

Lecture Notes
EG-296
Flight Mechanics

**fundamentals of aircraft performance,
stability and control**

W. G. Dettmer

College of Engineering

Swansea University

recommended literature:

- John D. Anderson, Jr., *Introduction to Flight*, 5th edition, McGraw-Hill, 2005
- Thomas R. Yechout *et al*, *Introduction to Aircraft Flight Mechanics*, American Institute of Aeronautics and Astronautics (AIAA), 2003
- Barnes W. McCormick, *Aerodynamics, Aeronautics and Flight Mechanics*, 2nd edition, John Wiley & Sons, 1995
- <http://en.wikipedia.org>

Contents

1	Basic Aerodynamics	1
1.1	Physical Units	1
1.2	The Standard Atmosphere	3
1.3	Mach Number	5
1.4	Reynolds Number	6
1.5	Boundary Layer	7
1.6	Bernoulli Equation for Incompressible Flow	8
1.7	Pressure Distribution and Flow Separation	9
1.8	Airfoil Fundamentals	11
1.9	High Lift Systems	20
1.10	Finite Wings	24
1.11	Aircraft Aerodynamics	31
1.12	Remarks on Trans-/Supersonic Flight	39
2	Aircraft Performance	43
2.1	Preliminaries	43
2.2	Brief Introduction to Aeroplane Propulsion	46
2.3	Straight, Level and Unaccelerated Flight	55
2.4	Climbing Flight and Flight Envelope	63
2.5	Gliding Flight	69
2.6	Take-Off and Landing	71
2.7	Range and Endurance	77
2.8	Turning Flight	83
2.9	$V-n$ Diagram	86
2.10	Energy Method for Accelerated Flight	89

3	Static Stability and Control	93
3.1	Static and Dynamic Stability	93
3.2	Aircraft Rotations and Control Surfaces	95
3.3	Longitudinal Static Stability	97
3.4	Longitudinal Control	108
3.5	Stick-Free Longitudinal Static Stability	113
3.6	Directional Static Stability and Control	118
3.7	Lateral Control	120
3.8	Coupling Effects	124

Chapter 1

Basic Aerodynamics

1.1 Physical Units

Basic physical units:

length	$1 \text{ in [inch]} = 0.0254 \text{ m [metre]}$ $1 \text{ ft [foot]} = 0.3048 \text{ m}$ $1 \text{ km [kilometre]} = 1,000 \text{ m}$ $1 \text{ mi [mile]} = 1,609 \text{ m}$ $1 \text{ nm [nautical mile]} = 1,852 \text{ m}$
mass	$1 \text{ lb [pound]} = 0.453592 \text{ kg [kilogram]}$ $1 \text{ t [ton]} = 1,000 \text{ kg}$
time	$1 \text{ h [hour]} = 3,600 \text{ s [seconds]}$

Derived physical units:

force	$1 \text{ N [Newton]} = 1 \text{ kg m s}^{-2}$ $1 \text{ kp [kilopond]} = 9.80665 \text{ kg m s}^{-2} = 1 \text{ kg} \cdot g$ $1 \text{ kN [kilonewton]} = 1,000 \text{ kg m s}^{-2}$
stress, pressure	$1 \text{ Pa [Pascal]} = 1 \text{ N m}^{-2} = 1 \text{ kg m}^{-1} \text{ s}^{-2}$ $1 \text{ kPa [kilo Pascal]} = 1,000 \text{ Pa}$ $1 \text{ MPa [mega Pascal]} = 1,000,000 \text{ Pa}$ $1 \text{ bar} = 100,000 \text{ Pa} = 10 \text{ N cm}^{-2}$
energy, work	$1 \text{ J [Joule]} = 1 \text{ N m} = 1 \text{ kg m}^2 \text{ s}^{-2}$
power	$1 \text{ W [Watt]} = 1 \text{ J s}^{-1} = 1 \text{ kg m}^2 \text{ s}^{-3}$ $1 \text{ kW [kilo Watt]} = 1,000 \text{ W}$ $1 \text{ MW [mega Watt]} = 1,000,000 \text{ W}$ $1 \text{ bhp [brake horse power]} = 745.7 \text{ W}$ $1 \text{ PS [Pferdestärke]} = 735.5 \text{ W} = 75 \text{ kp m s}^{-1}$

The quantity $g = 9.80665 \text{ m s}^{-2}$ denotes the gravitational acceleration of the earth.

For calculations involving angles we will need the relation

$$360 \text{ deg} = 2\pi \text{ rad} .$$

1.2 The Standard Atmosphere

Generally, in the atmosphere of the earth, the pressure, the temperature and the density of the air are functions of altitude. The variations of these quantities with time and location are negligible and mostly due to weather conditions.

The altitude of an aircraft is typically determined by measuring the free stream air pressure and subsequent calculation of the altitude. In order to ensure that the pilots of any aeroplanes at the same time in the same location have consistent altimeters the international community introduced the notion of the *standard atmosphere*, which relates the pressure, the temperature and the density of the air uniquely to the altitude and ignores local variations.

The standard atmosphere is composed of layers with constant temperature gradients, *i. e.* $dT/dh = \text{const.}$ in each layer:

$$\text{troposphere} : 0 - 11 \text{ km} \quad : T = 288.2 \text{ K} - \frac{71.5 \text{ K}}{11 \text{ km}} h \quad (1.1)$$

$$\text{stratosphere} : 11 \text{ km} - 20 \text{ km} : T = 216.7 \text{ K} \quad (1.2)$$

$$20 \text{ km} - \quad : T = 216.7 \text{ K} + \frac{\text{K}}{\text{km}} h \quad (1.3)$$

The equation for the perfect gas

$$p = \rho R T \quad \text{with } R \text{ specific gas constant, } R_{\text{air}} = 287 \text{ J (kg K)}^{-1}, \quad (1.4)$$

the hydrostatic equation

$$\frac{dp}{dh} = -\rho g \quad \text{with gravity acceleration } g = 9.81 \text{ m s}^{-2} \quad (1.5)$$

and the boundary condition $p = p_0 = 101,325 \text{ N m}^{-2}$ at $h = 0$ suffice to determine the pressure p . Using (1.1) and (1.4) in (1.5) and solving the differential equation for p renders

$$p = p_0 \left(1 - \frac{71.5}{288.2} \frac{h}{11 \text{ km}} \right)^{\frac{g}{R} \frac{11 \text{ km}}{71.5 \text{ K}}}. \quad (1.6)$$

Similarly, (1.2), (1.4) and (1.5) give

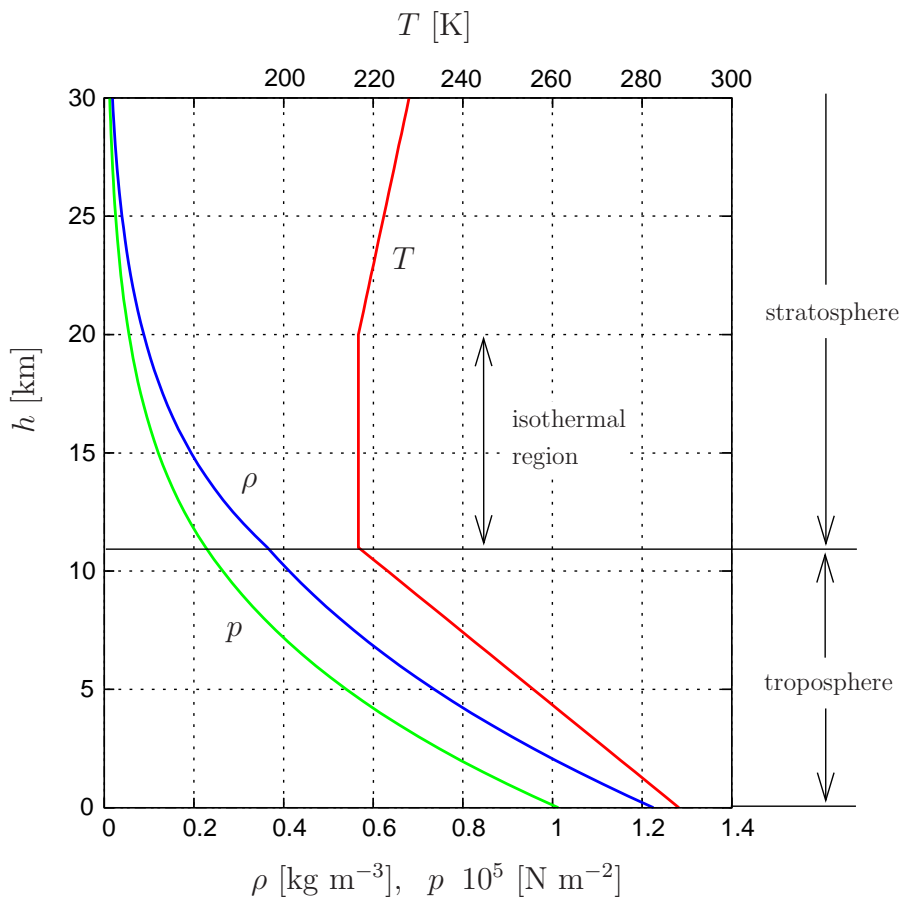
$$p = p_{11} \exp \left(-\frac{g}{R} \frac{h - 11 \text{ km}}{216.7 \text{ K}} \right), \quad (1.7)$$

where $p_{11} = 22,621 \text{ N m}^{-2}$. The density ρ may then be calculated from (1.4). At sea-level, the air density is obtained as $\rho_0 = 1.225 \text{ kg m}^{-3}$.

Tables of the standard atmosphere are provided in most text books on air flight.

We also note the dependency of the *speed of sound* a on the temperature, *i. e.*

$$a = \sqrt{\gamma R T} \quad \text{with } \gamma \text{ ratio of specific heats, } \gamma_{\text{air}} \approx 1.4. \quad (1.8)$$



	at sea-level	at 8000 m
density	$\rho_0 = 1.225 \text{ kg m}^{-3}$	0.526 kg m^{-3}
pressure	$p_0 = 101,325 \text{ N m}^{-2}$	$35,651 \text{ N m}^{-2}$
speed of sound	$340 \text{ m s}^{-1} = 1,225 \text{ km h}^{-1}$	$308 \text{ m s}^{-1} = 1,109 \text{ km h}^{-1}$

1.3 Mach Number

The dimensionless *Mach number* is defined in every point of the fluid flow field as

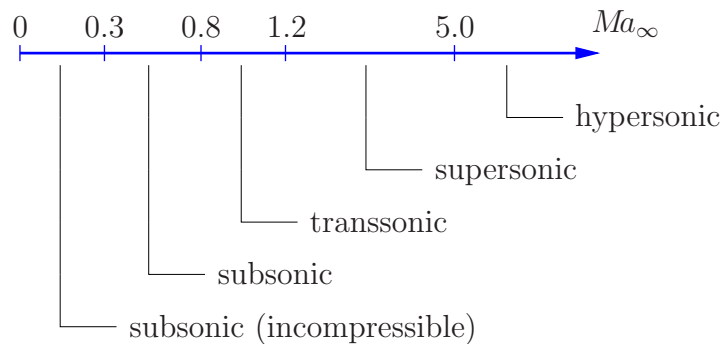
$$Ma = \frac{v}{a}, \tag{1.9}$$

where v is the local flow velocity. In order to characterise the flight of an airplane we introduce the *freestream Mach number*

$$Ma_\infty = \frac{v_\infty}{a}, \tag{1.10}$$

where v_∞ corresponds to the *true airspeed* or *free stream velocity*. Importantly, for $Ma_\infty < 0.3$, the air flow can be assumed to be incompressible, whereas, for $Ma_\infty > 1.0$, we expect the occurrence of pressure *shock waves*.

Characterisation of flow:



In transsonic flow, we typically have local areas of the flow field where the flow is subsonic and others where the flow is supersonic.

1.4 Reynolds Number

The dimensionless *Reynolds number* is defined as

$$Re = \frac{\rho v_{\infty} h}{\mu}, \quad (1.11)$$

where h is the characteristic length scale of the problem under consideration and μ is the viscosity of the fluid medium. The Reynolds number describes the ratio of the inertia forces to the viscous forces, both of which act on the fluid particles.

If the Reynolds number is small, then the fluid flow is typically *laminar*, *i.e.* the streamlines are smooth and regular.

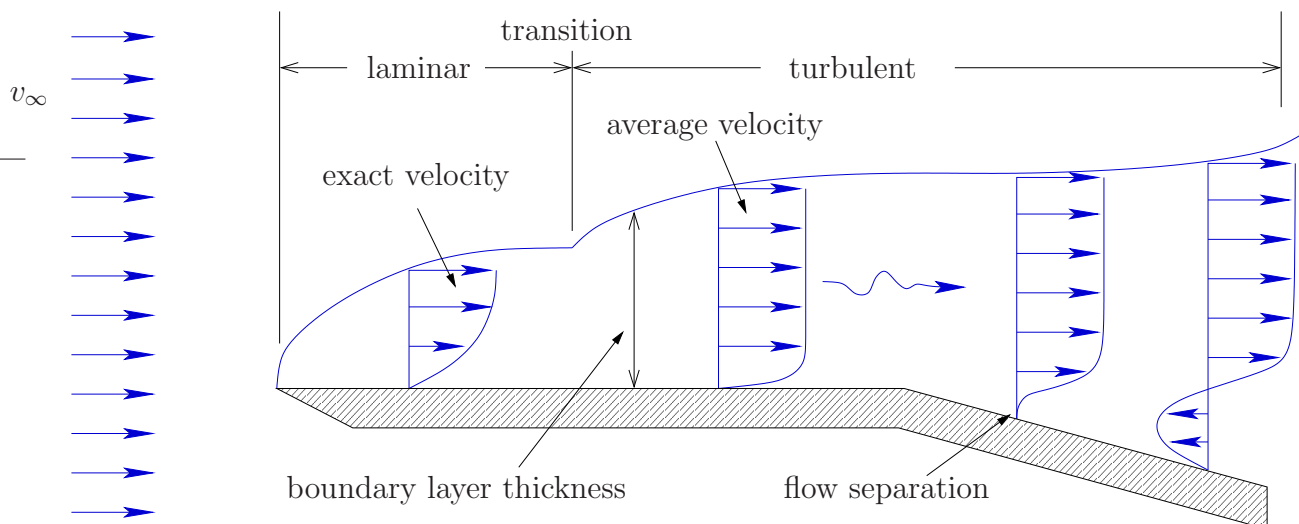
If the Reynolds number is large, then the fluid flow is likely to be *turbulent* in at least some areas of the flow field, *i.e.* the streamlines break up and the fluid particles move in a random irregular fashion. Turbulent fluid flow is always unsteady. In the presence of turbulence, we are interested in *average* velocities and *average* properties of the flow.

The *critical Reynolds number* Re_{crit} , which is associated with the transition from laminar to turbulent flow is extremely problem dependent. For the flow through a circular pipe it is approximately 2300.

1.5 Boundary Layer

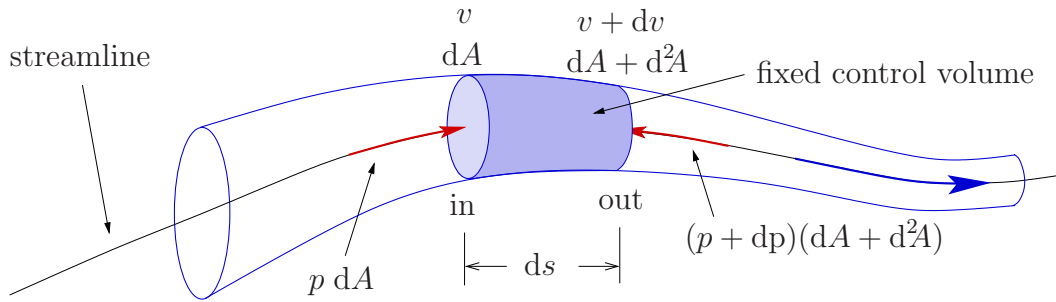
The flow field around a submerged body can be divided into the *boundary layer* and the region outside the boundary layer. The boundary layer is a thin region adjacent to the surface of the solid body, where the fluid flow is dominated by viscous forces (*friction*). Outside the boundary layer, the effect of the fluid viscosity is negligible (*potential flow*).

In a boundary layer we often observe transition from laminar to turbulent flow. Laminar boundary layers are thinner than turbulent ones. *Skin friction* is smaller in laminar boundary layers than in turbulent ones.



1.6 Bernoulli Equation for Incompressible Flow

Consider a stream tube of infinitesimal thickness in steady inviscid fluid flow:



By definition mass transport along the tube is constant: $\dot{m} = \rho dA v = \text{const.}$
Conservation of momentum in flow direction renders

$$0 = p dA - (p + dp)(dA + d^2A) + (\rho dA v) v - (\rho dA v) (v + dv).$$

Neglect of higher order terms gives the *Euler equation*

$$0 = dp + \rho v dv. \quad (1.12)$$

Using $\rho = \text{const.}$ and integrating along a streamline between points A and B we obtain for incompressible fluid flow

$$0 = \int_A^B dp + \rho \int_A^B v dv = p_B - p_A + \frac{1}{2} \rho (v_B^2 - v_A^2).$$

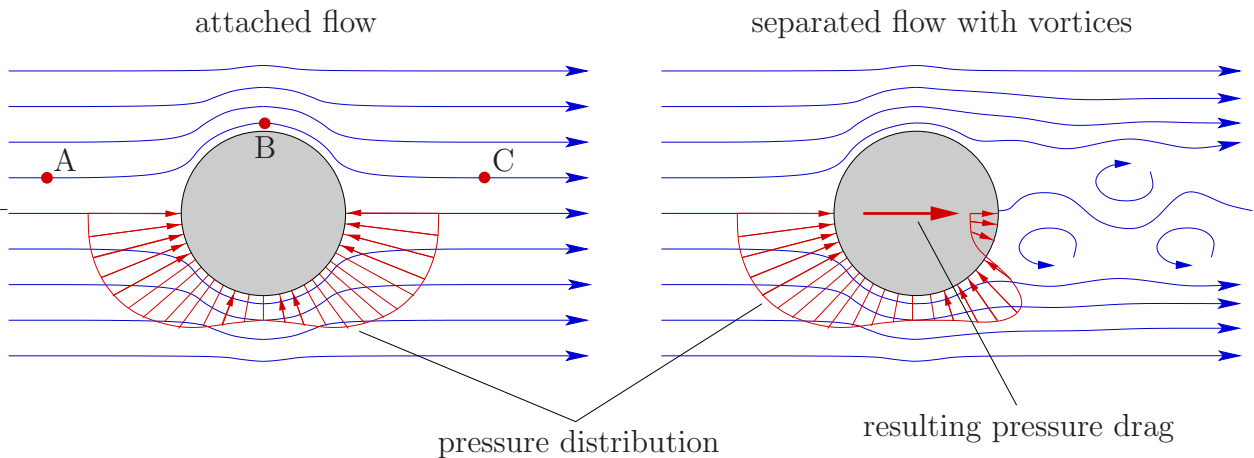
The *Bernoulli equation* for incompressible flow follows as

$$p_A + \frac{1}{2} \rho v_A^2 = p_B + \frac{1}{2} \rho v_B^2. \quad (1.13)$$

1.7 Pressure Distribution and Flow Separation

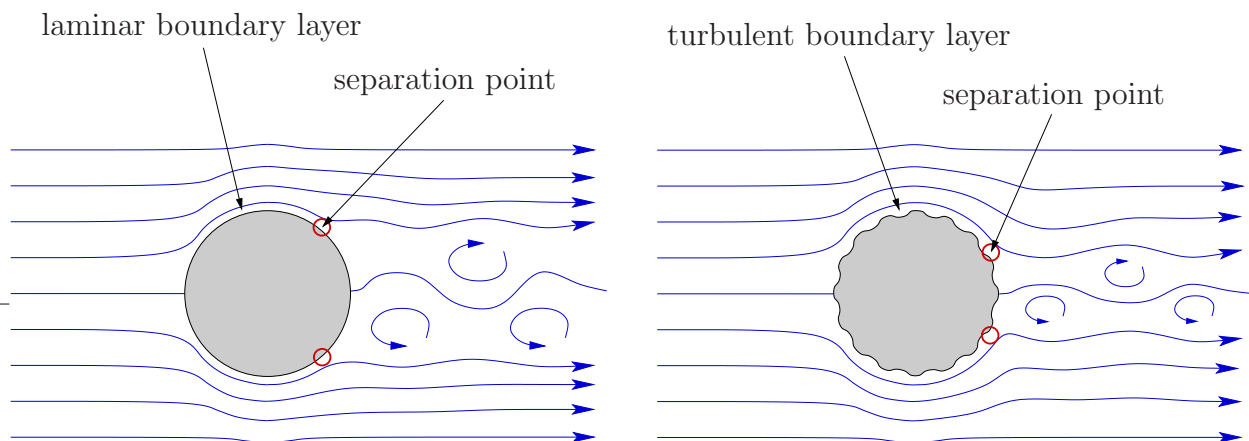
Consider the incompressible fluid flow around a sphere and assume *attached flow*. The stream tubes passing over the surface of the sphere are longer and narrower than the others. Those fluid particles, which travel from point A to B and then on to C are first accelerated and then decelerated, *i.e.* $v_\infty = v_A = v_C < v_B$. It then follows from (1.13), that these particles encounter first a drop and then an increase of pressure, *i.e.* $p_{\text{atmos}} = p_A = p_C > p_B$. At the same time, they have to work against skin friction on the surface of the solid sphere. Between point B and C, both the *adverse pressure gradient* and the skin friction slow down the particles.

Therefore, the attached flow pattern is only physically possible if the adverse pressure gradient is sufficiently small. Otherwise, the particles are decelerated and finally move in the opposite direction, which causes *flow separation*. Flow separation creates a wake region dominated by *vortices*.



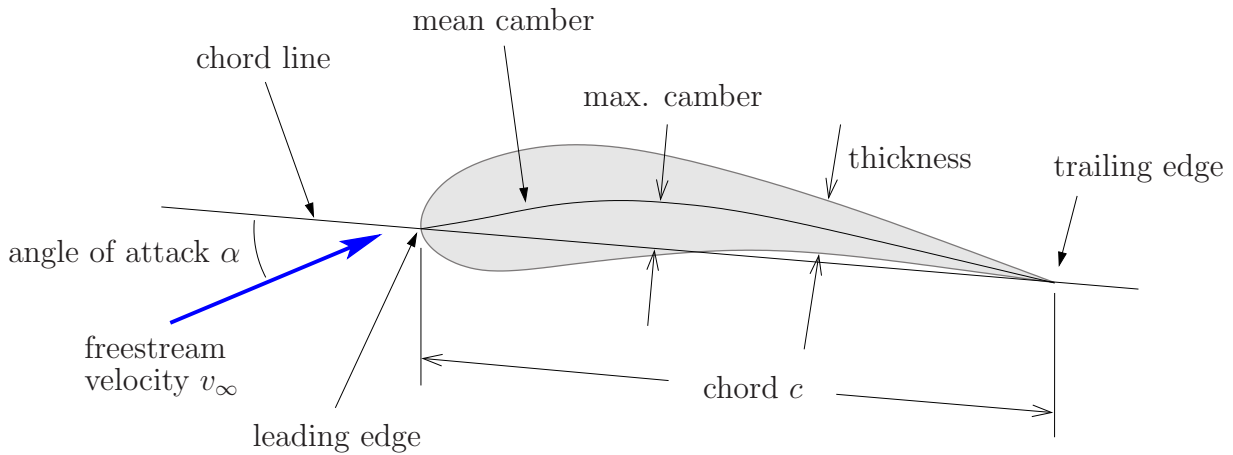
The integral of the pressure over the surface of the solid sphere renders the force which is exerted by the fluid flow on the submerged sphere. This force is denoted as the *pressure drag* and must not be confused with the skin friction. For attached flow, the pressure drag is zero. However, flow separation typically results in a pressure drag which is significantly larger than skin friction drag. This is due to the failure of the flow to recover the high pressure at the rear of the body.

The flow in turbulent boundary layers possesses more kinematic energy than laminar flow, and therefore has a greater potential to overcome adverse pressure gradients. Thus, turbulent boundary layers are often created deliberately (dimples on golf ball) in order to repress separation and consequently reduce the pressure drag (despite the increase in friction drag the overall drag reduction is significant).



1.8 Airfoil Fundamentals

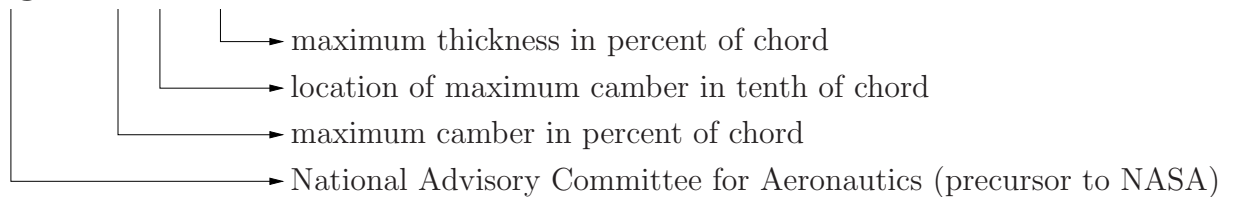
Geometry and Terminology



The angle of attack α is defined as the angle between the freestream velocity and the chord line. The latter corresponds to the straight line connecting the leading and the trailing edges.

The NACA four digit code describes the airfoil geometry:

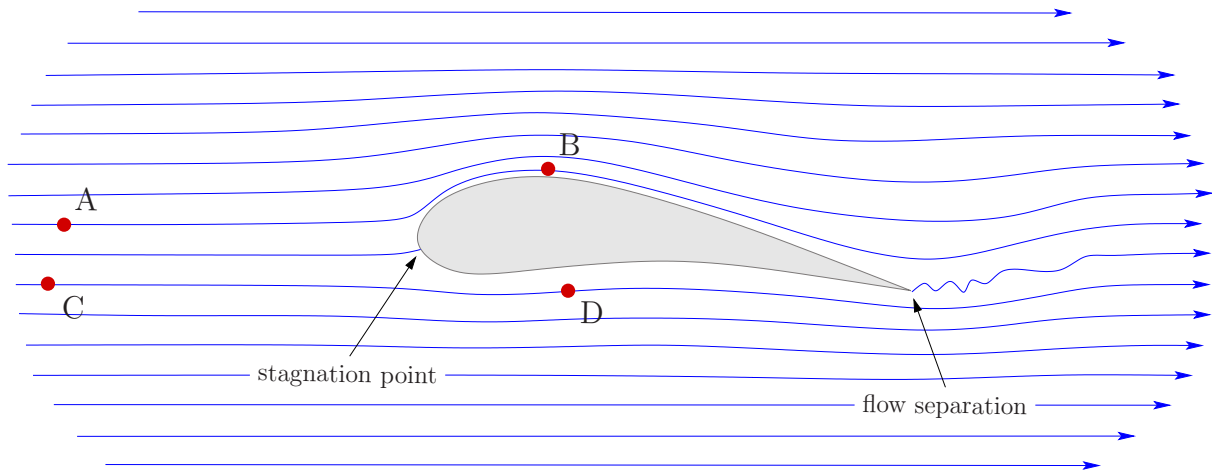
NACA 2 4 12



Note that, besides this classical family of airfoils, there are several other series. Modern airfoils, such as the *supercritical* airfoil, are typically designed with complex computer analysis tools for specific requirements and feature very individual geometries.

Generation of Lift and Origin of Drag

We consider the airflow past an airfoil. For simplicity, we assume incompressibility of the air ($Ma_\infty < 0.3$).



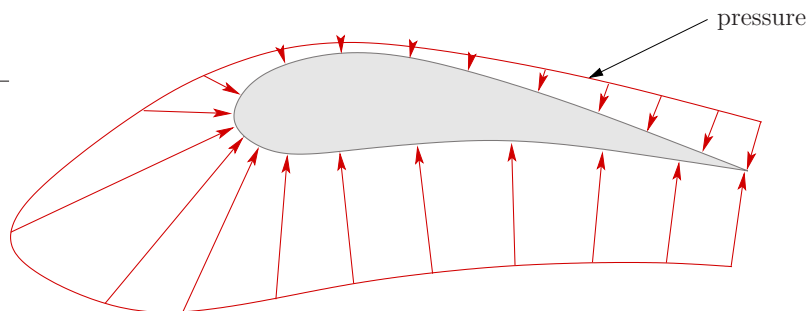
The streamlines passing over the top of the airfoil are longer, the space between them is narrower, than at the bottom. The air particles flowing over the airfoil evidently need to accelerate more than those passing underneath, *i. e.*

$$v_A = v_C = v_\infty < v_D < v_B . \quad (1.14)$$

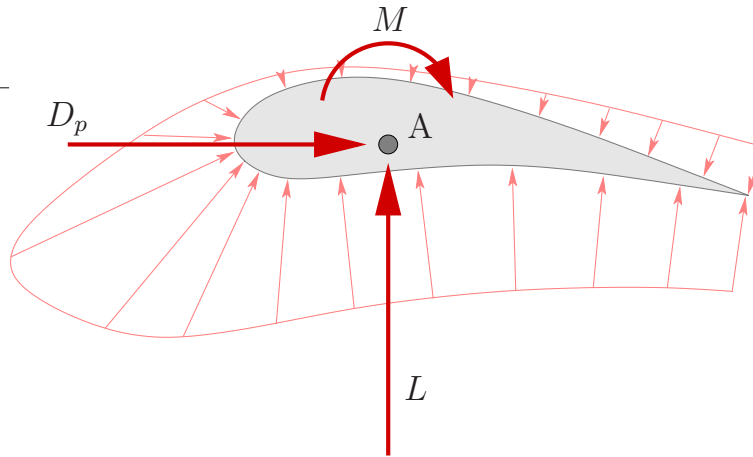
It then follows from (1.13) that

$$p_A = p_C = p_{\text{atmos}} > p_D > p_B . \quad (1.15)$$

In the stagnation point, we have $v = 0$ and thus $p > p_{\text{atmos}}$. We obtain a qualitative pressure distribution as displayed below.



The integration of the pressure renders the *lift force* L (perpendicular to v_∞), the *pressure drag force* D_p (parallel to v_∞) and the *moment* M . The moment M depends on the choice of point A.



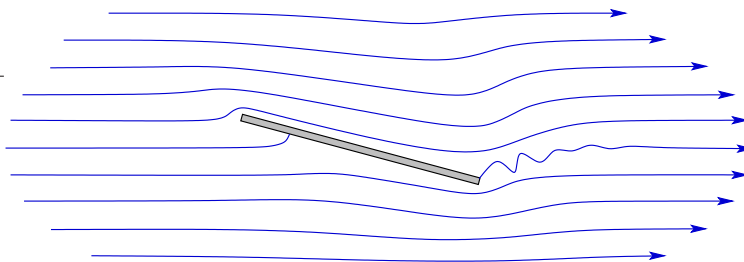
For subsonic flows, the total drag force acting on the airfoil includes the pressure drag D_p and the *skin friction drag* D_f due to the air viscosity, *i. e.*

$$D = D_p + D_f . \tag{1.16}$$

The effect of skin friction in lift direction is negligible. For transsonic and supersonic flows, another drag component is observed, which arises from the formation of shock waves, see Section 1.12.

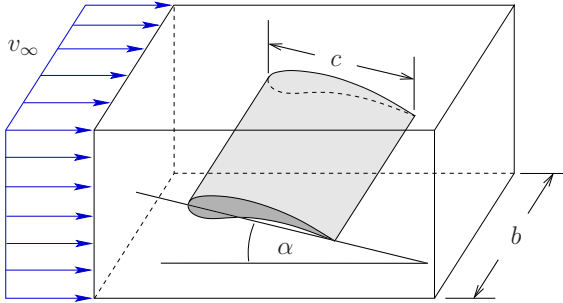
For a given airfoil geometry, lift and drag forces depend on the angle of attack α and the velocity v_∞ . Note that there exists a point A, such that M is the same for all angles of attack α . This point is called the *aerodynamic centre* of the airfoil and is of crucial importance in the design of aeroplanes.

Note also that lift can be generated with bodies of very primitive geometries as shown below.



Aerodynamic Coefficients

For the characterisation of airfoil geometries, we introduce coefficients which are independent of the airfoil size and the velocity v_∞



$$\text{lift: } C_l = \frac{L}{q_\infty c b} \quad (1.17)$$

$$\text{drag: } C_d = \frac{D}{q_\infty c b} \quad (1.18)$$

$$\text{moment: } C_m = \frac{M}{q_\infty c^2 b} \quad (1.19)$$

The dynamic pressure q_∞ in the stagnation point is obtained from (1.13)

$$p_{\text{atmos}} + 0 + \frac{1}{2} \rho v_\infty^2 = p_{\text{atmos}} + q_\infty + 0 \quad \Rightarrow \quad q_\infty = \frac{1}{2} \rho v_\infty^2 \quad (1.20)$$

The aerodynamic coefficients C_l , C_d , C_m depend primarily on the angle of attack α . In the range of very large velocities, they also depend on the Reynolds number Re and the Mach number Ma .

For the design and study of airfoils, it is useful to introduce the drag coefficients $C_{d,f}$ and $C_{d,p}$, which relate to friction drag and pressure drag, respectively, *i. e.*

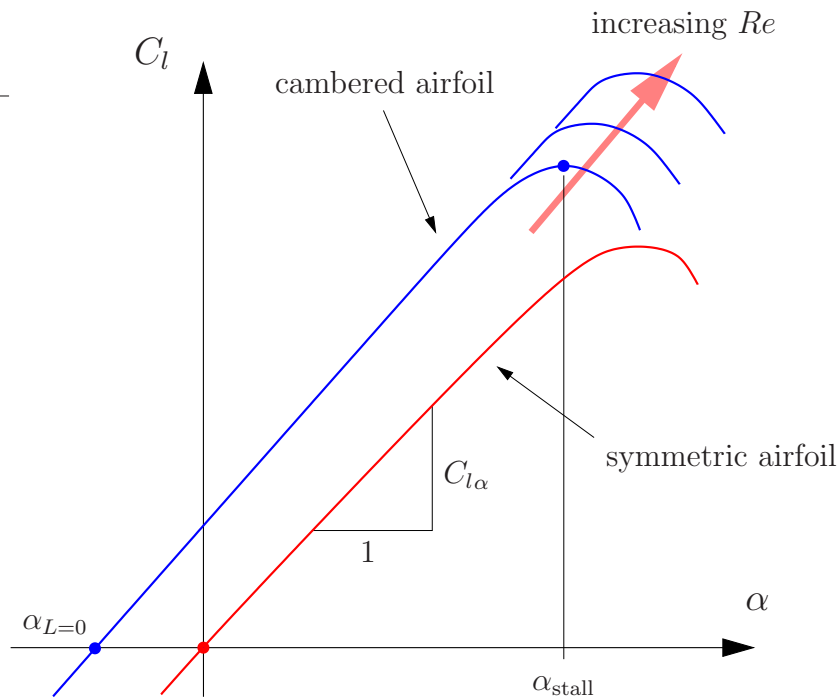
$$C_{d,f} = \frac{D_f}{q_\infty c b}, \quad C_{d,p} = \frac{D_p}{q_\infty c b}. \quad (1.21)$$

Thus, with (1.16), we have for subsonic flow

$$C_d = C_{d,f} + C_{d,p}. \quad (1.22)$$

Airfoil Lift Curve

By measuring the lift force L for different angles of attack α (wind tunnel tests), we can obtain the characteristic lift curve of a specific airfoil.



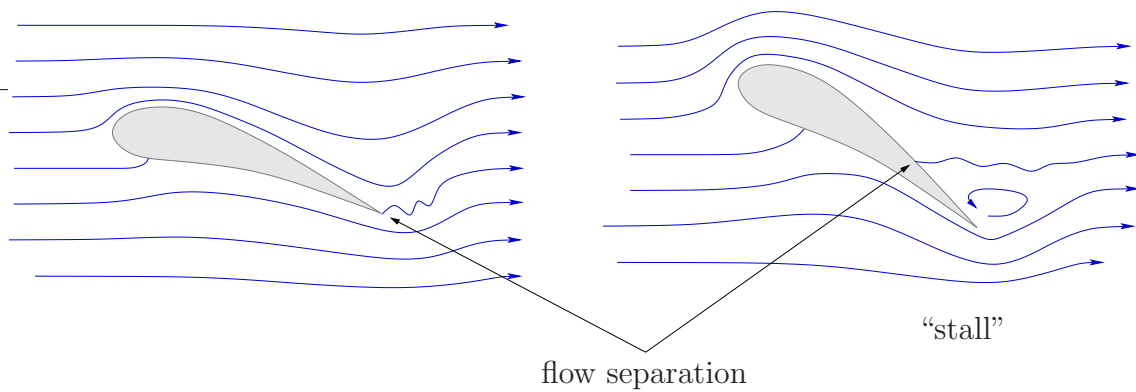
For reasonable angles of attack, we observe a linear relation between C_l and α . For symmetric airfoils (zero camber), we clearly have zero lift at $\alpha = 0$. The derivative of C_l with respect to α is denoted as $C_{l\alpha}$.

A good approximation of $C_l(\alpha)$ may be written as

$$C_l(\alpha) = C_{l\alpha} \cdot (\alpha - \alpha_{L=0}) . \tag{1.23}$$

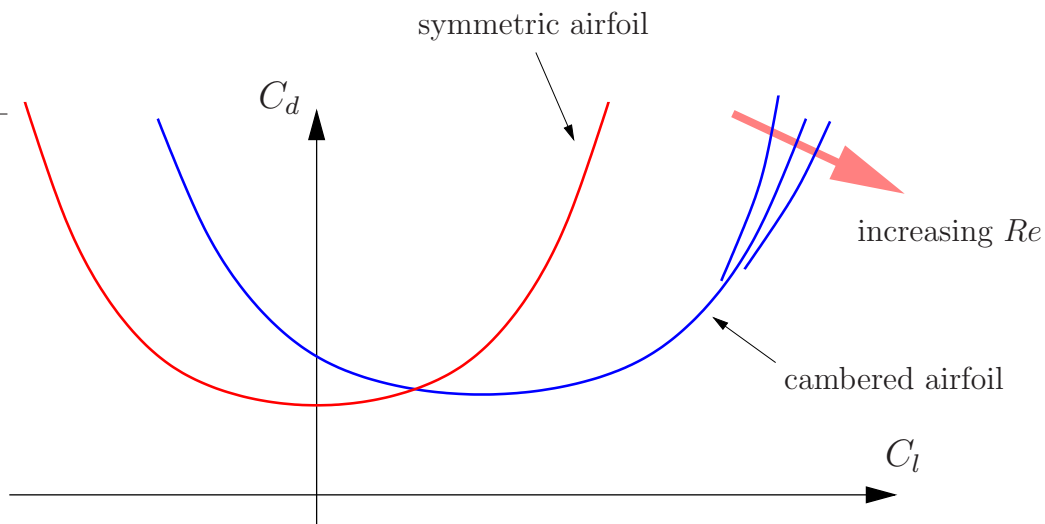
The sudden drop of the lift coefficient at α_{stall} is due to flow separation before the trailing edge. This destroys the desired pressure distribution over the airfoil surface and may lead to the complete loss of lift: We say “the airfoil *stalls*”.

An increase of the Reynolds number extends the turbulent boundary layer and thereby represses undesired flow separation. This typically leads to larger $C_{l_{\text{max}}}$.



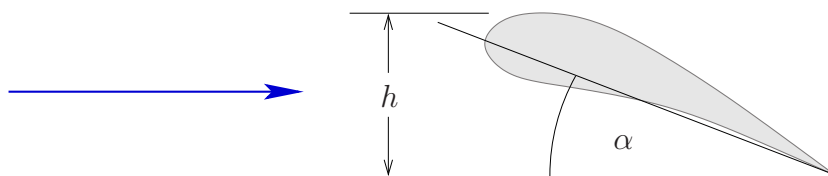
Airfoil Drag Polar

Similarly to the lift, we can measure the drag force for different angles of attack in a wind tunnel experiment. The graph, which displays the drag coefficient C_d against the lift coefficient C_l , is known as the *drag polar* of the airfoil.

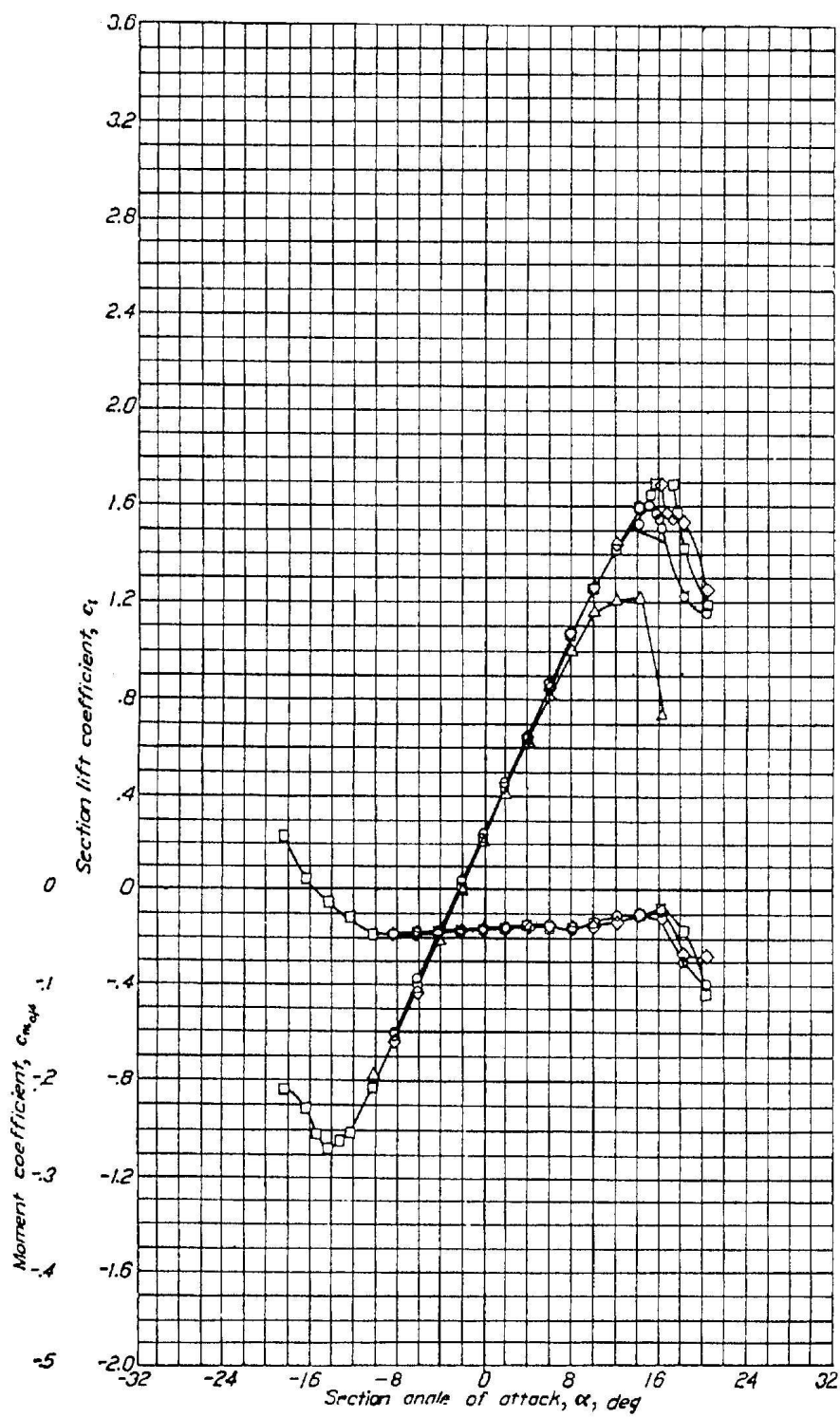


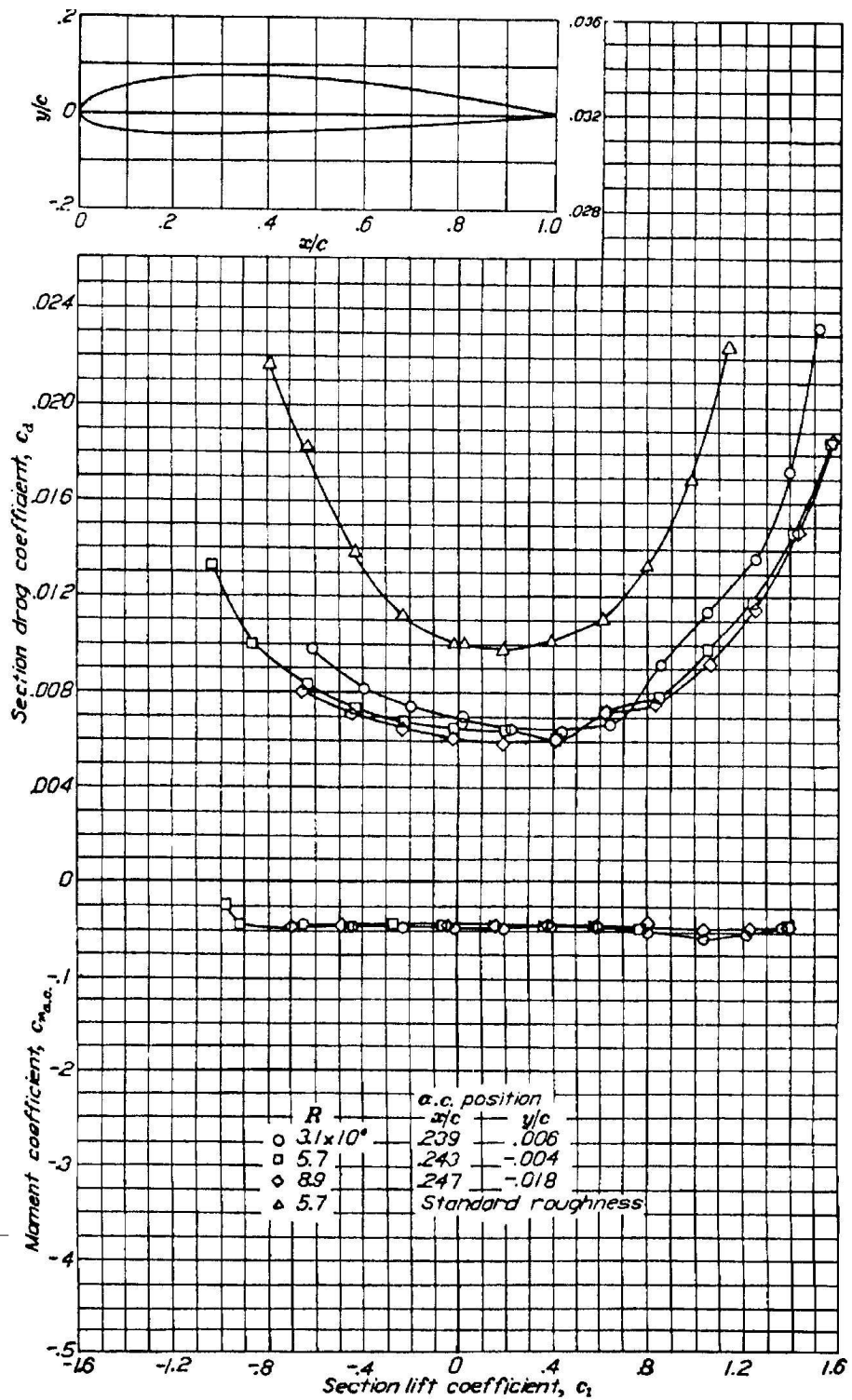
For interpretation, recall the linear relation between C_l and α . The pressure drag or “separation drag” $C_{d,p}$ is closely related to the airfoil thickness “seen” by the coming flow and denoted by h in the diagram below. Therefore, $C_{d,p}$ becomes larger as α (and C_l) increase. The skin friction drag $C_{d,f}$ is fairly independent of α and dominates the drag associated with small α (small C_l).

Higher Reynolds numbers suppress flow separation and allow to achieve larger lift coefficients with less pressure drag despite the increase in skin friction drag.



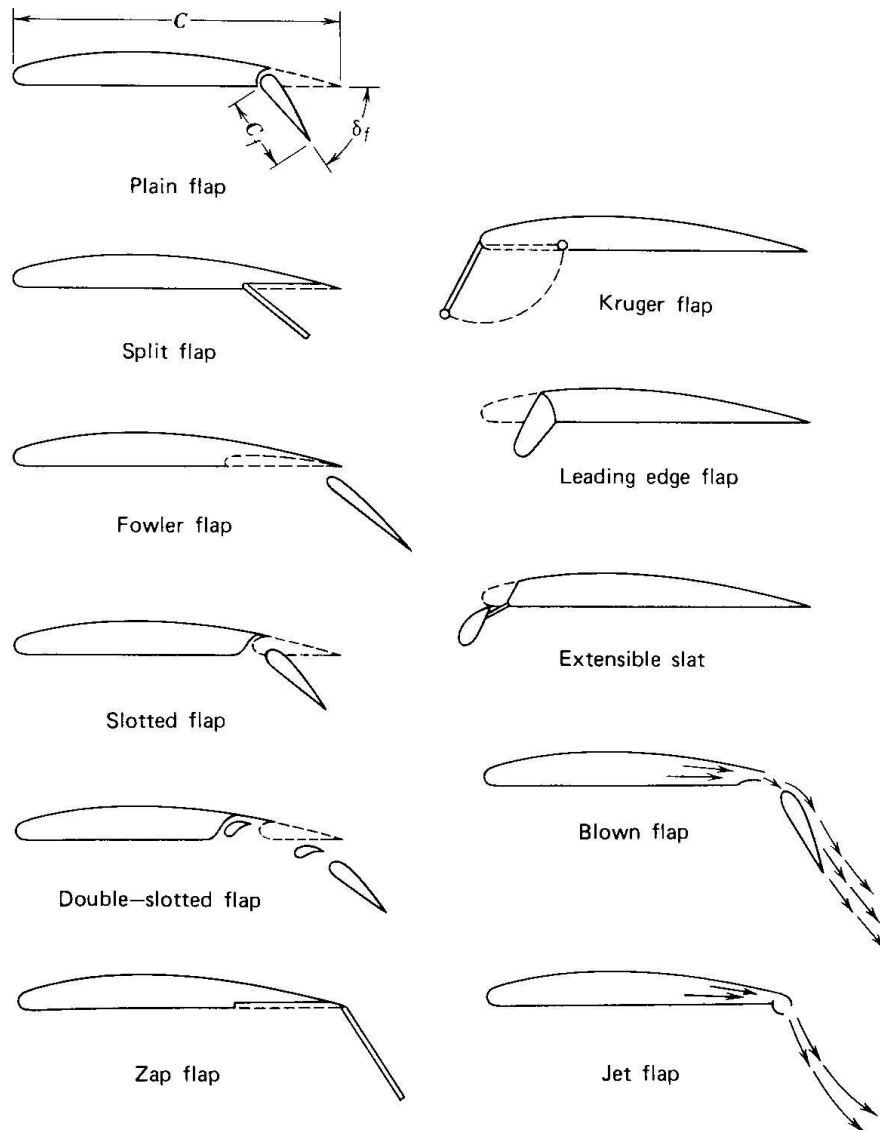
Drag and Lift Coefficients of NACA 2412



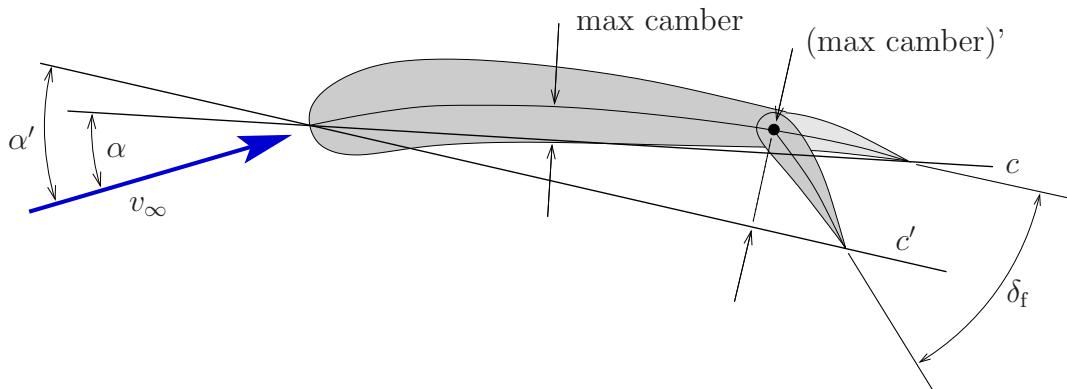


1.9 High Lift Systems

For certain manoeuvres, such as take-off and landing, very high lift systems are desirable. However, we have seen in the drag polar, that high lift is typically associated with large drag forces, which need to be overcome by engine thrust. Therefore, in order not to jeopardise the cruising performance of the aeroplane, we desire high lift systems that can be activated when needed, *e. g.* to allow short ground roll at take-off. For that purpose, a variety of *flaps* have been developed.



For most flap types, the increase of the lift coefficient is due to the increased camber of the airfoil and the increased angle of attack with respect to the new chord line c' . The flap deflection is typically denoted as δ_f .



plain flaps:

- The optimum flap chord ratio is approximately $\frac{c_f}{c} = 0.25$.
- The optimum flap angle is approximately 60 deg.
- The maximum achievable increment in $C_{l_{max}}$ is approximately 0.9.

split flaps:

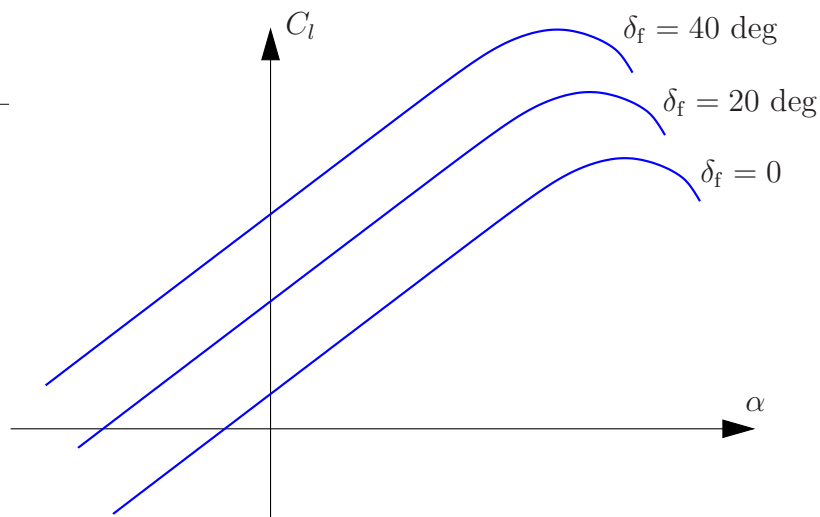
- The optimum flap chord ratio varies with the airfoil thickness: $0.3 < \frac{c_f}{c} < 0.4$.
- The optimum flap angle is approximately 70 deg.
- The maximum achievable increment in $C_{l_{max}}$ is approximately 0.9.

slotted flaps:

- The optimum flap chord ratio is approximately $\frac{c_f}{c} = 0.3$.
- The optimum flap angle is approximately 40 deg for single slots and 70 deg for double-slotted flaps.
- The maximum achievable increment in $C_{l_{max}}$ is approximately 1.5 for single slots and 1.9 for double-slotted flaps.

powered systems:

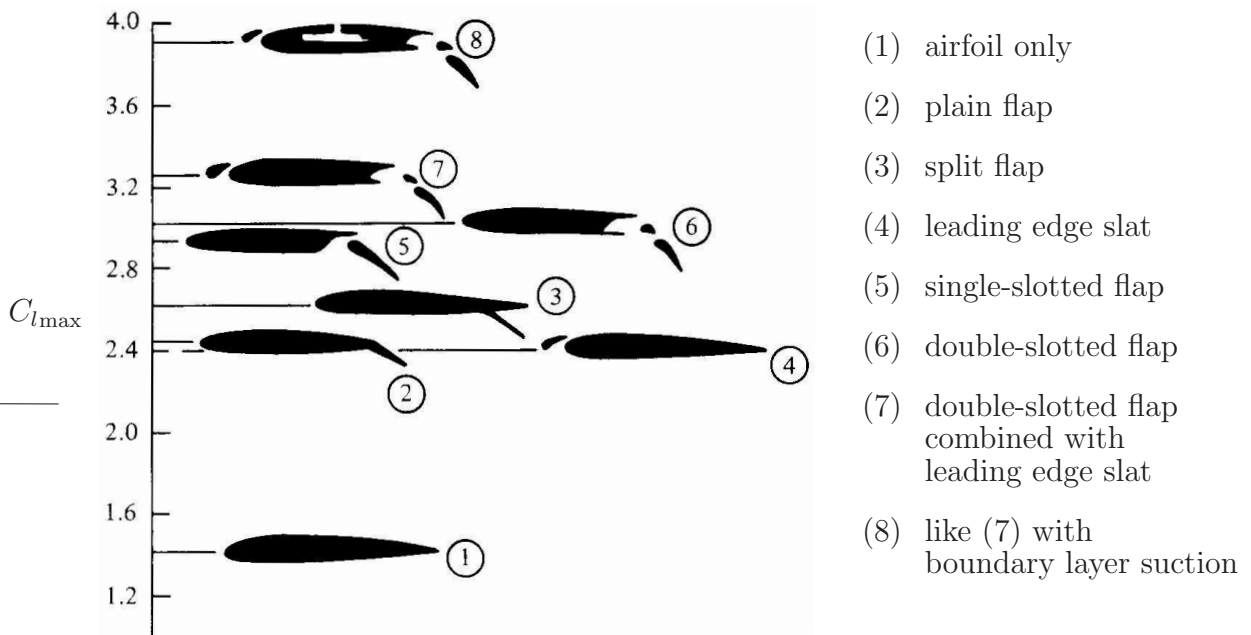
- Directed air jets blown through nozzles near the trailing edge can act as “virtual” flaps.
- Distributed suction over the wing surface may be used to delay flow separation.
- Powered high lift systems have the capability to provide values of $C_{l_{\max}}$ large enough to achieve extremely short takeoff ground roll of the aircraft.



The effect of standard flaps on the slope $C_{l\alpha}$ of the lift curve is typically negligible. Introducing the *flap effectiveness factor* τ , which can be determined from wind tunnel tests, the lift coefficient of an airfoil with a flap may be written as

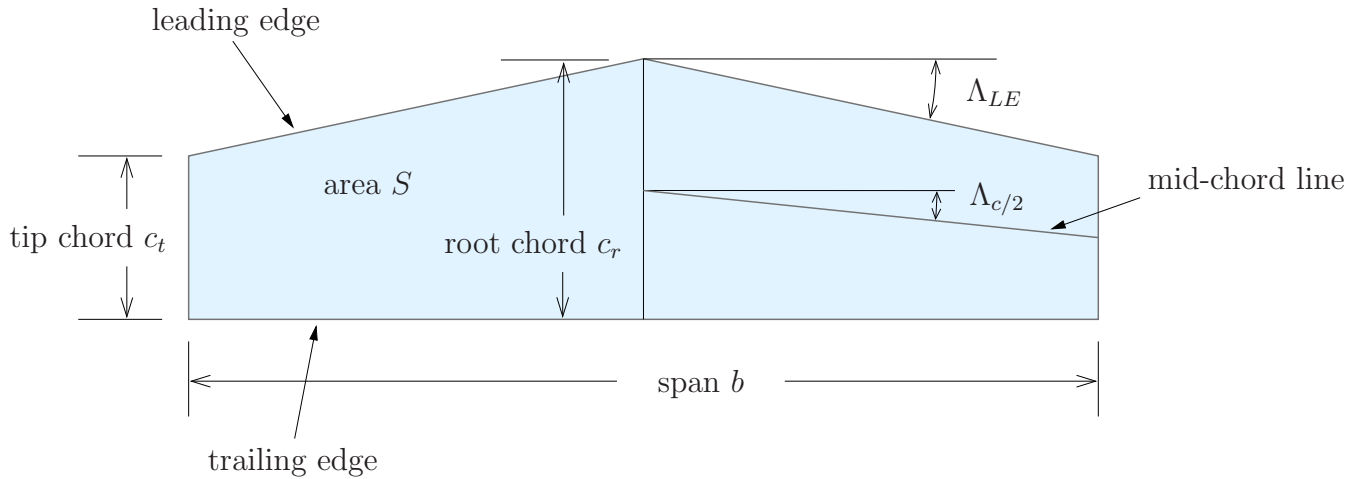
$$C_l = C_{l\alpha} (\alpha - \alpha_{L=0} + \tau \delta_f) . \quad (1.24)$$

The dependency of the flap effectiveness on the flap deflection δ_f is beyond the scope of this course.



1.10 Finite Wings

Geometry and Terminology



$$\text{aspect ratio} \quad AR = \frac{b^2}{S} \quad (1.25)$$

$$\text{taper ratio} \quad \lambda = \frac{c_t}{c_r} \quad (1.26)$$

The angles Λ_{LE} and $\Lambda_{c/2}$ or $\Lambda_{c/4}$ are known as *sweep angles*.

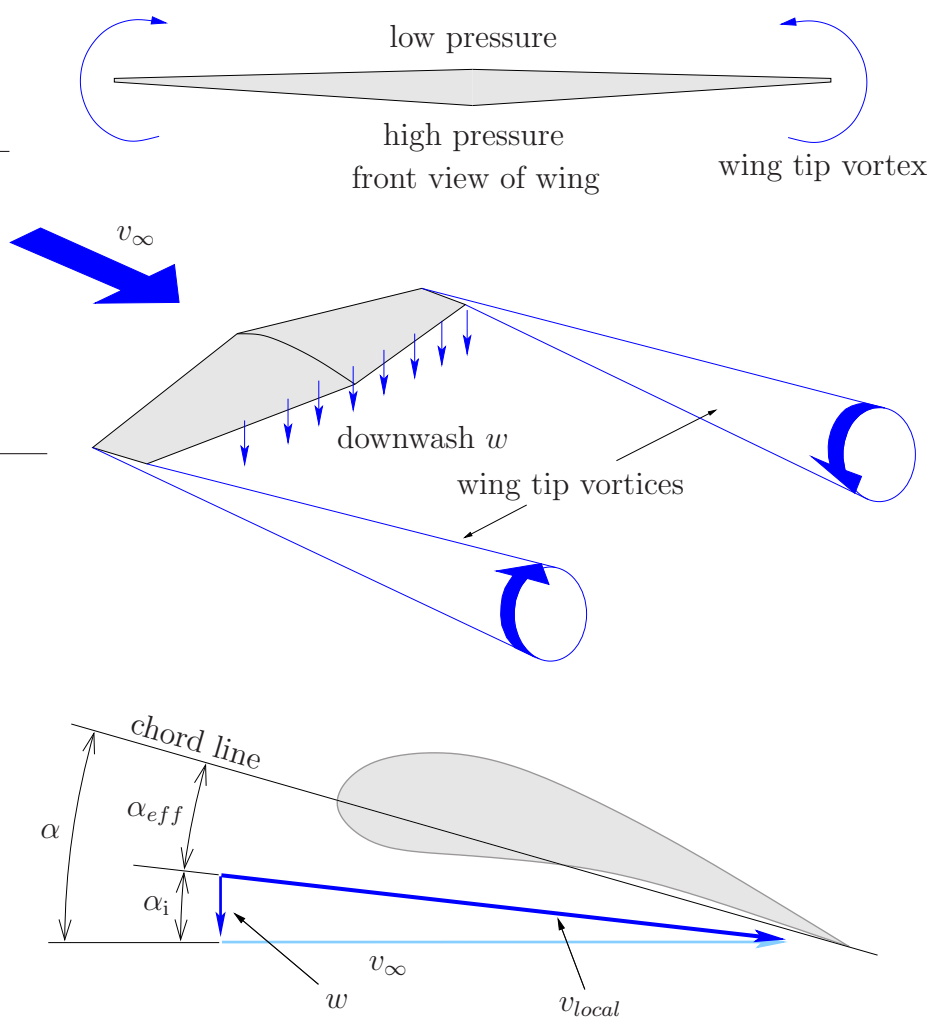
A wing with a large span b and small chord lengths has a large aspect ratio AR . The imaginary wing with $AR \rightarrow \infty$ is known as the “infinite wing”.

A rectangular wing “has no taper” ($\lambda = 1$); a delta wing has a taper ratio $\lambda = 0$.

Lift, drag and moment coefficients for the finite wing are denoted as C_L , C_D , C_M to avoid confusion with airfoil data C_l , C_d , C_m .

Wing Tip Vortices and Induced Angle of Attack

A wing generates lift by creating a pressure difference between the upper and lower surfaces. *Wing tip vortices* are generated as the high-pressure air on the lower wing surface seeks the relatively lower pressure on the upper surface. These vortices induce a downward component of velocity called *downwash* w .



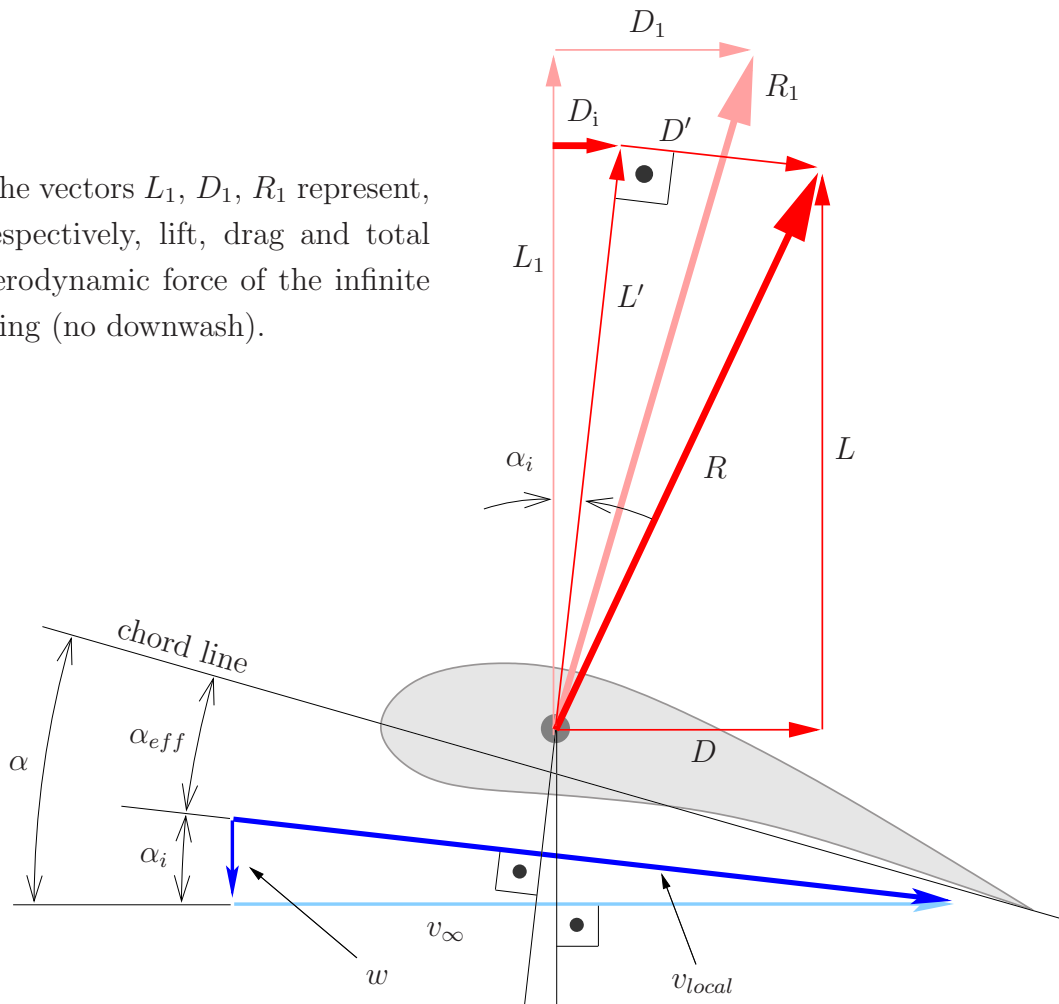
The velocity v_{local} “seen” by the wing consists of the superposition of the velocity v_∞ and the downwash w . It follows that the *effective* angle of attack α_{eff} is related to α and to the *induced* angle of attack α_i by

$$\alpha_{eff} = \alpha - \alpha_i . \quad (1.27)$$

Induced Drag

According to (1.27), the effective angle of attack α_{eff} between the velocity v_{local} and the chord line of the wing section is smaller than α . Relating the direction of the lift force to the effective freestream velocity v_{local} corresponds to a rearward rotation of the lift force by α_i . However, we would like to continue to define the directions of lift and drag forces L and D with respect to the original freestream velocity v_∞ . Thus, we see that the tilted lift force L' contributes a certain component of drag. This drag is known as the *induced drag* D_i .

The vectors L_1 , D_1 , R_1 represent, respectively, lift, drag and total aerodynamic force of the infinite wing (no downwash).



The angle α_i is typically very small. Generally, we also have $L \gg D$. Thus,

$$L' = L, \quad D_i = \alpha_i L. \quad (1.28)$$

Under certain assumptions, such as incompressible flow, it can be derived that

$$\alpha_i = \frac{C_L}{\pi e AR} , \quad (1.29)$$

where e is the geometry dependent *span efficiency factor*. Typically, $0.9 < e < 1$; for an elliptic wing $e = 1$. Note that α_i is obtained in radians.

Equation (1.29) reflects the following correlations:

- A large lift coefficient C_L implies a large pressure difference between lower and upper wing surfaces. This causes a strong downwash, which, turn produces a large α_i .
- The smaller the aspect ratio AR , *i. e.* the shorter the wing, the more dominant are the wing vortices. This causes a strong downwash and leads to a large α_i .

Defining the *induced drag coefficient* as
$$C_{D,i} = \frac{D_i}{q_\infty S} \quad (1.30)$$

and using (1.28), (1.29) and (1.17) for the finite wing, we obtain

$$C_{D,i} = \frac{C_L}{\pi e AR} \frac{L}{q_\infty S} = \frac{C_L^2}{\pi e AR} . \quad (1.31)$$

It follows for the total drag C_D of a finite wing at subsonic speeds that

$$C_D = C_d + \frac{C_L^2}{\pi e AR} . \quad (1.32)$$

The airfoil section drag or *profile drag* C_d accounts for skin friction and pressure drag and is given by (1.22). Recall the dependency of C_d on the lift coefficient C_l of the airfoil. However, the variation of C_d is typically significantly smaller than the induced drag coefficient $C_{D,i}$.

The most effective remedy for induced drag is the design of large aspect ratio wings. Also the addition of vertical surfaces at the wing tips (“winglets”) reduces the strength of the wing tip vortices and thereby decreases the induced drag.

Page 29 shows a qualitative representation of the drag polar of a finite wing.

Lift of the Finite Wing

In Equation (1.28) we have $L = L'$. Furthermore, we can write

$$L = q_\infty S C_L(\alpha), \quad L' = q_\infty S C_l(\alpha_{\text{eff}}). \quad (1.33)$$

Thus, we obtain

$$C_L(\alpha) = C_l(\alpha_{\text{eff}}). \quad (1.34)$$

Using (1.23), (1.27) and (1.29), we can deduce

$$\begin{aligned} C_L(\alpha) &= C_l(\alpha - \alpha_i) \\ &= C_{l_\alpha} \cdot (\alpha - \alpha_i - \alpha_{L=0}) \\ &= C_{l_\alpha} \cdot \left(\alpha - \frac{C_L(\alpha)}{\pi e AR} - \alpha_{L=0} \right). \end{aligned} \quad (1.35)$$

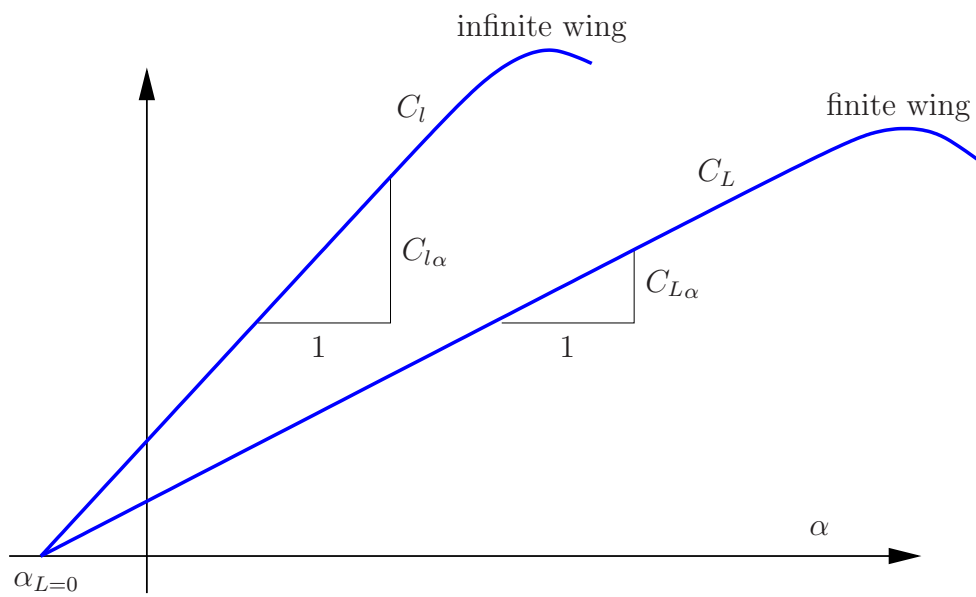
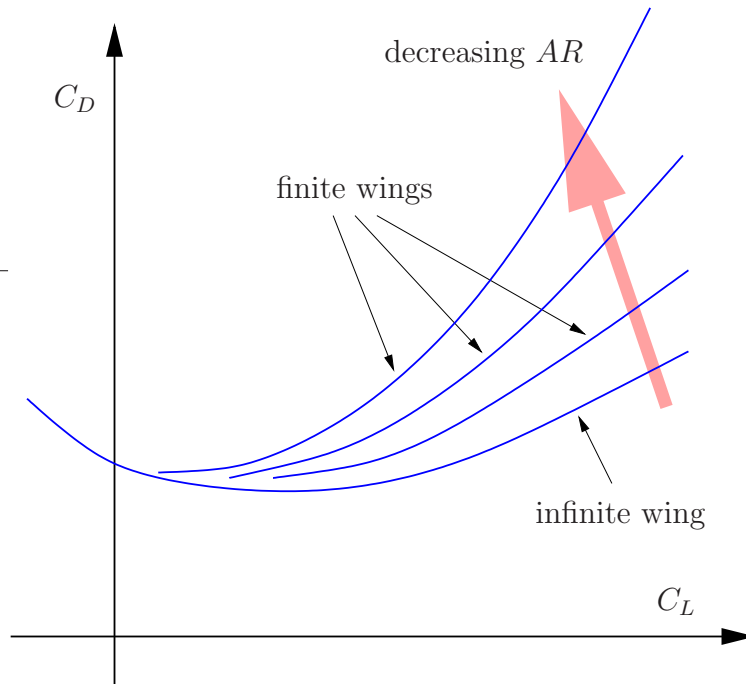
Rearranging (1.35) gives

$$C_L(\alpha) = C_{L\alpha} \cdot (\alpha - \alpha_{L=0}) \quad \text{with} \quad C_{L\alpha} = \frac{C_{l_\alpha}}{1 + \frac{C_{l_\alpha}}{\pi e AR}}. \quad (1.36)$$

For $\alpha = \alpha_{L=0}$ no lift is generated, thus there are no wing tip vortices and consequently, $\alpha_{L=0}$ is identical for the finite wing and the airfoil (“infinite wing”). From (1.36) we understand that $C_{L\alpha} < C_{l_\alpha}$.

It follows that $C_L(\alpha) < C_l(\alpha)$, which is consistent with the original starting point of the reduced effective angle of attack.

Drag Polar and Lift Curve



Estimation of C_L and C_D for the Finite Wing

Given the lift curve and the drag polar of the NACA 2412 airfoil on pages 18 and 19 as well as the wing geometry properties $AR = 10$ and $e = 0.95$, estimate the lift and drag coefficients C_L and C_D of the corresponding finite wing for the angle of attack $\alpha = 4$ deg with $Re < 3 \cdot 10^4$.

Solution:

From the lift curve of the NACA 2412 airfoil we deduce

$$\alpha_{L=0} = -2 \text{ deg} \quad \text{and} \quad C_{l\alpha} = 0.1 \text{ deg}^{-1} .$$

From (1.36) we get

$$C_{L\alpha} = \frac{0.1 \text{ deg}^{-1}}{1 + \frac{0.1 \frac{180}{\pi}}{\pi \cdot 0.95 \cdot 10}} = 0.839 \text{ deg}^{-1}$$

and

$$C_L = 0.839 (4 - (-2)) = \underline{0.503} .$$

With (1.34)

$$C_l(\alpha_{\text{eff}}) = C_L(\alpha) = 0.503 .$$

Thus, we get from the drag polar of the NACA 2412 airfoil that

$$C_d(C_l = 0.503) = 0.0065 .$$

Finally, we use (1.32) to obtain

$$C_{D,i} = \frac{0.503^2}{\pi \cdot 0.95 \cdot 10} = 0.00849$$

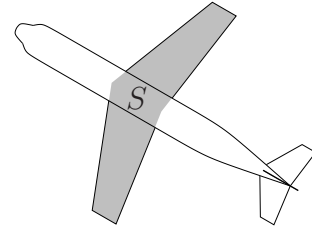
$$C_D = 0.0065 + 0.00849 = \underline{0.0150} .$$

Note that even for this moderate angle of attack the induced drag coefficient $C_{D,i}$ is larger than the profile drag coefficient C_d .

1.11 Aircraft Aerodynamics

Preliminaries

The entire aeroplane consists of the wings, the tail, the fuselage and possibly other components such as engine nacelles, stores, weapons.



We introduce the *wing reference area* S as illustrated.

The coefficients C_L and C_D for the total aeroplane must not be confused with those for the wing. Let L and D denote the lift and drag forces acting on the entire aeroplane, then

$$C_L = \frac{L}{q_\infty S}, \quad C_D = \frac{D}{q_\infty S}. \quad (1.37)$$

Using (1.20), (1.37) and (1.37), we can solve for the freestream velocity to obtain

$$v_\infty = \sqrt{\frac{2L}{\rho S C_L}}. \quad (1.38)$$

The slowest speed an aeroplane can fly in straight, level, unaccelerated flight is called the *stall speed* v_{stall} . In straight, level flight, we have $L = W$, where W is the weight of the aeroplane. The minimum of v_∞ is achieved with maximum C_L . Therefore,

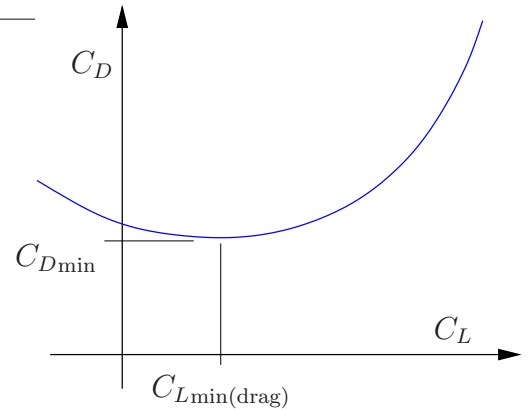
$$v_{\text{stall}} = \sqrt{\frac{2W}{\rho S C_{L\text{max}}}}. \quad (1.39)$$

Aircraft Drag Polar

The drag polar of an aeroplane can be obtained from wind-tunnel experiments or flight tests. It can generally be approximated quite accurately by a quadratic parabola. Therefore, there exists a factor \tilde{e} , such that the drag polar for an aircraft can be represented as

$$C_D = C_{D\min} + \frac{(C_L - C_{L\min(\text{drag})})^2}{\pi \tilde{e} AR}. \quad (1.40)$$

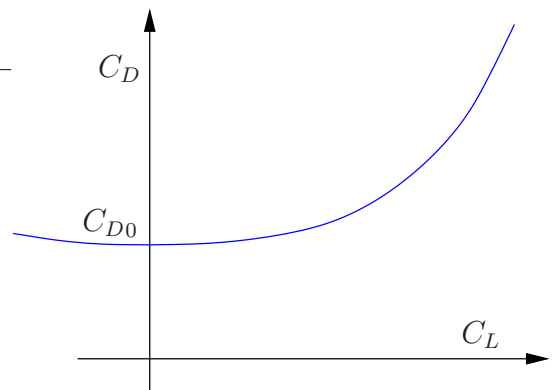
Equation (1.40) accounts for the fact that the minimum drag $C_{D\min}$ of a well designed aeroplane is associated with a small positive lift $C_{L\min(\text{drag})} > 0$; *i. e.* zero lift is usually associated with a nose-down orientation of the aircraft, which does not render minimum drag.



A convenient approximation of the aircraft drag polar (1.40), sufficiently accurate for most calculations, is given by

$$C_D = C_{D0} + \frac{C_L^2}{\pi e AR}, \quad (1.41)$$

where e denotes the *Oswald efficiency factor* and must not be confused with the span efficiency factor. Always $e \leq 1$ and for many aircraft, $e \approx 0.8$.



In Equation (1.41), the constant C_{D0} is called *zero lift drag coefficient* or *parasite drag* and includes zero lift pressure drag, skin friction and *interference drag*. Interference drag is generated when more than one body (*e.g.* stores on a wing) are placed in the same flow field. The coefficient C_{D0} is a very important aerodynamic characteristic of an aeroplane (see diagram on page 36).

The second term in (1.41) represents the drag due to lift. Thus, it includes the induced drag on all lifting surfaces (mainly wings and horizontal tail) and the increment of the pressure drag when lift is generated. It is denoted as *aircraft induced drag* $C_{D,i}$, but must not be confused with the “pure” induced drag of the wing in Equation (1.31)

$$C_{D,i} = \frac{C_L^2}{\pi e AR} . \quad (1.42)$$

Total Aircraft Drag Force

We are now in a position to express the total drag force acting on an aeroplane in straight level unaccelerated flight as a function of the freestream velocity v_∞ . Using (1.37) and (1.41), we can deduce

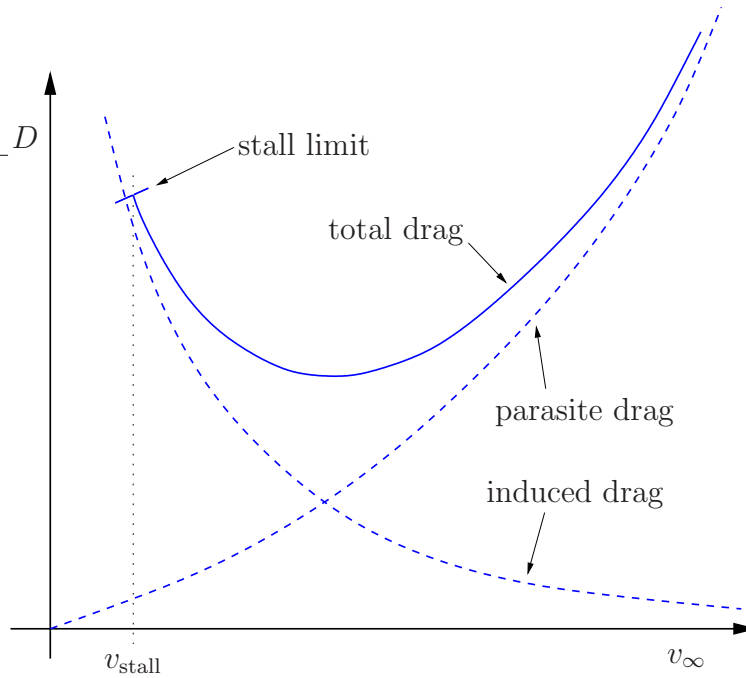
$$D = C_D q_\infty S = \left(C_{D0} + \frac{C_L^2}{\pi e AR} \right) q_\infty S = C_{D0} S q_\infty + \frac{L^2}{\pi e AR S q_\infty}. \quad (1.43)$$

With (1.20) and $L = W$ from straight level unaccelerated flight, it follows that

$$D = \underbrace{\left(\frac{1}{2} C_{D0} \rho S \right) v_\infty^2}_{\text{parasite drag}} + \underbrace{\left(\frac{2W^2}{\pi e AR \rho S} \right) \frac{1}{v_\infty^2}}_{\text{induced drag}}. \quad (1.44)$$

Equation (1.44) describes how changes in altitude (ρ), load (W) and configuration (C_{D0} , S , e , AR) affect an aircraft's total drag.

Note that different points on the D - v_∞ diagram are associated with different angles of attack. As v_∞ increases, α decreases.



At the drag minimum we have

$$\frac{dD}{dv_\infty} = C_{D0} \rho S v_\infty - \frac{4W^2}{\pi e AR \rho S} \frac{1}{v_\infty^3} = 0. \quad (1.45)$$

Solving for C_{D0} and eliminating v_∞ with (1.20), (1.37) and $L = W$ gives

$$C_{D0} = \frac{4W^2}{\pi e AR (\rho S)^2} \frac{1}{v_\infty^4} = \frac{W^2}{\pi e AR S^2} \frac{1}{q_\infty^2} = \frac{C_L^2}{\pi e AR}. \quad (1.46)$$

Recalling (1.42) it follows that in the drag minimum the induced drag is equal to the parasite drag

$$D \Rightarrow MIN \quad \rightarrow \quad C_{D0} = C_{D,i}. \quad (1.47)$$

With $L = W$ we may write for straight, level and unaccelerated flight

$$D = W \frac{D}{L} = W \frac{C_D}{C_L} = \frac{W}{C_L/C_D}. \quad (1.48)$$

Thus, the drag is inverse proportional to the lift over drag ratio. Consequently, the minimum of drag must coincide with the maximum of C_L/C_D , which explains the fundamental importance of $(C_L/C_D)_{\max}$ (see diagram on page 36). To verify this, we express the ratio C_L/C_D as a function of C_L , *i. e.*

$$\frac{C_L}{C_D} = \frac{C_L}{C_{D0} + \frac{C_L^2}{\pi e AR}}, \quad (1.49)$$

and equate the derivative with zero to obtain

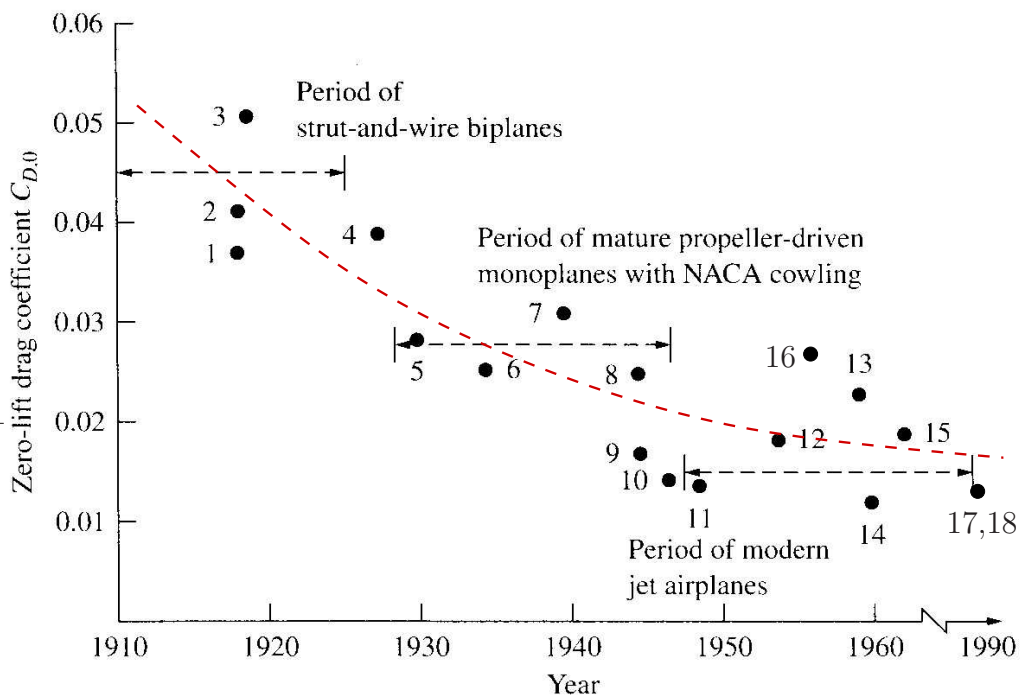
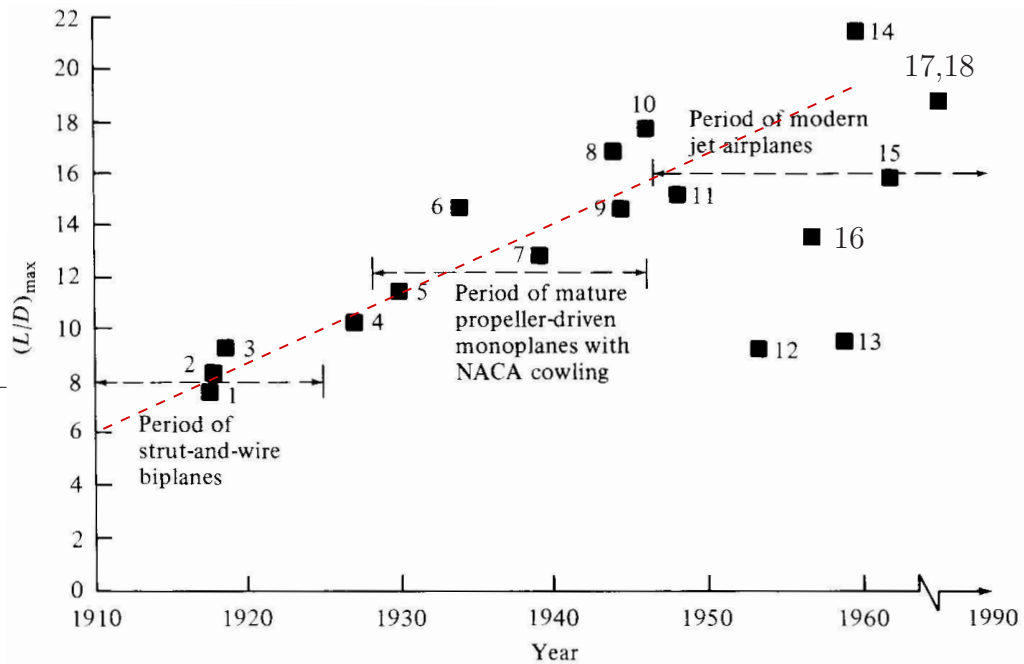
$$\frac{d(C_L/C_D)}{dC_L} = \frac{1}{C_{D0} + \frac{C_L^2}{\pi e AR}} - \frac{C_L \frac{2C_L}{\pi e AR}}{\left(C_{D0} + \frac{C_L^2}{\pi e AR}\right)^2} = 0, \quad (1.50)$$

which can be simplified to give the same result as (1.47), *i. e.*

$$L/D \Rightarrow MAX \quad \rightarrow \quad C_{D0} = C_{D,i}. \quad (1.51)$$

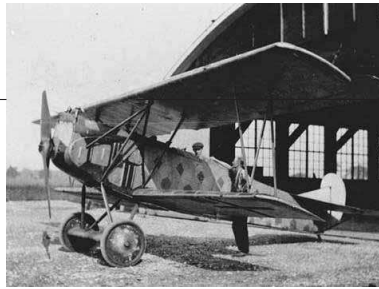
Thus, when the total drag of an aircraft is minimal, the parasite and the induced drag are equal and the lift over drag ratio is maximal.

Historical Developments





(1) SPAD XIII



(2) Fokker D-VII



(3) Curtiss JN-4



(4) Spirit of St. Louis



(5) Lockheed Vega



(6) Douglas DC-3



(7) Boeing B-17



(8) Boeing B-29



(9) Mustang P-51



(10) Lockheed P-80



(11) North American F-86

(12) Lockheed F-104
Starfighter(13) McDonnell F-4
Phantom II

(14) Boeing B-52

(15) General Dynamics
F-111

(16) Cessna 172 Skyhawk



(17) Boeing B-747



(18) Airbus A-380

1.12 Remarks on Trans-/Supersonic Flight

Airfoil Critical Mach Number and Wave Drag

Consider the two dimensional flow around an airfoil. The *critical Mach number* Ma_{cr} is defined as the smallest Mach number Ma_{∞} , for which there is at least one point of the flow field where the local Mach number is $Ma = 1$. Due to the larger velocity differences in the flow field, the critical Mach number is larger for thick than for thin airfoils.

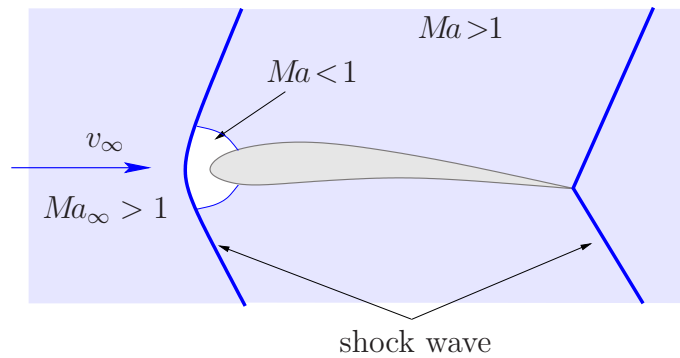
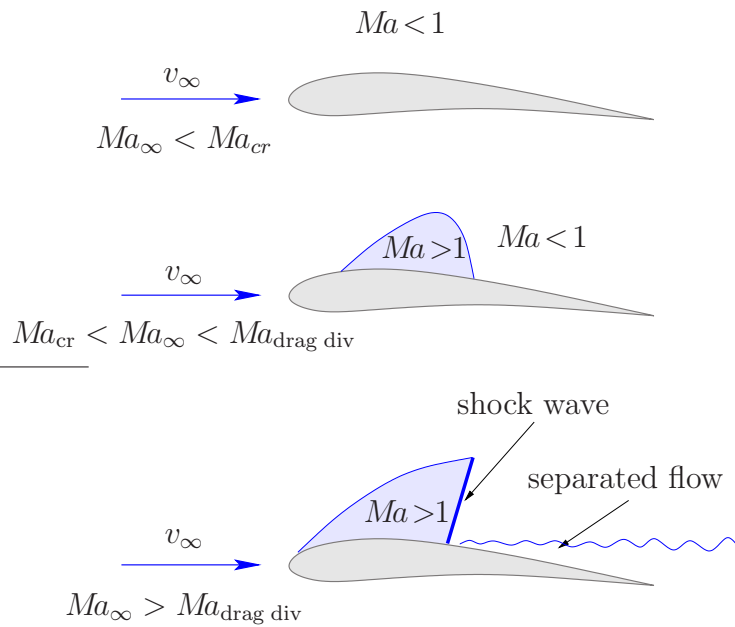
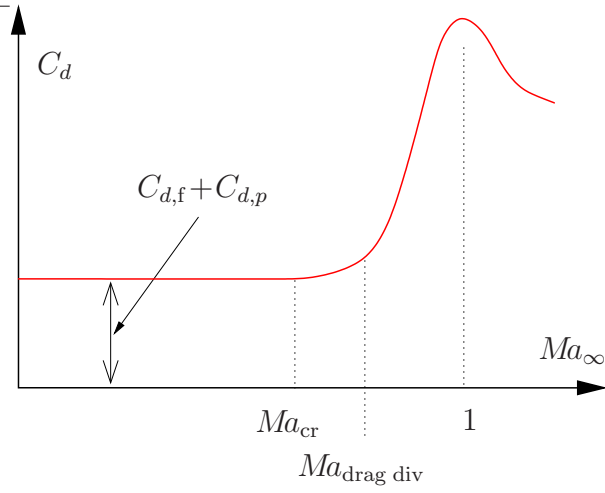
The *drag divergence Mach number* $Ma_{drag\ div}$ of an airfoil is the smallest Mach number Ma_{∞} , for which a shock wave is generated in the flow field. The sudden increase of the drag as Ma_{∞} is increased beyond $Ma_{drag\ div}$ is denoted as the *wave drag*. This is partly due to the dissipative nature of the shock wave itself and partly due to a significant increase of separation drag caused by the pressure discontinuity along the shock wave. The shock wave pattern changes as the velocity is increased even further. Shock waves also significantly affect the generation of lift.

Note that generally $Ma_{cr} < Ma_{drag\ div} < 1$. (1.52)

For $Ma_{\infty} > Ma_{drag\ div}$, the drag coefficient for an airfoil becomes

$$C_d = C_{d,f} + C_{d,p} + C_{d,wave} . \quad (1.53)$$

For the entire aeroplane, the effect of wave drag may be included in (1.41). Thus, the discussions in the next chapters do not generally require to distinguish subsonic or supersonic flight.

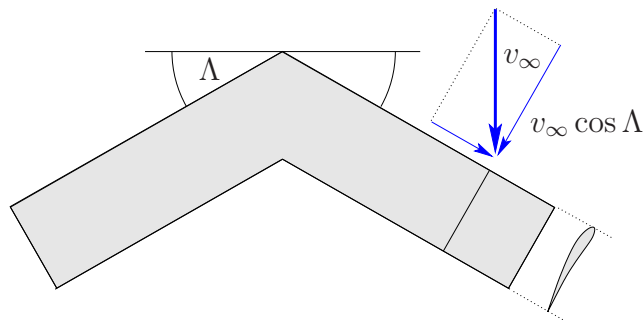


Sweep Angle

By sweeping the wings of a subsonic aircraft, the Mach numbers Ma_{cr} and $Ma_{drag\ div}$ are increased, *i. e.* the onset of wave drag is delayed to higher velocities.

We typically obtain

$$Ma_{cr}^{airfoil} < Ma_{cr}^{swept\ wing} < \frac{Ma_{cr}^{airfoil}}{\cos \Lambda} . \quad (1.54)$$

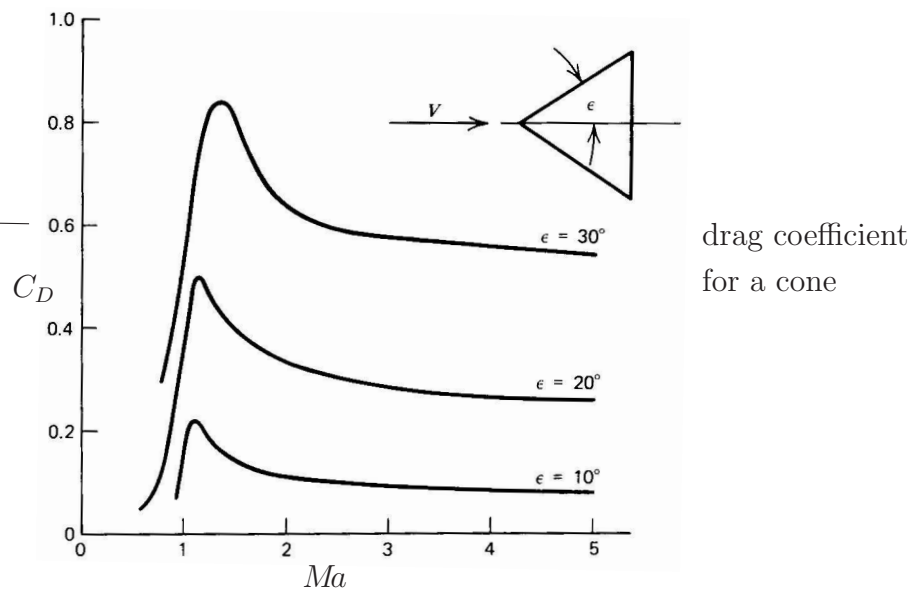
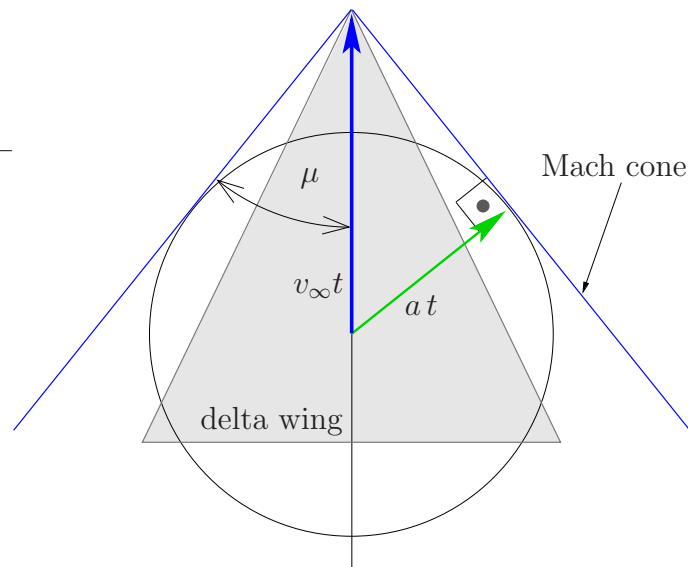


However, note that sweeping the wing adversely affects the generation of lift. Due to the different aerodynamic loading, wing sweep also requires stiffer and stronger wing structures.

A reliable investigation of the behaviour of swept wings needs to be based on wind tunnel experiments or on sophisticated computer analysis.

Extreme Sweep and Delta Wings for Supersonic Speeds

In supersonic flight, the wave drag is reduced significantly if the sweep angle Λ is chosen smaller than the *Mach cone* angle μ . The velocity component normal to the leading edge is then subsonic. This tends to reduce the intensity and the complexity of the shock wave pattern for the aircraft.

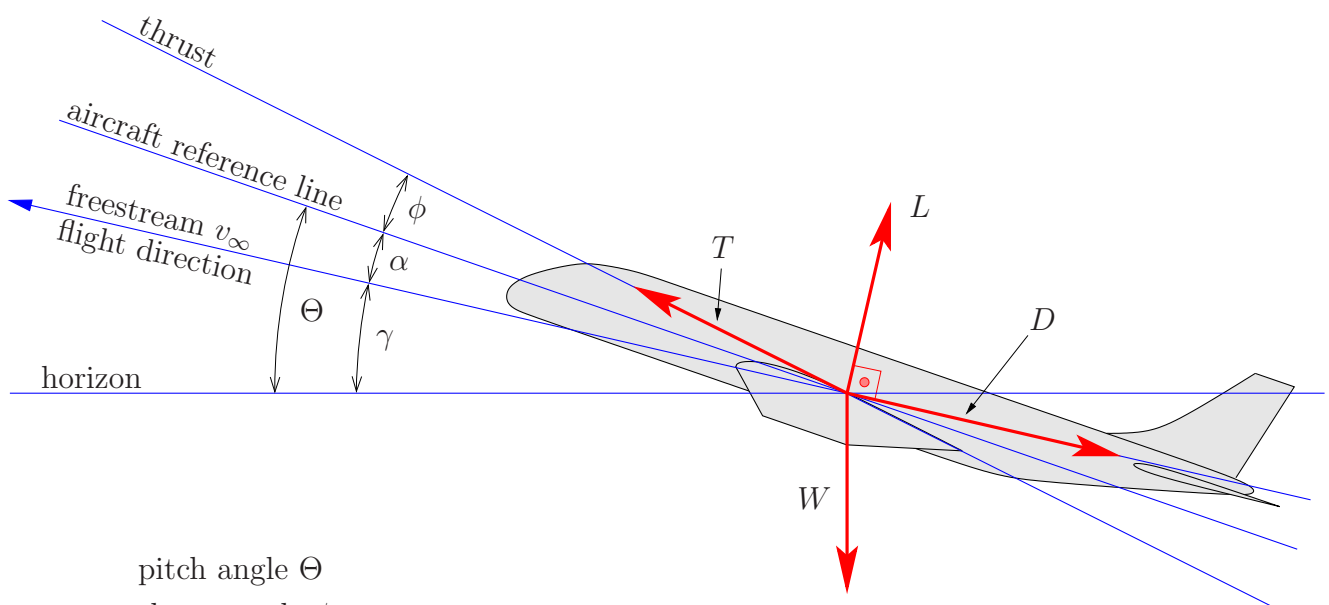


Chapter 2

Aircraft Performance

2.1 Preliminaries

Some Geometry and Terminology



- pitch angle Θ
- thrust angle ϕ
- angle of attack α
- flight path angle γ
- engine thrust T

Basic Equations of Motion

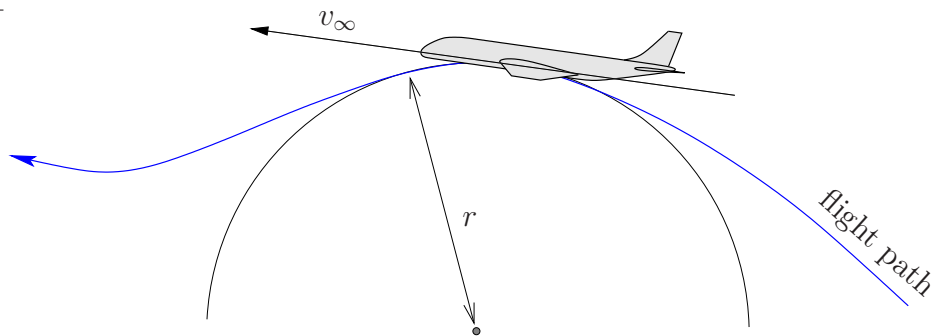
For simplicity, we regard the aircraft as a point mass m with two degrees of freedom (horizontal and vertical translation).

Using Newton’s second law “*force = mass \times acceleration*” and performing the summation of the forces parallel and perpendicular to the flight path, we obtain

$$m \frac{dv_\infty}{dt} = T \cos(\alpha + \phi) - D - W \sin \gamma \quad (2.1)$$

$$m \frac{v_\infty^2}{r} = -T \sin(\alpha + \phi) - L + W \cos \gamma, \quad (2.2)$$

where $\frac{dv_\infty}{dt}$ is the acceleration of the aircraft in flight direction and $\frac{v_\infty^2}{r}$ is the acceleration due to the local curvature of the flight path (centripetal acceleration).



Load Factor

We introduce the *load factor* n as the ratio of lift force over aeroplane weight, *i. e.*

$$n = \frac{L}{W} . \quad (2.3)$$

We will see that in different flight manoeuvres the load factor takes different values.

At this stage, it is convenient to rewrite the expression (1.44) such that it holds, at least approximately, for all flight manoeuvres. To this end, we use (2.3) in (1.43). With (1.20), *i. e.* $q_\infty = \frac{1}{2} \rho v_\infty^2$, we then obtain

$$D = \left(\frac{1}{2} C_{D0} \rho S \right) v_\infty^2 + \left(\frac{2(nW)^2}{\pi e AR \rho S} \right) \frac{1}{v_\infty^2} . \quad (2.4)$$

We may also express the velocity v_∞ in terms of nW rather than L . The expression (1.38) may then be rewritten as

$$v_\infty = \sqrt{\frac{2nW}{\rho S C_L}} . \quad (2.5)$$

2.2 Brief Introduction to Aeroplane Propulsion

Before we enter into the detailed discussion of aircraft performance, we ought to have a basic understanding of aircraft propulsion systems. Clearly, we can expect the qualitative and quantitative properties of the aircraft engines to have substantial impact on the overall performance of the aeroplane. However, the detailed discussion of aircraft engines is beyond the scope of this course.

The most commonly known types of propulsion systems include

- propeller with piston engine,
- turbojet engine,
- turbofan engine,
- turboprop engine,
- ramjet,
- rocket engine.

On the following pages we present some basic information on the piston propeller and the gas turbine engines. The ramjet may be seen as a primitive turbojet engine without any rotating components. The incoming air is compressed solely by the high freestream velocity. Therefore, ramjets only work at very large speeds and are rather impractical. Rocket engines were initially mounted on high speed aeroplanes, but were quickly replaced by the more efficient jet engines.

Propeller with Piston Engine

Until about 1940, the piston engine represented the only practical means of aeroplane propulsion. It was sufficiently powerful and, at the same time, light enough to be mounted on an aeroplane. It was continuously further developed, such that several engine types are now available. The main differences include the different types of cooling systems and different piston arrangements. However, as shown in the diagram, the *specific fuel consumption SFC* is very similar for most engines. It decreases slightly with the engine power. *SFC* denotes the weight (or mass!) of fuel burnt per time unit to generate a certain amount of power. For piston engines, *SFC* is nearly independent of the throttle setting, *i. e.*

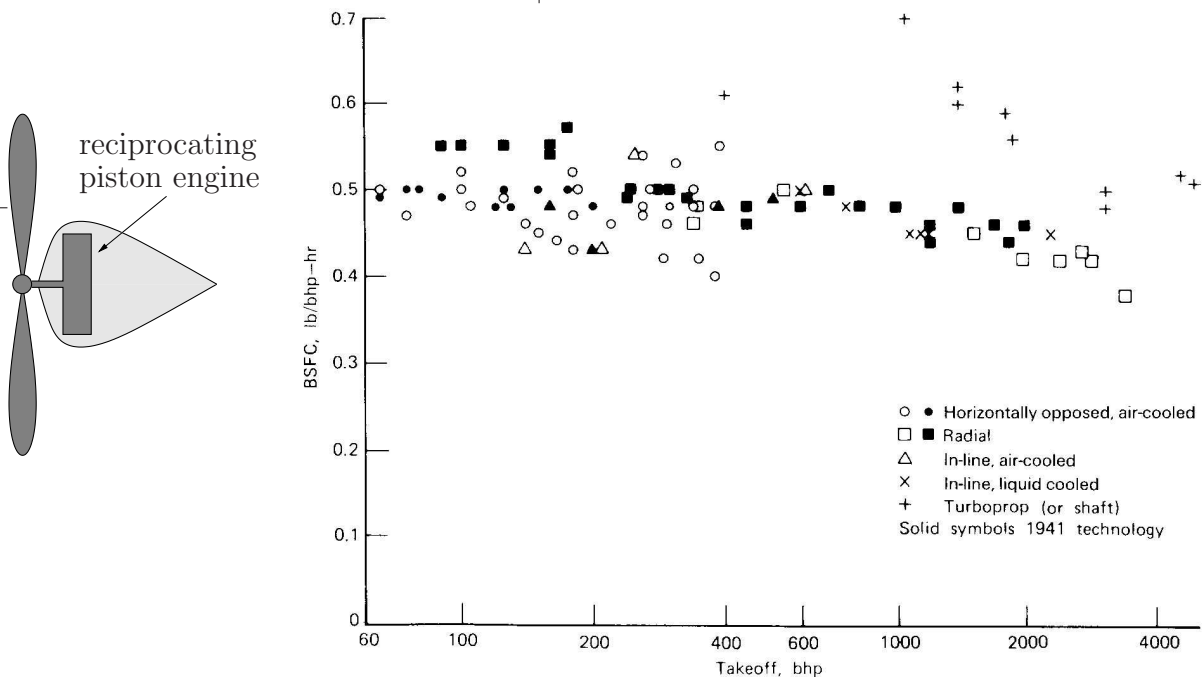
$$SFC = \frac{-dW_{\text{fuel}}/dt}{P} = \text{const.} \quad (2.6)$$

In English units *SFC* (also known as *brake specific fuel consumption BSFC*) is measured in [lb/(bhp h)]. In the SI system, we typically use [N/(kW h)]. With $g = 9.81 \text{ m s}^{-2}$, we have

$$1 \frac{\text{lb}}{\text{bhp h}} \cdot g = \frac{0.453592 \cdot 9.81}{0.7457} \frac{\text{N}}{\text{kW h}} = 5.97 \frac{\text{N}}{\text{kW h}}. \quad (2.7)$$

A valid guess for any piston engine is $SFC = 0.5 \text{ lb (bhp h)}^{-1}$, which corresponds to approximately

$$SFC = 3 \frac{\text{N}}{\text{kW h}}. \quad (2.8)$$



Mounted to the shaft of the piston engine is the propeller, which consists of a number of blades. These blades have airfoil-like sections and are generally *pitched* significantly. The pitch angle β denotes the angle between the section chord line and the plane of rotation. The pitch of modern propellers changes with the radius. Many propellers have *variable pitch* (pilot-controlled pitch), as opposed to *fixed pitch*.

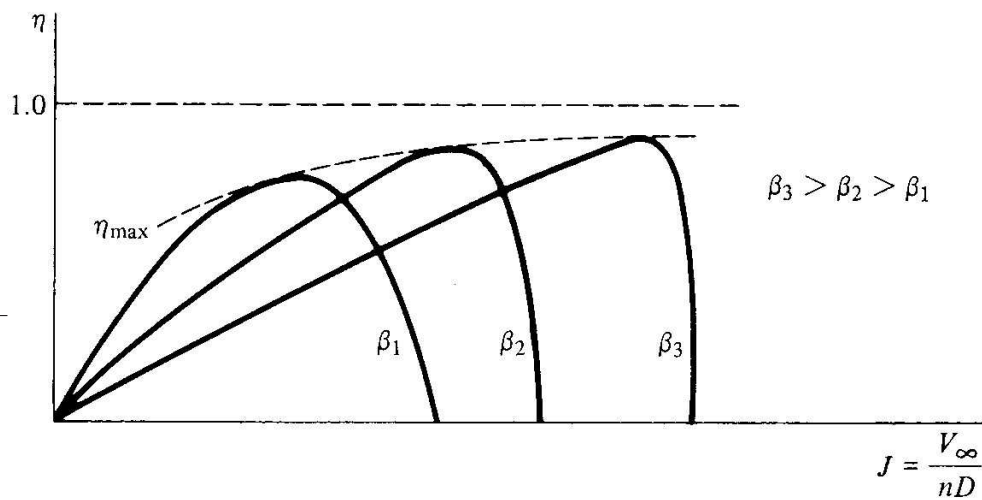
The airflow around the propeller blades is extremely complicated, since it involves induced flow velocities (similar to the finite wing) as well as rotational flow and substantial interference phenomena. It is therefore evident that the engine power P can not be transformed into propulsive power available P_A without loss. We may write

$$P_A = \eta P, \quad (2.9)$$

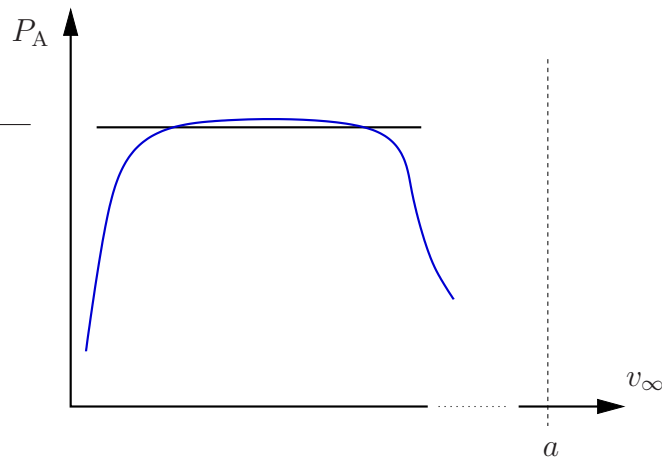
where η is the propeller efficiency factor. It can be shown with experiments that η depends on the propeller geometry (parameter β for propellers with variable pitch) and on the so-called dimensionless *advance ratio* J , which is defined as

$$J = \frac{v_\infty}{nD}, \quad (2.10)$$

where n is the number of rotations per time unit and D is the propeller diameter. The advance ratio corresponds to the ratio of the velocity with which the propeller advances through the air over the tangential velocity of the blade tips in the plane of rotation. The diagram below shows the typical efficiency for a propeller with variable pitch.



For the discussion of airplane performance we need the dependency of power available P_A on the velocity v_∞ . Assuming variable pitch which is always adjusted to the aeroplane speed v_∞ , we obtain the qualitative diagram displayed below. For rough estimates of the airplane performance, we may approximate the power available diagram by the straight line $P_A = \text{const.}$ as shown. Note the drop of P_A as the Mach number $Ma_\infty = v_\infty/a$ leaves the incompressibility range.



For piston propellers, the dependency of power available on altitude is approximated fairly well by assuming that P_A is proportional to the air density, *i. e.*

$$P_{A,\text{alt}} = \frac{\rho_{\text{alt}}}{\rho_{\text{sea}}} P_{A,\text{sea}} , \quad (2.11)$$

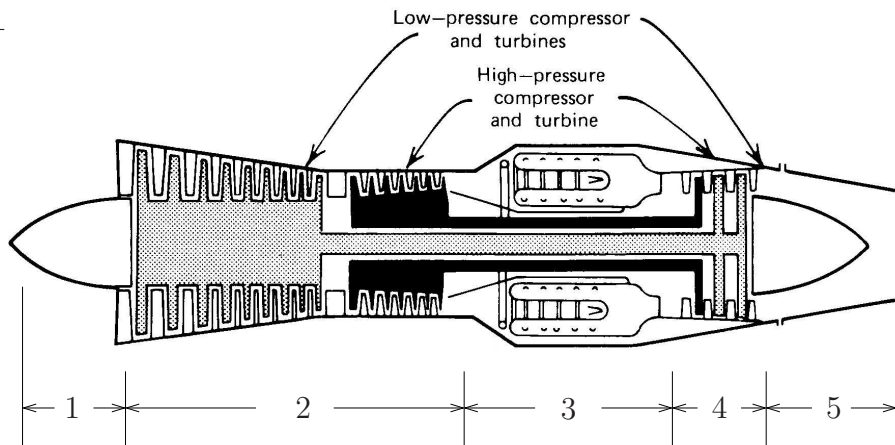
where the subscripts “sea” and “alt” denote quantities at sea level and at some higher altitude, respectively. We conclude from $\rho_{\text{alt}}/\rho_{\text{sea}} < 1$ that power available decreases as the altitude is increased.

Gas Turbine Engines

In 1903, the first gas turbine was constructed that was able to produce more power than needed to run its own components. However, the first substantial working gas turbine engine was constructed as late as 1937 and the first aeroplane with a turbojet engine flew in 1939. The first operational jet fighter began service in 1942. The first jet propelled passenger flight took place in 1952 and may be seen as the beginning of mass travelling. Today most commercial and military aeroplanes employ gas turbine engines.

We distinguish the turbojet, the turbofan and the turboprop engines. The most characteristic feature of a gas turbine is the continuous nature of the thermodynamic processes in the gas turbine as opposed to the reciprocating engine.

turbojet engine: The three basic components of the turbojet engine are the compressor, the burner and the gas turbine.



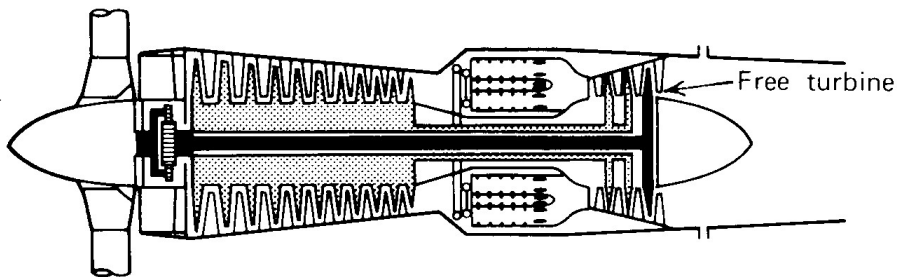
- 1 inlet diffuser
- 2 compressor
- 3 burner
- 4 turbine
- 5 exhaust nozzle

The compressor consists of a combination of rotating and stationary blades. In the burner, the fuel is injected into the compressed air and the mixture is burnt, whereby heat is generated and the volume of the gas mixture expands significantly. Typically the ratio of air to fuel by weight is about 60/1. However, only approximately 25% of

the air is used to support combustion. The remainder bypasses the fuel nozzles and mixes downstream of the burner to cool the hot gases before they enter the turbine. The mixed air, still very hot (about 1100°C), passes through the turbine, which is composed of rotating and stationary blades. The turbine extracts energy from the moving gases, which is used to drive the compressor. In fact, nearly 75% of the combustion energy is required by the compressor. The remaining 25% represent the kinetic energy of the exhaust, which provides the thrust. The number of rotations per minute of the turbine wheel is generally in the order of 10,000 rpm. Turbojet engines can be designed to work at speeds far beyond the sound barrier.

A turbojet engine may be equipped with an afterburner, which relies on injecting fuel into the extended exhaust nozzle (afterburner duct). Since only 25% or so of the air is used to support combustion in the burner, there is sufficient oxygen in the turbine exhaust mixture to support additional burning. The additional heat further expands the exhaust and thereby increases the exhaust velocity. Afterburning can more than double the thrust of a gas turbine engine, but at a proportionately greater increase in fuel consumption.

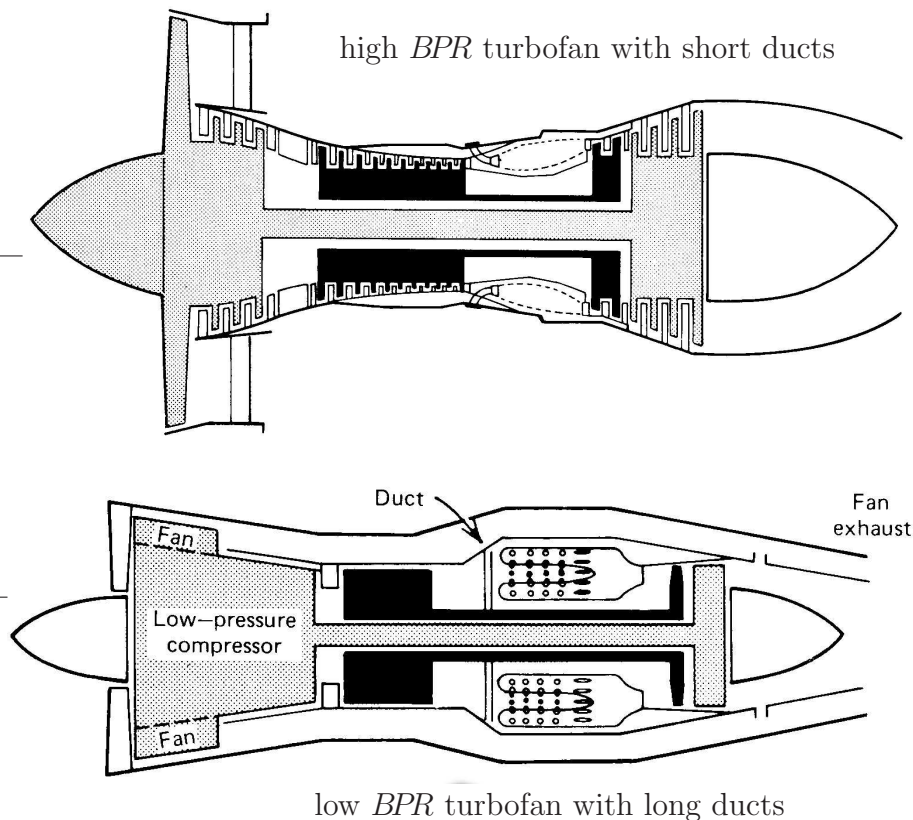
turboprop engine: This engine may be regarded as a turbojet engine, which is equipped with a modified gas turbine that extracts nearly all the energy from the moving gases, leaving only a small residual thrust. This turbine drives not only the compressor, but also provides the shaft power for the propeller. Alternatively the compressor and the propeller may be driven by two sequential gas turbines as shown below.



Due to the fact that turboprops basically represent propellers powered by a gas engine, their use is limited to speeds far below the sound barrier. However, the development of high speed turboprops is ongoing and they are already being employed for Mach numbers much larger than the incompressibility limit of $Ma_{\infty} = 0.3$.

Like turbojets, turboprops may be equipped with afterburners. Note that turboshaft engines, which work similarly to turboprops, are commonly used to drive the rotors of modern helicopters.

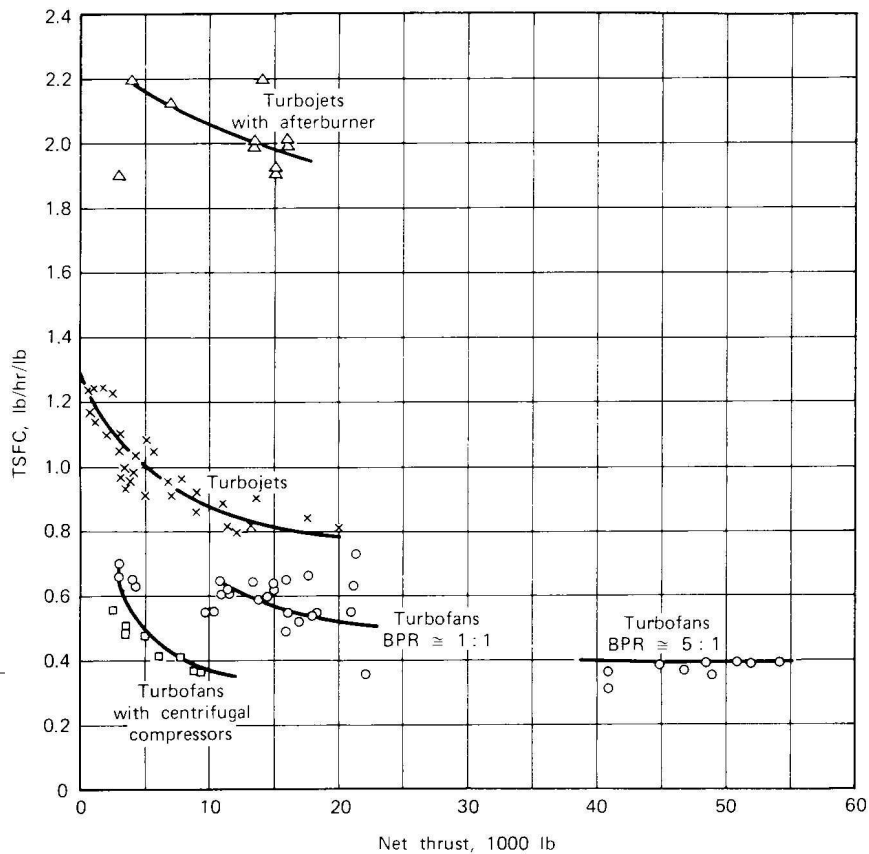
turbofan engine: The turbofan engine may be regarded as a compromise between the turbojet engine and the turboprop. The turbines drive the compressor and a fan, but they do not absorb as much energy as in the turboprop, such that the exhaust jet provides a major part of the thrust. The fan may be regarded as a propeller with a large number of blades rotating inside a duct, which suppresses radial airflow. Such a fan is capable of providing thrust at velocities in the whole range of subsonic speeds. The ratio by weight of the air that passes through the fan (secondary flow) to the air that passes through the gas engine (primary flow) is called the *bypass ratio BPR*. Early turbofan engines had bypass ratios of around 1/1; the latest engines have ratios of up to 10/1. Turbofan engines are generally quieter and much lighter and consume less fuel than turbojets. Since the 1970ies, most commercial aircraft have been equipped with large *BPR* turbofans, allowing for fuel efficient subsonic flight with most of the thrust being provided by the fan, whereas a typical configuration for military aircraft is the low *BPR* turbofan with afterburners.



For turbojets and turbofans the fuel consumption is expressed in terms of *thrust specific fuel consumption* $TSFC$. This expression denotes the weight of fuel burnt per time unit to generate a certain amount of constant thrust. In English units, $TSFC$ is typically given in terms of mass rather than forces, *i. e.* [lb/(h lb)], whereas in SI units we have [N/(h N)]. However, due to mass (or force) cancelling out of the expression, the dimension of $TSFC$ is always 1/time, and there is no need for unit conversion. Independently of the throttle setting, the fuel burnt per unit of time and thrust is nearly constant for turbojets and may be approximated as constant for turbofans, *i. e.*

$$TSFC = \frac{-dW_{fuel}/dt}{T} = const. \tag{2.12}$$

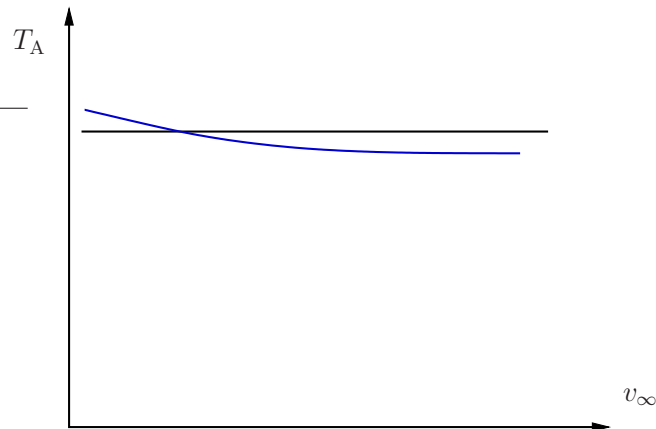
The diagram below shows some representative values for $TSFC$. We note that $TSFC$ is lower for very strong engines than it is for smaller ones.



For the study of airplane performance, we need to know the dependency of thrust available T_A on the flight velocity (v_∞) and on the altitude (ρ). At constant altitude, the thrust available of turbojets and turbofans typically decreases slightly as the velocity increases. Depending on the air pressure, this decrease may amount to 30% or so. For rough estimates and for the qualitative understanding of the flight mechanics of a specific aeroplane, it is sufficiently accurate to approximate the thrust available by $T_A = \text{const.}$ at a given altitude. As the altitude is changed, T_A is proportional to the change of the air density, *i. e.*

$$T_{A,\text{alt}} = \frac{\rho_{\text{alt}}}{\rho_{\text{sea}}} T_{A,\text{sea}} , \quad (2.13)$$

where the subscripts “sea” and “alt” denote quantities at sea level and at some higher altitude, respectively. We conclude from $\rho_{\text{alt}}/\rho_{\text{sea}} < 1$ that thrust available decreases as the altitude is increased.



2.3 Straight, Level and Unaccelerated Flight

Thrust Required

We will see that the study of the simplest of flight situations, *i. e.* straight, level and unaccelerated flight, often abbreviated by “SLUF”, allows to draw a variety of conclusions about the performance of the specific aeroplane under consideration.

By definition, we have
$$\frac{d v_{\infty}}{d t} = \frac{v_{\infty}^2}{r} = 0, \quad \text{and} \quad \gamma = 0 . \quad (2.14)$$

Furthermore, we assume that $\phi + \alpha$ is small; thus

$$\sin(\phi + \alpha) \approx 0 \quad \text{and} \quad \cos(\phi + \alpha) \approx 1 . \quad (2.15)$$

Hence, (2.1) and (2.2) reduce to

$$T = D, \quad L = W . \quad (2.16)$$

We conclude that the lift required to sustain SLUF is equal to the weight of the aeroplane. With (2.3) it follows that the load factor is unity, *i. e.* $n = 1$. The thrust required to sustain SLUF is equal to the drag. Henceforth, we denote the *thrust required* as T_R .

With (2.16) and (1.48) it follows that
$$T_R = \frac{W}{C_L/C_D} . \quad (2.17)$$

The thrust required is proportional to the inverse of the lift over drag ratio. The minimum thrust required is associated with the maximum lift over drag ratio. Equation (2.17) demonstrates the fundamental importance of the aircraft drag polar, *i. e.* the ratio C_L/C_D , for the choice of the aircraft weight and the aircraft engine.

Recalling (2.4) with $n = 1$, we note that T_R depends on the aircraft weight (W), the aircraft configuration (C_{D0} , S , e , AR), the flight altitude (ρ) and the flight velocity (v_{∞}), *i. e.*

$$T_R = D = \underbrace{\left(\frac{1}{2} C_{D0} \rho S\right) v_{\infty}^2}_{\text{parasite drag}} + \underbrace{\left(\frac{2 W^2}{\pi e AR \rho S}\right) \frac{1}{v_{\infty}^2}}_{\text{induced drag}} . \quad (2.18)$$

Power Required and Power Available

Typically, thrust required and thrust available are compared in terms of power, “power = force \times velocity”, therefore,

$$P_R = T_R v_\infty \quad \text{and} \quad P_A = T_A v_\infty . \quad (2.19)$$

Note that the minimum of power required P_R does not coincide with the minimum of thrust required T_R . It can be shown that the velocity associated with the drag minimum $v_{\min T_R}$ can be constructed from the tangent through the origin as illustrated.

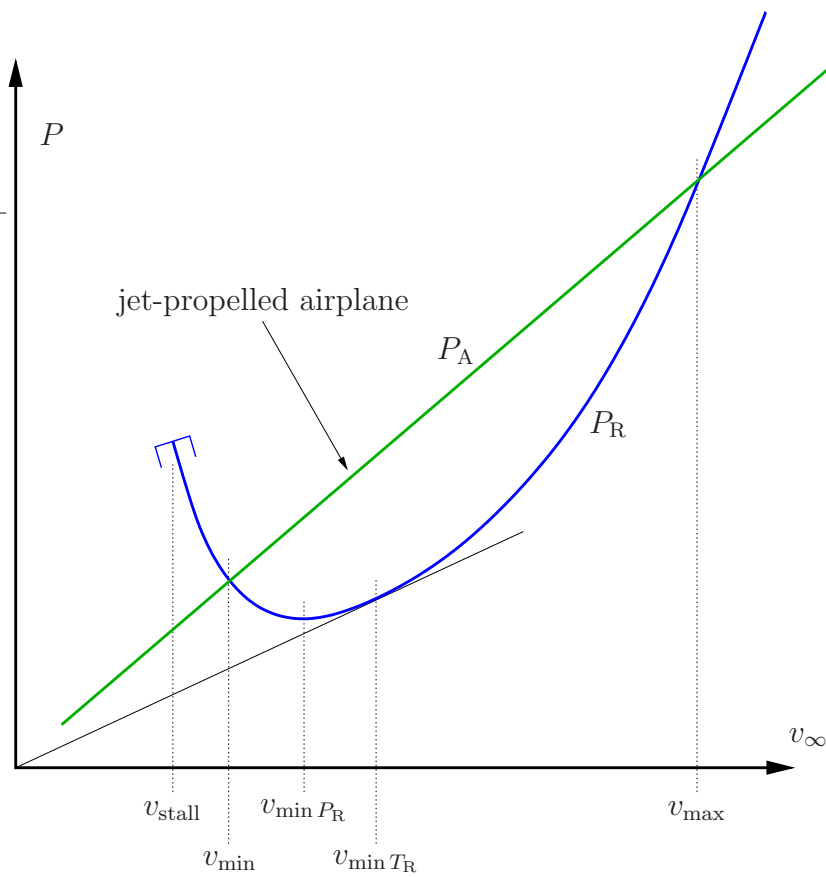
With $L = W$, (1.38) and (2.17) we get from (2.19) that

$$P_R = W \frac{C_D}{C_L} \sqrt{\frac{2W}{\rho S C_L}} = \sqrt{\frac{2W^3}{\rho S}} \frac{C_D}{C_L^{3/2}} , \quad (2.20)$$

It follows from (2.20) that the minimum power required is associated with the maximum of $C_L^{3/2}/C_D$.

Power required can straightforwardly be expressed as a function of velocity by combining (2.19) and (2.18), *i. e.*

$$P_R = \left(\frac{1}{2} C_{D0} \rho S \right) v_\infty^3 + \left(\frac{2W^2}{\pi e AR \rho S} \right) \frac{1}{v_\infty} . \quad (2.21)$$



Note that flight at different velocities v_∞ with $v_{min} \leq v_\infty \leq v_{max}$ is associated with different angles of attack and different throttle settings. In order to reduce the flight velocity the pilot generally has to increase the angle of attack and adjust the throttle setting such that the power provided by the engine equals P_R .

Three Important Velocities

First we rearrange (1.42) to give $C_L = \sqrt{\pi e AR C_{D,i}}$. (2.22)

With $T_R = D$, we conclude from (1.47), (1.51) and (2.22) that, for the minimum of thrust required,

$$T_R \Rightarrow MIN \quad \rightarrow \quad \begin{cases} v_\infty = v_{\min T_R} \\ C_{D,i} = C_{D0} \\ \frac{C_L}{C_D} = (C_L/C_D)_{\max} \\ C_L = \sqrt{\pi e AR C_{D0}} . \end{cases} \quad (2.23)$$

Using (2.21), we can derive for the minimum of power required that

$$\frac{dP_R}{dv_\infty} = \frac{d(T_R v_\infty)}{dv_\infty} = \frac{3}{2} C_{D0} \rho S v_\infty^2 - \frac{2W^2}{\pi e AR \rho S} \frac{1}{v_\infty^2} = 0 . \quad (2.24)$$

It follows that

$$3 C_{D0} = \left(\frac{2L}{S \rho v_\infty^2} \right)^2 \frac{1}{\pi e AR} = \frac{C_L^2}{\pi e AR} = C_{D,i} . \quad (2.25)$$

Recalling (2.20) and (2.22) we may summarise

$$P_R \Rightarrow MIN \quad \rightarrow \quad \begin{cases} v_\infty = v_{\min P_R} \\ C_{D,i} = 3 C_{D0} \\ \frac{C_L^{3/2}}{C_D} = (C_L^{3/2}/C_D)_{\max} \\ C_L = \sqrt{3 \pi e AR C_{D0}} . \end{cases} \quad (2.26)$$

Furthermore, we introduce the velocity \hat{v}_∞ , which renders a maximum of $(C_L^{1/2}/C_D)$. It is convenient to introduce \hat{v}_∞ at this stage, even though we will not need it before the discussion of range and endurance in Section 2.7. With (1.41) the expression $(C_L^{1/2}/C_D)$ may be written as a function of C_L , *i. e.*

$$\frac{C_L^{1/2}}{C_D}(C_L) = \frac{\sqrt{C_L}}{C_{D0} + \frac{C_L^2}{\pi e AR}}. \quad (2.27)$$

At the maximum we have

$$\frac{d(C_L^{1/2}/C_D)}{dC_L} = \frac{1}{2\sqrt{C_L}(C_{D0} + C_{D,i})} - \frac{\sqrt{C_L}}{(C_{D0} + C_{D,i})^2} \frac{2C_L}{\pi e AR} = 0. \quad (2.28)$$

Resubstituting (1.42) into (2.28), we find $C_{D0} = 3 C_{D,i}$. (2.29)

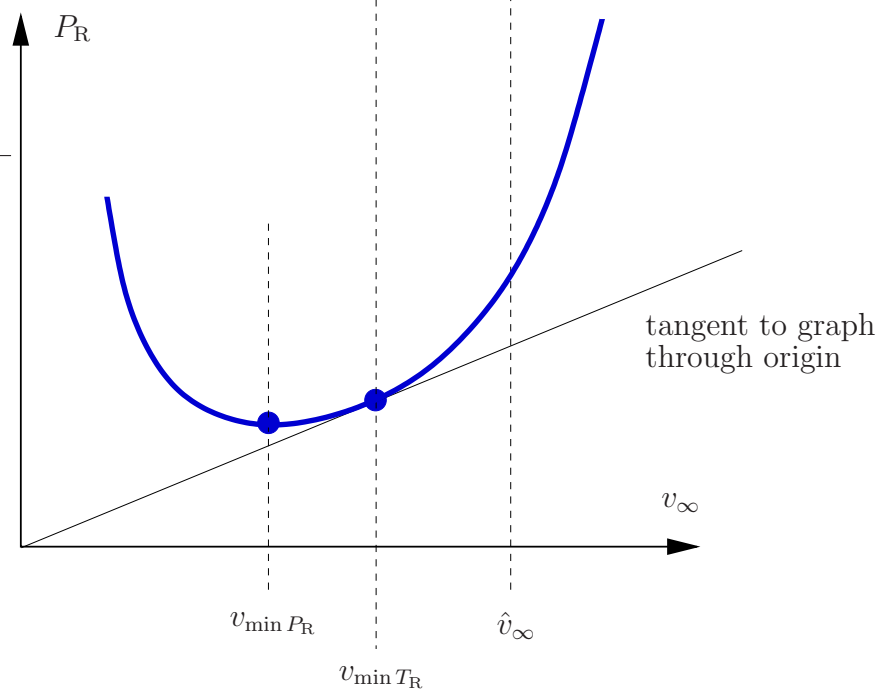
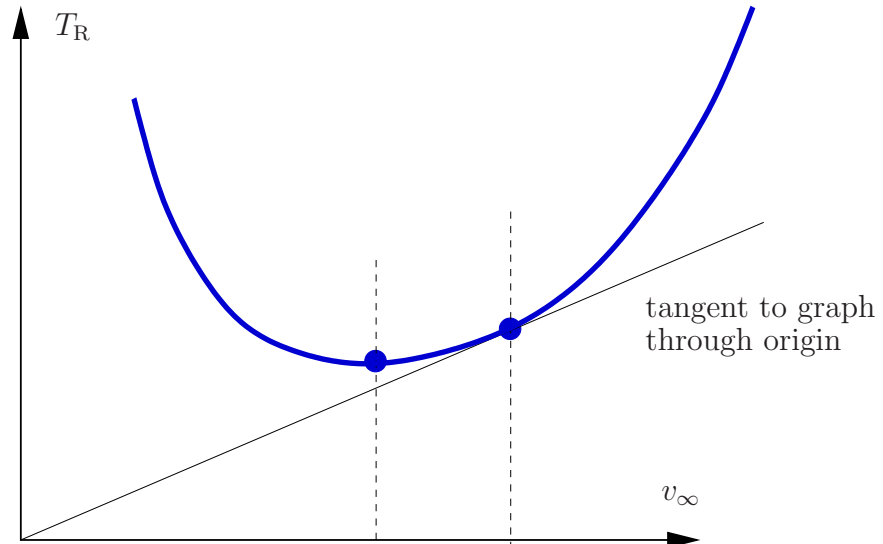
Thus, using (2.22), we can state that

$$\text{for flight at } v_\infty = \hat{v}_\infty \quad \rightarrow \quad \left\{ \begin{array}{l} C_{D,i} = \frac{1}{3} C_{D0} \\ \frac{C_L^{1/2}}{C_D} = (C_L^{1/2}/C_D)_{\max} \\ C_L = \sqrt{\frac{\pi}{3} e AR C_{D0}}. \end{array} \right. \quad (2.30)$$

The velocities $v_{\min T_R}$, $v_{\min P_R}$ and \hat{v}_∞ can then be found by using $n = \frac{L}{W} = 1$ and the expression for C_L given in (2.23)₄, (2.26)₄, (2.30)₃, respectively, in Equation (2.5).

We obtain $v_{\min P_R} < v_{\min T_R} < \hat{v}_\infty$. (2.31)

A graphical interpretation of the velocities is shown on the next page.



Effect of Altitude on Power Diagrams

Let the subscripts “sea” and “alt” denote quantities at sea level or at a higher altitude, respectively. With (1.38) we can then relate the flight velocities v_{alt} and v_{sea} as follows

$$v_{\text{alt}} = \sqrt{\frac{2W}{\rho_{\text{alt}} S C_L}} = \sqrt{\frac{\rho_{\text{sea}}}{\rho_{\text{alt}}}} \sqrt{\frac{2W}{\rho_{\text{sea}} S C_L}} = \sqrt{\frac{\rho_{\text{sea}}}{\rho_{\text{alt}}}} v_{\text{sea}} . \quad (2.32)$$

Similarly, equation (2.20) renders

$$P_{\text{R,alt}} = \sqrt{\frac{2W^3}{\rho_{\text{alt}} S} \frac{C_D}{C_L^{3/2}}} = \sqrt{\frac{\rho_{\text{sea}}}{\rho_{\text{alt}}}} \sqrt{\frac{2W^3}{\rho_{\text{sea}} S} \frac{C_D}{C_L^{3/2}}} = \sqrt{\frac{\rho_{\text{sea}}}{\rho_{\text{alt}}}} P_{\text{R,sea}} . \quad (2.33)$$

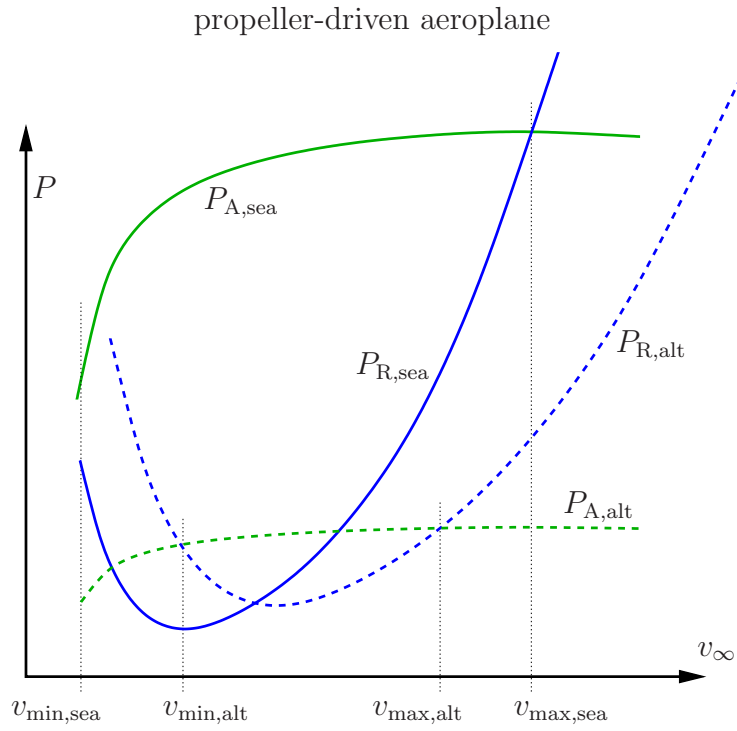
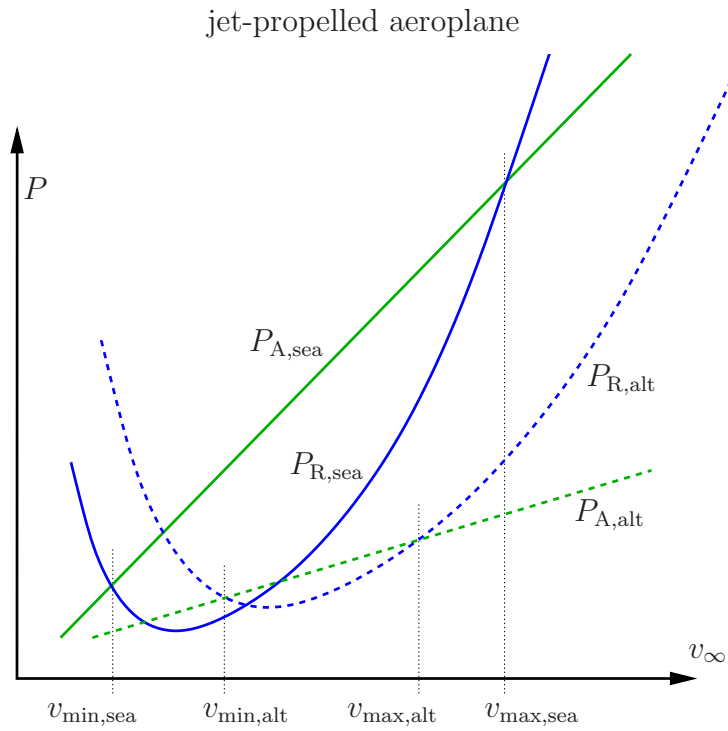
Thus, the graph for P_{R} at a certain altitude is obtained from the graph at sea level by scaling both axis with the factor $\sqrt{\rho_{\text{sea}}/\rho_{\text{alt}}} > 1$.

For power available of the propeller-driven aeroplane, we recall from (2.11) that

$$P_{\text{A,alt}} = \frac{\rho_{\text{alt}}}{\rho_{\text{sea}}} P_{\text{A,sea}} . \quad (2.34)$$

For the jet-propelled aeroplane a similar relation as given by (2.13) holds for thrust available. Combining (2.13) and (2.19) renders (2.34). Thus, power available at a specific altitude is generally obtained by scaling down power available at sea level with $\rho_{\text{alt}}/\rho_{\text{sea}} < 1$.

The qualitative diagrams on the next page illustrate that v_{max} changes significantly with altitude. The interval $[v_{\text{min}}, v_{\text{max}}]$ becomes smaller as the altitude increases. Note however, that a higher altitude means larger velocities $v_{\text{min } P_{\text{R}}}$ and $v_{\text{min } T_{\text{R}}}$.



2.4 Climbing Flight and Flight Envelope

We assume that $\phi + \alpha$ is small; thus $\sin(\phi + \alpha) \approx 0$ and $\cos(\phi + \alpha) \approx 1$. For straight, unaccelerated climbing flight, (2.1) and (2.2) then reduce to

$$T = D + W \sin \gamma, \quad L = W \cos \gamma. \quad (2.35)$$

From (2.35)₂, we obtain for the load factor

$$n = \frac{L}{W} = \cos \gamma \leq 1. \quad (2.36)$$

The *rate of climb ROC* is related to v_∞ by

$$ROC = v_{\text{climb}} = v_\infty \sin \gamma. \quad (2.37)$$

With (2.35), it follows that

$$ROC = v_\infty \frac{T - D}{W}. \quad (2.38)$$

We recall that $v_\infty D = v_\infty T_R = P_R$. By replacing $T v_\infty$ with power available P_A we obtain the maximum rate of climb for a specific velocity v_∞ and altitude, *i. e.*

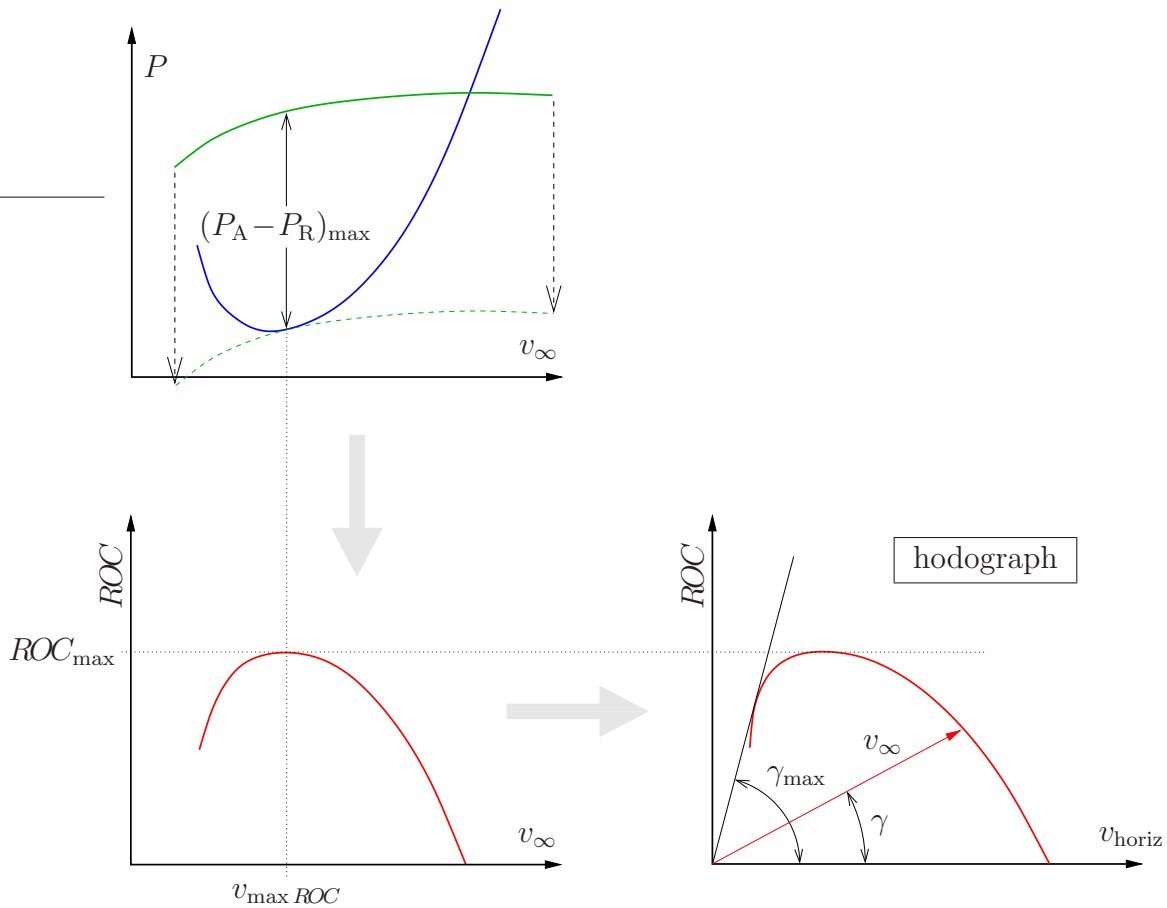
$$ROC = \frac{P_A - P_R}{W}. \quad (2.39)$$

The term $P_A - P_R$ is identified as the *excess power*. The maximum climb rate is calculated as

$$ROC_{\text{max}} = \frac{(P_A - P_R)_{\text{max}}}{W}. \quad (2.40)$$

Remark: It follows from (2.36) and (2.4) with $P_R = v_\infty T_R = v_\infty D$ that P_R depends on γ . With $ROC = v_\infty \sin \gamma$ and $P_R(v_\infty, \gamma)$, the Equations (2.38) – (2.40) are nonlinear in terms of v_∞ and γ . For flight path angles $\gamma < 20^\circ$, we may use $n = \cos \gamma \approx 1$ and ignore the dependency of P_R on γ . This allows the straightforward evaluation of γ for a given v_∞ . \square

Hodograph for Climbing Flight



The maximum excess power $(P_A - P_R)_{\max}$ and the associated freestream velocity $v_\infty = v_{\max ROC}$ can be obtained graphically by shifting the $P_A(v_\infty)$ curve as illustrated.

The *hodograph* is obtained from the $ROC(v_\infty)$ diagram by exploiting

$$v_{\text{horiz}} = v_\infty \cos \gamma . \quad (2.41)$$

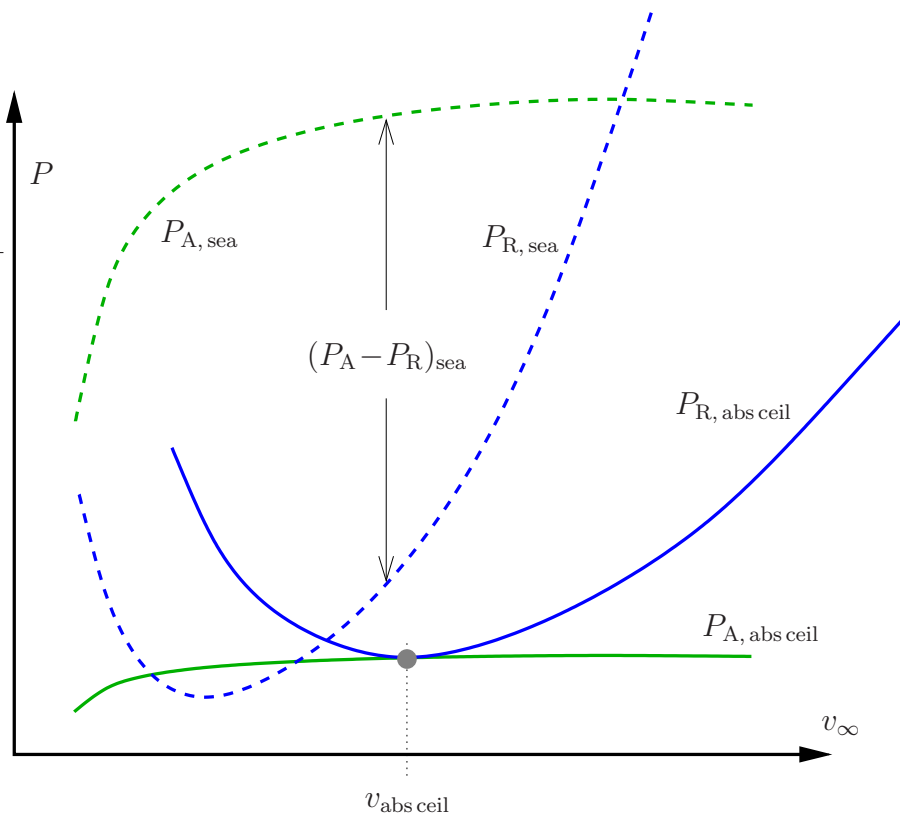
Note that the *maximum climb angle* γ_{\max} is not associated with ROC_{\max} and that the hodograph changes with altitude.

At low velocities v_∞ , a propeller-driven airplane possesses a larger proportion of excess power $P_A - P_R$ than a jet-propelled aircraft. Consequently, ROC at low v_∞ and the maximum climb angle γ_{\max} are typically larger for propeller-driven airplanes.

How high can an airplane fly?

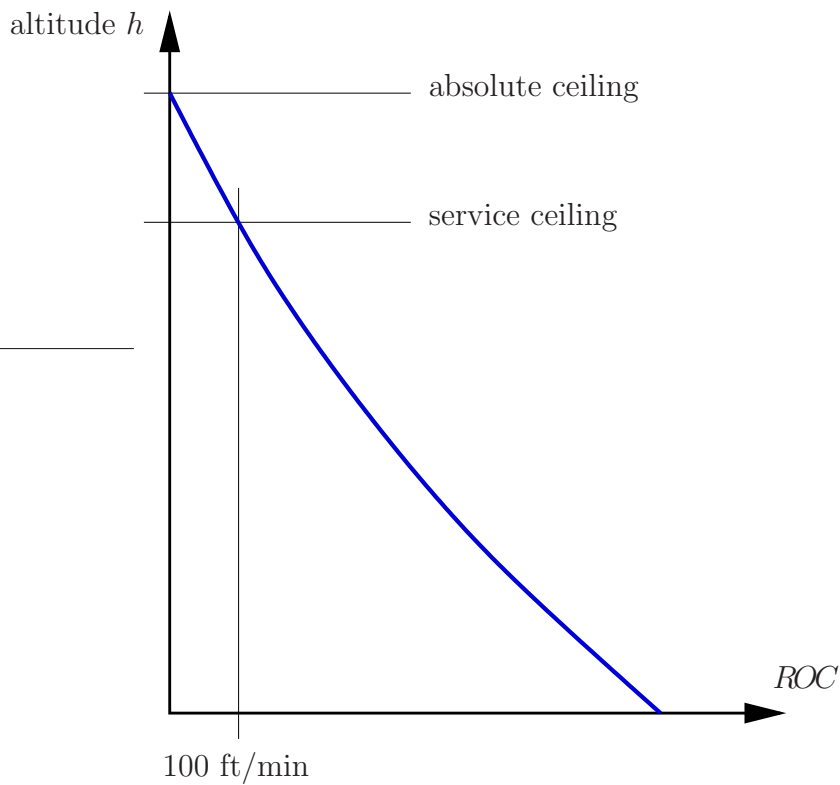
The effect of altitude on power required and power available is described by (2.33) and (2.34), respectively. If $h_2 > h_1$ denote two different altitudes, such that $\rho_2 < \rho_1$, then P_R is scaled with $\sqrt{\rho_1/\rho_2} > 1$, whereas P_A is scaled with $\rho_2/\rho_1 < 1$. Thus, the excess power $P_A - P_R$ decreases as the altitude increases.

Consequently, there is an altitude with $P_A - P_R = 0$ for exactly one velocity v_∞ , as shown in the diagram below. There is no potential for further climb. This altitude is called the *absolute ceiling* of the aircraft. At the absolute ceiling, straight, level and unaccelerated flight can only be sustained for one specific velocity v_∞ .



Service Ceiling

The so-called *service ceiling* for jet-propelled aeroplanes is defined by the altitude which allows for a maximum climb rate $ROC_{\max} = 100 \text{ ft/min} = 0.508 \text{ m/s}$. At this altitude the velocities v_{\min} and v_{\max} still provide a margin for different flight manoeuvres. Thus, it is, for example, possible to avoid collision with another aeroplane by climbing to a higher altitude. The service ceiling is of substantial importance to jet-propelled aeroplanes since the fuel efficiency increases with altitude as we will show in Section 2.7.



Time to Climb

For the calculation of the time Δt required to climb from altitude h_1 to altitude h_2 , we need to express the rate of climb ROC as a function of altitude h . The graph of $ROC(h)$ is displayed qualitatively on the previous page. It may be approximated with sufficient accuracy by one or more linear sections. We then have

$$ROC(h) = ROC_1 - \frac{h - h_1}{h_2 - h_1} (ROC_1 - ROC_2), \quad (2.42)$$

where ROC_1 and ROC_2 denote the rates of climb at altitudes h_1 and h_2 , respectively.

The time required to climb from altitude h_1 to altitude h_2 may then be obtained as

$$\Delta t = \int_{h_1}^{h_2} \frac{dh}{ROC(h)} = a \int_{h_1}^{h_2} \frac{dh}{b + h}, \quad (2.43)$$

where

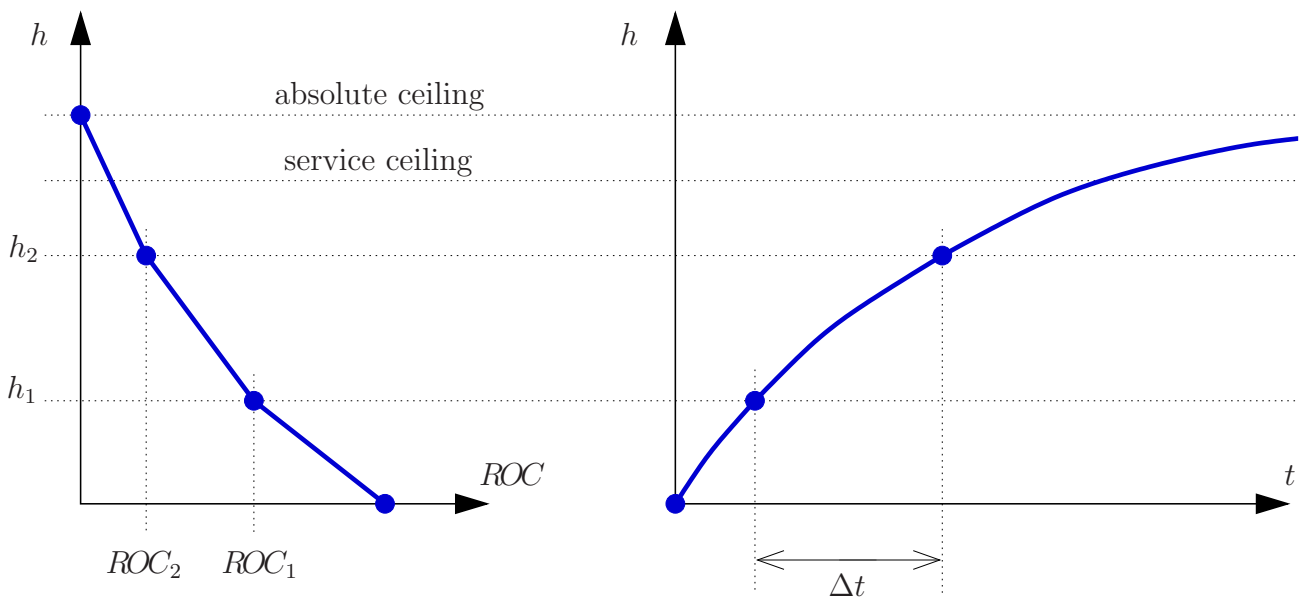
$$a = \frac{h_2 - h_1}{ROC_2 - ROC_1}, \quad b = \frac{ROC_1 h_2 - ROC_2 h_1}{ROC_2 - ROC_1}. \quad (2.44)$$

The integration renders

$$\Delta t = a \ln(b + h_2) - a \ln(b + h_1) = a \ln\left(\frac{b + h_2}{b + h_1}\right), \quad (2.45)$$

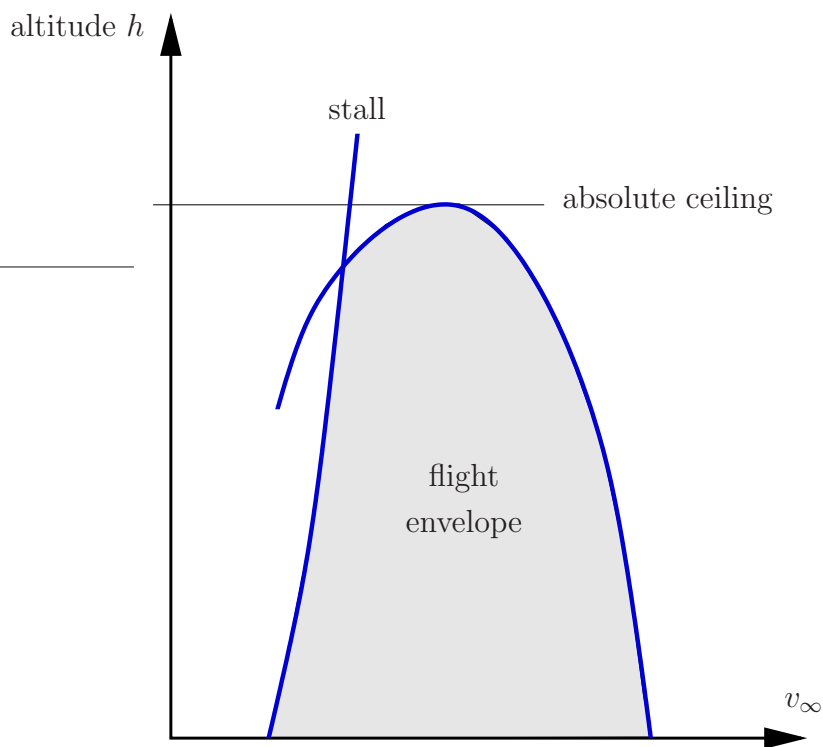
which becomes

$$\Delta t = \frac{h_2 - h_1}{ROC_2 - ROC_1} \ln\left(\frac{ROC_2}{ROC_1}\right). \quad (2.46)$$

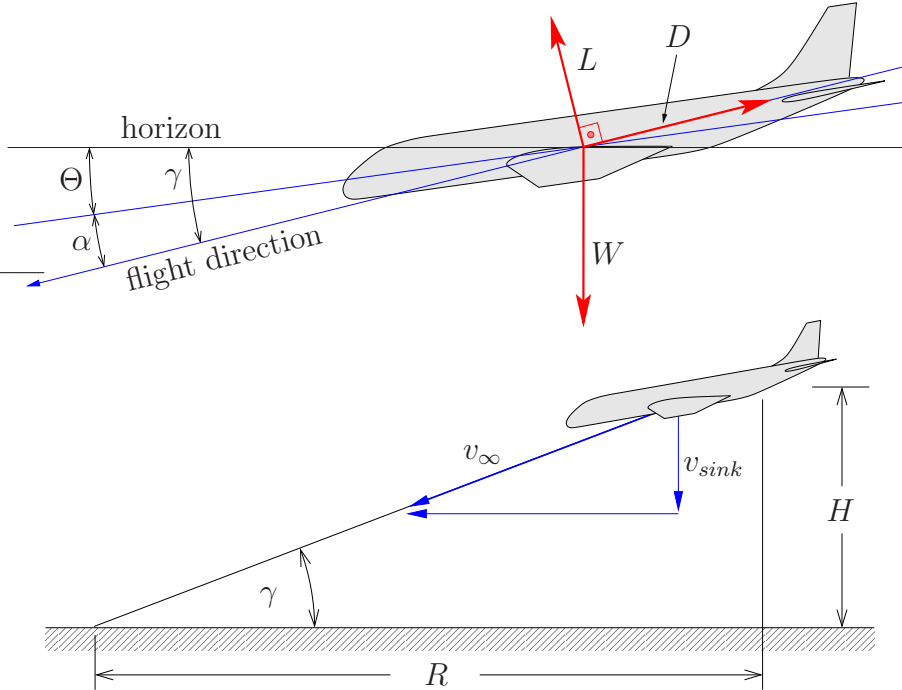


Flight Envelope

The *flight envelope* is an important diagram for any aeroplane. It shows the flight altitude displayed against the freestream velocity v_∞ or Mach number Ma_∞ . We obtain the flight envelope by evaluating v_{\min} and v_{\max} from the power required and power available diagrams (see *e. g.* page 57) at different altitudes. Note that v_{\min} may be determined by the stall phenomena.



2.5 Gliding Flight



Assuming straight, unaccelerated flight with $T = 0$, and taking into account the orientation of γ , the equations (2.1) and (2.2) reduce to

$$L - W \cos \gamma = 0, \quad D - W \sin \gamma = 0. \quad (2.47)$$

It follows that

$$\frac{D}{W} = \sin \gamma, \quad n = \frac{L}{W} = \cos \gamma \leq 1, \quad (2.48)$$

and thus,

$$\tan \gamma = \frac{\sin \gamma}{\cos \gamma} = \frac{D}{L} = \frac{1}{C_L / C_D}. \quad (2.49)$$

Defining H and R as illustrated, it follows from (2.49) that

$$\frac{1}{\tan \gamma} = \frac{R}{H} = \frac{L}{D} = \frac{C_L}{C_D}. \quad (2.50)$$

Thus, in order to minimise the *glide angle* γ and maximise the *glide range* R , the airplane should be flown at $L/D = (L/D)_{\max} = (C_L/C_D)_{\max}$. We recall from (2.23), that this is associated with the freestream velocity $v_\infty = v_{\min T_R} = v_{\min D}$. In the context of sailplanes, the expression $1/\tan \gamma$ is also known as the *glide number*.

With (2.19) and (2.49) it follows that

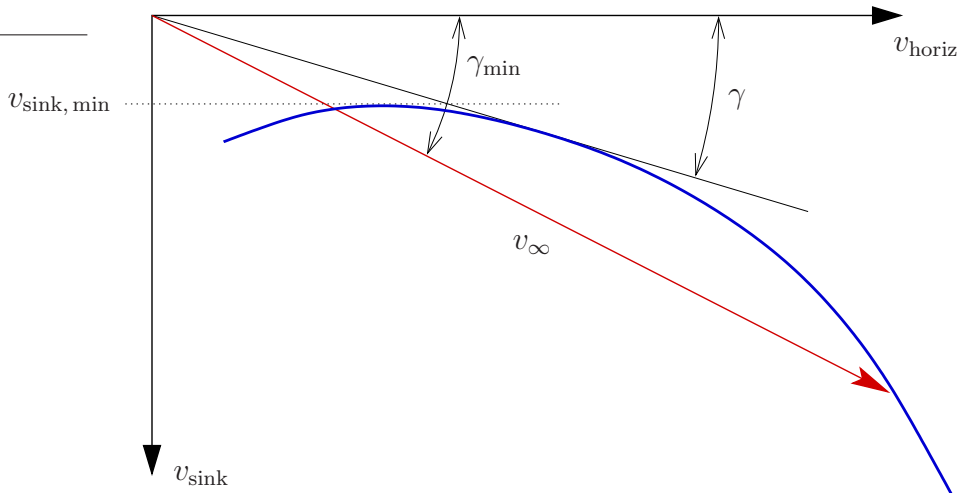
$$v_{\text{sink}} = v_{\infty} \sin \gamma = v_{\infty} \frac{D}{W} = \frac{P_{\text{R}}}{W}. \quad (2.51)$$

Thus, the sink rate v_{sink} is minimised by flying at the minimum of P_{R} , *i. e.* with velocity $v_{\text{min } P_{\text{R}}}$. Note that (2.26)₂–(2.26)₄ only hold for SLUF or small γ .

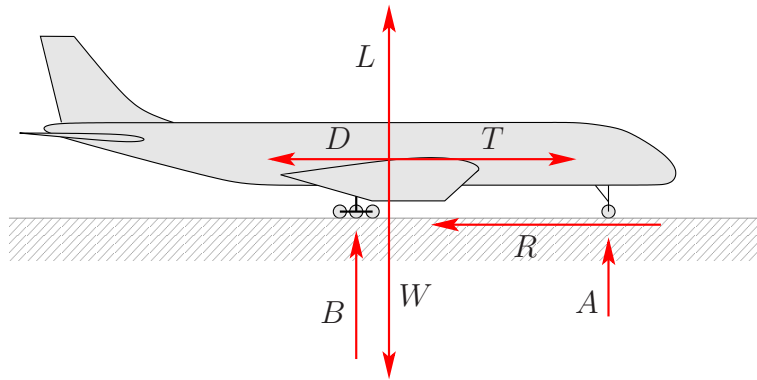
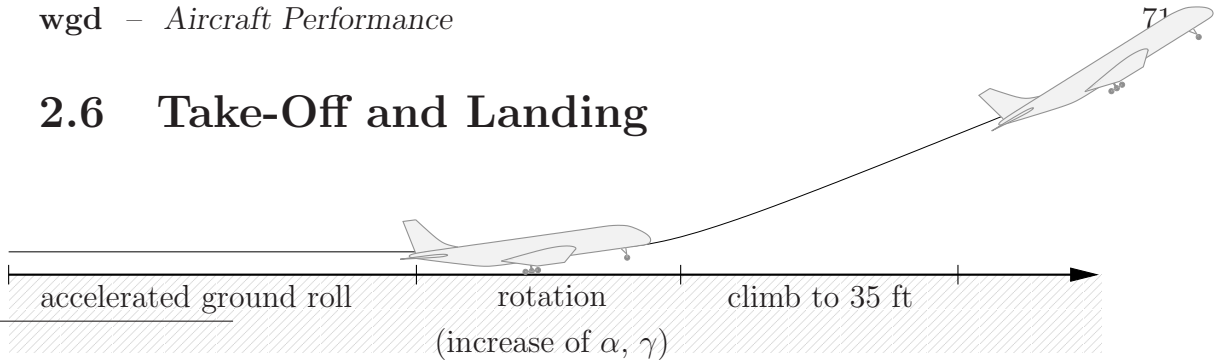
For some average air density (ignoring the dependency of P_{R} on altitude), the maximum *glide endurance* can be obtained from the minimum sink rate as

$$E_{\text{glide, max}} = \frac{H}{v_{\text{sink, min}}} = \frac{H W}{P_{\text{R min}}}. \quad (2.52)$$

For small angles γ (sailplane, gliders), an approximation of the gliding hodograph may be obtained by evaluating (2.51) for a range of velocities v_{∞} and by using $v_{\text{horiz}} = v_{\infty} \cos \gamma \approx v_{\infty}$. However, large angles γ require to resolve the dependency of P_{R} on γ in (2.51) and also in (2.52). The exact hodograph may be obtained from evaluating v_{sink} and v_{horiz} for a range of lift coefficients C_L . It is important to understand that the minimum glide angle (maximum range) is not associated with the minimum sink rate.



2.6 Take-Off and Landing



During ground roll, we have for the angle of attack and the flight path angle that $\alpha = \gamma = 0$. Furthermore, the thrust angle ϕ is assumed to be small. With Newton's second law and summation of the forces parallel to the runway it follows that

$$m \frac{dv_\infty}{dt} = T - D - R, \quad (2.53)$$

where $m = W/g$ is the mass of the aeroplane.

Rolling friction R is proportional to the normal force $A+B = W-L$ acting between the tires and the ground, *i. e.*

$$R = \mu_R (W - L), \quad (2.54)$$

where typically $\mu_R \approx 0.02$ for take-off on a smooth runway, or $\mu_R \approx 0.4$ for landing ground roll with the brakes deployed.

With (1.20), (1.37), (1.41), (2.53) and (2.54) the equations which govern ground roll of an aeroplane are

$$m \frac{dv}{dt} = T - D - \mu_R (W - L) \quad (2.55)$$

$$L = \frac{1}{2} \rho v_\infty^2 S C_L \quad (2.56)$$

$$D = \frac{1}{2} \rho v_\infty^2 S \left(C_{D0} + \phi \frac{C_L^2}{\pi e AR} \right). \quad (2.57)$$

Due to the vicinity of the wings to the ground, the wing tip vortices and consequently the downwash and induced drag do not develop to the same extent as at a higher altitude. This phenomena is termed the *ground effect* and is accounted for by the dimensionless factor ϕ . A good approximation is

$$\phi = \frac{(16 h/b)^2}{1 + (16 h/b)^2} < 1, \quad (2.58)$$

where h is the height of the wings above the ground.

In order to calculate the ground roll distances required for take-off and landing, we first consider

$$\frac{dv}{dt} = \frac{dv}{ds} \frac{ds}{dt} = v \frac{dv}{ds} = \frac{1}{2} \frac{d(v^2)}{ds}. \quad (2.59)$$

Defining the force F by
$$F = T - D - \mu_R (W - L), \quad (2.60)$$

Equation (2.55) can be rewritten as
$$F = m \frac{dv_\infty}{dt} = \frac{m}{2} \frac{d(v_\infty^2)}{ds}, \quad (2.61)$$

which renders
$$ds = \frac{m}{2F} d(v_\infty^2). \quad (2.62)$$

From integration we obtain the ground roll distance required to accelerate or decelerate from v_1 to v_2 as

$$s = \int_{v_1^2}^{v_2^2} \frac{m}{2F} d(v_\infty^2). \quad (2.63)$$

Take-Off Ground Roll

The smallest velocity v_∞ , with which flight can be sustained, is v_{stall} . Therefore, the ground roll distance required for acceleration before lift-off is minimal for $v_{\text{LO}} = v_{\text{stall}}$. The quantity v_{LO} denotes the lift-off velocity and the stalling velocity v_{stall} is given by (1.39). However, in order to provide a safety margin, it is common practice to define

$$v_{\text{LO}} = 1.2 v_{\text{stall}} = 1.2 \sqrt{\frac{2W}{\rho S C_{L_{\text{max}}}}} \quad (2.64)$$

We note that care must be taken to determine the value of $C_L = C_{L_{\text{max}}}$ to be used in (2.56), (2.57) and in (2.64). On the one hand, the angle of attack is restricted by the horizontal orientation of the aeroplane during ground roll, which decreases $C_{L_{\text{max}}}$, on the other hand, high lift systems such as flaps may be used to increase $C_{L_{\text{max}}}$.

Exact Solution: The thrust T usually varies with the velocity v_∞ . However, particularly for jet-propelled aircraft, it is sufficiently accurate to assume $T = \text{const.}$ for constant altitude.

Thus, with (2.55) – (2.58) we obtain the lift-off ground roll distance s_{LO} from (2.63) by the following manipulations

$$s_{\text{LO}} = \int_0^{v_{\text{LO}}^2} \frac{d(v_\infty^2)}{a v_\infty^2 + b} = \frac{1}{a} \ln \frac{a v_{\text{LO}}^2 + b}{b}, \quad (2.65)$$

where

$$a = \left(\mu_R C_L - C_{D0} - \frac{\phi C_L^2}{\pi e AR} \right) \frac{\rho S g}{W} \quad \text{and} \quad b = \frac{2g}{W} (T - \mu_R W). \quad (2.66)$$

If the thrust varies significantly as v_∞ increases, then a numerical integration technique may be required.

Approximation 1: A commonly employed approximation for s_{LO} is based on the assumption of constant acceleration with an average force $F_{av} = const.$ Typically, we choose $F_{av} = F(v_{\infty} = 0.7 v_{LO})$. With (2.63) and (2.64) it then follows that

$$s_{LO} \approx \frac{1.44 W^2}{g \rho S C_{L_{max}} [T - D - \mu_R(W - L)]_{0.7v_{LO}}} . \quad (2.67)$$

Approximation 2: If T is much larger than $D + R$, then (2.67) becomes

$$s_{LO} \approx \frac{1.44 W^2}{g \rho S C_{L_{max}} T} . \quad (2.68)$$

Despite this being a very rough approximation, it demonstrates that s_{LO} is proportional to W^2 , rather than just W . Furthermore, if we recall from (2.19) and (2.34) that thrust T is proportional to air density ρ , we find with (2.68) that the lift-off ground roll s_{LO} is inverse proportional to ρ^2 . Consequently, airports which are located at higher altitudes require longer runways.

The dependency of s_{LO} on the wing reference area S and the maximum lift coefficient $C_{L_{max}}$ is evident.

Landing Ground Roll

The typical touch-down velocity of an aeroplane is

$$v_{\text{TD}} = 1.3 v_{\text{stall}} = 1.3 \sqrt{\frac{2W}{\rho S C_{L_{\text{max}}}}}, \quad (2.69)$$

which provides an appropriate safety margin. Generally, the forces during landing ground roll are described by (2.55) – (2.58). However, at touchdown, the thrust T has usually been reduced to zero or it has been *reversed*. The rolling friction now includes the effect of brakes such that $\mu_R \approx 0.4$, and the aerodynamic coefficients C_{D0} and C_L account for the application of spoilers or drag chutes.

Exact Solution: Assuming $T = \text{const.} \leq 0$, the landing ground roll distance is obtained from (2.63) as

$$s_L = \int_{v_{\text{TD}}^2}^0 \frac{d(v_{\infty}^2)}{a v_{\infty}^2 + b} = \frac{1}{a} \ln \frac{a v_{\text{TD}}^2 + b}{b}, \quad (2.70)$$

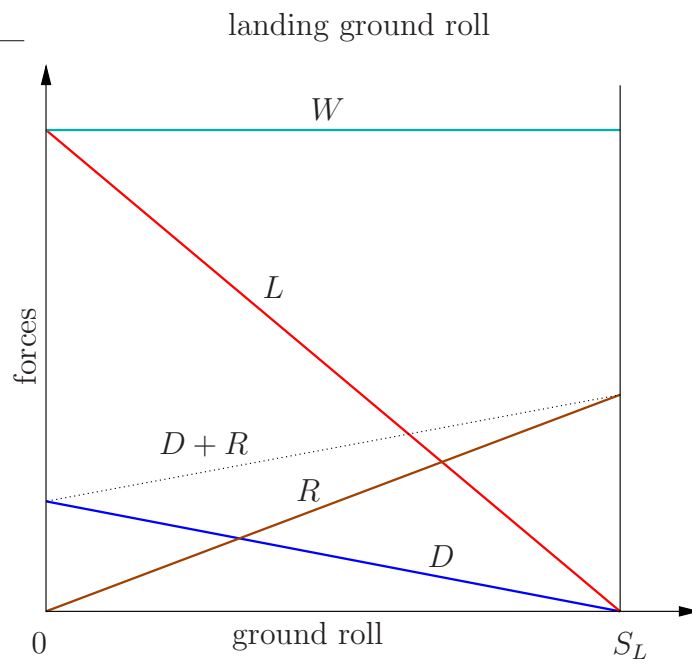
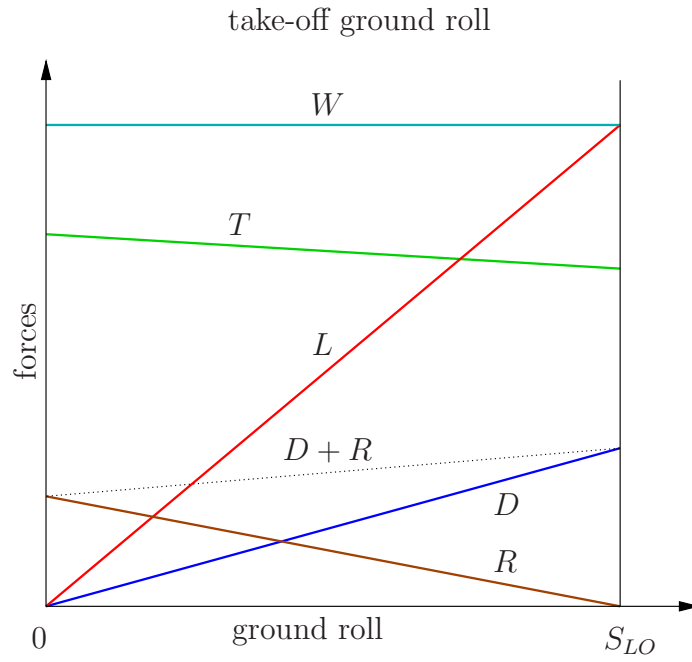
where the quantities a and b are defined as in (2.66).

Approximation: An approximation for s_L is obtained analogously to (2.67) as

$$s_L \approx \frac{1.69 W^2}{g \rho S C_{L_{\text{max}}} [-T + D + \mu_R(W - L)]_{0.7v_{\text{TD}}}}. \quad (2.71)$$

Recall that for landing $T \leq 0$.

Variation of Forces During Ground Roll



2.7 Range and Endurance

The maximum distance an aeroplane can traverse on a tank of fuel is denoted as *range* R . The maximum time which an aeroplane can stay airborne on a tank of fuel is denoted as *endurance* E .

Clearly, R and E are related to the fuel consumption of the aeroplane. According to Section 2.2, fuel consumption for the propeller-driven aeroplane is given in terms of fuel burnt per power and time (specific fuel consumption $SFC = const.$), whereas for the jet-propelled aeroplane fuel consumption is given in terms of fuel burnt per thrust and time (thrust specific fuel consumption $TSFC = const.$). Therefore, we have to develop separate sets or formula for range and endurance for the two types of aeroplanes.

In order to account for the changes of aeroplane weight as fuel is being burnt,

we define $\left\{ \begin{array}{l} W_f \text{ current weight of fuel,} \\ W_0 \text{ weight of aeroplane with full fuel load,} \\ W_1 \text{ weight of aeroplane without fuel.} \end{array} \right.$

The current total weight of the aeroplane may then be expressed as

$$W = W_1 + W_f. \quad (2.72)$$

Propeller-Driven Aeroplane

From (2.6) we recall that

$$SFC = \frac{-dW_f/dt}{P} \approx const. \quad (2.73)$$

Furthermore, we assume a constant propeller efficiency η and use (2.9) to write

$$SFC = \frac{-\eta dW_f/dt}{P_A} \approx const. \quad (2.74)$$

Rearranging gives

$$dt = -\frac{\eta}{SFC P_A} dW_f. \quad (2.75)$$

We obtain for the endurance

$$E = \int_0^E dt = -\int_{W_0}^{W_1} \frac{\eta}{SFC P_A} dW_f \quad (2.76)$$

It follows that maximum endurance E is achieved if the airplane is always flown at $v_{\min P_R}$ with minimum power required $P_A = P_{R,\min}$. Recalling (2.26), this is associated with $(C_L^{3/2}/C_D)_{\max}$.

Assuming straight level unaccelerated flight with a constant angle of attack, *i. e.*

$$P_A = T_A v_\infty = T_R v_\infty = D v_\infty, \quad W = L, \quad \frac{L}{D} = \frac{C_L}{C_D} = const. \quad (2.77)$$

we recall (2.5) for $n = 1$, *i. e.*
$$v_\infty = \sqrt{\frac{2W}{\rho S C_L}} \quad (2.78)$$

and obtain from (2.76)

$$E = \int_{W_1}^{W_0} \left(\frac{\eta}{SFC} \frac{1}{D v_\infty} \frac{L}{W} \right) dW = \int_{W_1}^{W_0} \left(\frac{\eta}{SFC} \frac{C_L^{3/2}}{C_D} \sqrt{\frac{\rho S}{2}} W^{-\frac{3}{2}} \right) dW, \quad (2.79)$$

which renders the *Breguet formula* for the endurance of a propeller-driven airplane flown at constant altitude, *i. e.* $\rho = const.$, as

$$E = \frac{\eta}{SFC} \frac{C_L^{3/2}}{C_D} \sqrt{2\rho S} \left(W_1^{-\frac{1}{2}} - W_0^{-\frac{1}{2}} \right). \quad (2.80)$$

In order to calculate the range, we manipulate (2.75) and use (2.19) to obtain

$$ds = - \frac{ds}{dt} \frac{\eta}{SFC P_A} dW_f = - \frac{\eta}{SFC P_A / v_\infty} dW_f = - \frac{\eta}{SFC T_A} dW_f. \quad (2.81)$$

Integration renders the range as

$$R = \int_0^R ds = \int_{W_1}^{W_0} \frac{\eta}{SFC T_A} dW. \quad (2.82)$$

Thus, the range is maximised if the airplane is always flown at $v_{\min T_R}$ with minimum thrust required $T_A = T_{R, \min}$. According to (2.23), this corresponds to $(C_L/C_D)_{\max}$.

For SLUF, we have $\frac{T_A}{W} \frac{C_L}{C_D} = 1$. Multiplication of the integrand in (2.82) with this term gives

$$R = \int_{W_1}^{W_0} \frac{\eta}{SFC} \frac{C_L}{C_D} \frac{1}{W} dW = \frac{\eta}{SFC} \frac{C_L}{C_D} \ln \frac{W_0}{W_1}. \quad (2.83)$$

Note that the endurance E as given by (2.80) for the propeller-driven aeroplane depends on the altitude (ρ), whereas maximum range R as given by (2.83) can be achieved at any altitude. The endurance is a maximum at sea-level, where ρ is large.

Jet-Propelled Aeroplane

With $T = T_A$ we obtain from (2.12)
$$dt = -\frac{1}{TSFC T_A} dW_f . \quad (2.84)$$

Integration renders the endurance as

$$E = \int_0^E dt = - \int_{W_0}^{W_1} \frac{1}{TSFC T_A} dW_f . \quad (2.85)$$

It follows that maximum endurance is achieved if the airplane is always flown at $v_{\min T_R}$ with minimum thrust required $T_A = T_{R, \min}$. Recalling (2.23), this is associated with $(C_L/C_D)_{\max}$.

Based on the assumptions of straight level unaccelerated flight and a constant angle of attack we may multiply (2.85) with $\frac{T_A}{W} \frac{C_L}{C_D} = 1$ to obtain the *Breguet formula* for the endurance of a jet-propelled aeroplane, *i. e.*

$$E = \int_{W_1}^{W_0} \frac{1}{TSFC} \frac{C_L}{C_D} \frac{dW}{W} = \frac{1}{TSFC} \frac{C_L}{C_D} \ln \frac{W_0}{W_1} . \quad (2.86)$$

Manipulating (2.84) and assuming SLUF with (2.78) and $\frac{T_A}{W} \frac{C_L}{C_D} = 1$ we may write

$$\begin{aligned} ds &= -\frac{ds/dt}{TSFC T_A} dW_f = -\frac{v_\infty}{TSFC} \frac{C_L}{C_D} \frac{dW_f}{W} \\ &= -\sqrt{\frac{2}{\rho S}} \frac{1}{TSFC} \frac{C_L^{1/2}}{C_D} \frac{dW_f}{\sqrt{W}} . \end{aligned} \quad (2.87)$$

Integration renders the range as

$$R = \int_0^R ds = - \int_{W_0}^{W_1} \sqrt{\frac{2}{\rho S}} \frac{1}{TSFC} \frac{C_L^{1/2}}{C_D} \frac{dW_f}{\sqrt{W}} . \quad (2.88)$$

Thus, for $\rho = \text{const.}$ (constant altitude), the range is maximised if the airplane is always flown at the velocity \hat{v}_∞ that renders maximum $C_L^{1/2}/C_D$ (see (2.30)). This velocity can be obtained graphically from the thrust required over velocity diagram by means of the tangent through the origin (analogously to $v_{\min T_R}$ in the power-required diagram).

Based on the assumption of SLUF, *i. e.* $C_L^{1/2}/C_D = \text{const.}$, we can derive the *Breguet formula* for the range of a jet-propelled airplane from (2.88) as

$$R = \frac{1}{TSFC} \sqrt{\frac{8}{\rho S}} \frac{C_L^{1/2}}{C_D} \left(\sqrt{W_0} - \sqrt{W_1} \right), \quad (2.89)$$

For the jet-propelled airplane the endurance as given by (2.86) is independent of the altitude, whereas the range as given by (2.89) increases with altitude. Maximum range can therefore be achieved when the airplane is flown near the absolute ceiling. That is the reason for the introduction of the “service ceiling” as described on page 66.

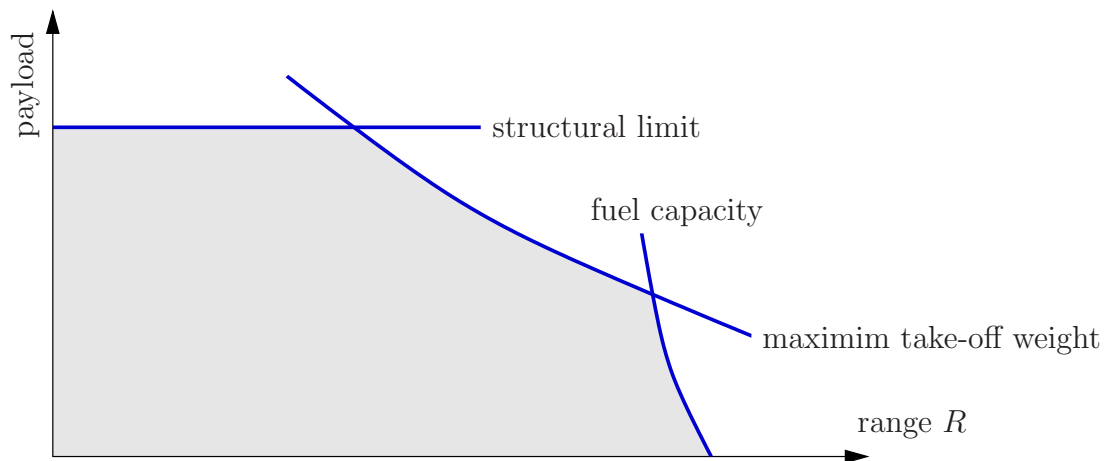
It is important to know that, in practice, for both propeller-driven and jet-propelled aeroplanes, range and endurance depend significantly on the weather conditions, the pilot skills, the climb to the cruising altitude *etc.* However, the Breguet formula (2.80), (2.83), (2.86) and (2.89) provide acceptable approximations and valuable insight into how range and endurance can be maximised.

Range and Payload

The specifications of larger aeroplanes typically include the *range–payload* curve. This is a graph which, for a particular mission profile, presents the effect of trading payload for fuel on the range of an airplane.

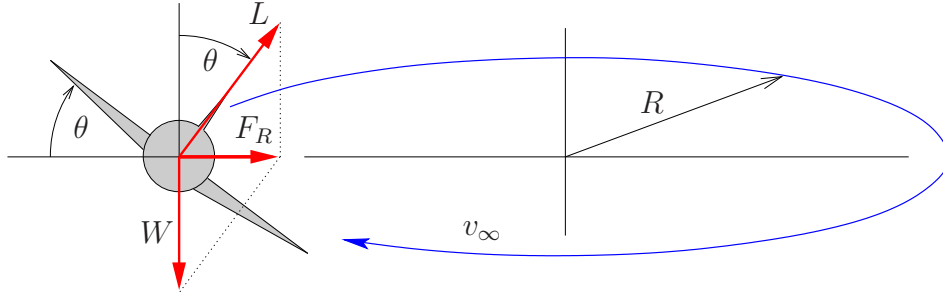
The specific design of any aeroplane renders a certain *maximum take-off weight*, which must not be exceeded by the total weight in order to ensure that the aeroplane is fully operational. Consequently, if the payload is very heavy, the fuel tanks can only be filled partially and the range is reduced significantly.

The range–payload diagram may also reflect structural limitations, *i. e.* the maximum load which can be supported by the airframe, and the limitation arising from the capacity of the fuel tanks.



2.8 Turning Flight

Level Turn



If the pilot increases the *bank angle* to $\theta > 0$, then the lift force is tilted as illustrated. Assuming that v_∞ and L are controlled such that $v_\infty = \text{const.}$ and

$$L \cos \theta = W , \quad (2.90)$$

then the aircraft performs a circular *level turn*. The load factor (2.3) associated with a level turn is

$$n = \frac{L}{W} = \frac{1}{\cos \theta} \geq 1 . \quad (2.91)$$

The component of lift directed towards the centre of the turn may be written as

$$F_R = \sqrt{L^2 - W^2} = W \sqrt{n^2 - 1} . \quad (2.92)$$

Using Newton's second law and the radial acceleration v_∞^2/R gives

$$F_R = m \frac{v_\infty^2}{R} . \quad (2.93)$$

Combining (2.92), (2.93) and $W = m g$ renders

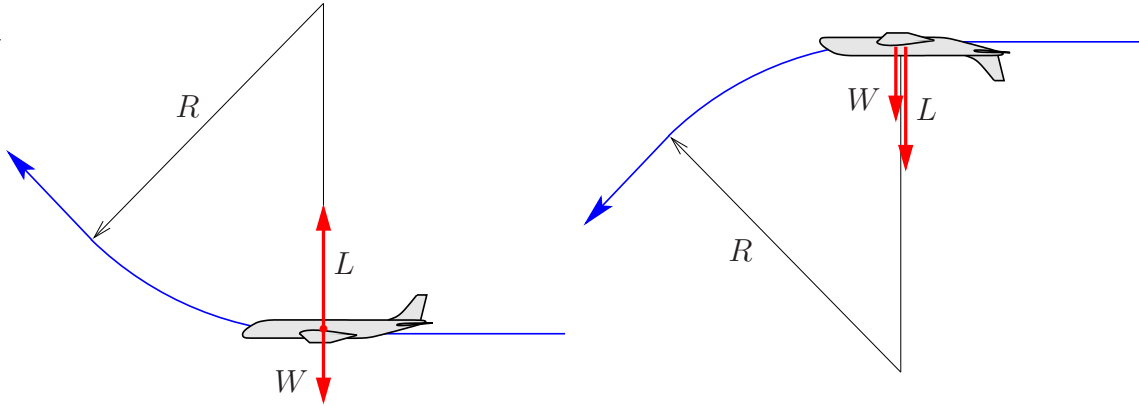
$$R = \frac{v_\infty^2}{g \sqrt{n^2 - 1}} . \quad (2.94)$$

The angular velocity or *turn rate* is obtained as

$$\omega = \frac{v_\infty}{R} = \frac{g \sqrt{n^2 - 1}}{v_\infty} . \quad (2.95)$$

Recall from (2.4) that the induced drag becomes larger as n increases. Thus, the thrust required to sustain a level turn is larger than that for straight level unaccelerated flight.

Pull-Up and Pull-Down



If the lift of an airplane, which is initially in straight, level flight, is suddenly increased, the airplane will perform a *pull-up* manoeuvre. We obtain

$$F_R = L - W = W(n - 1). \quad (2.96)$$

Similarly to (2.94) and (2.95) it follows that

$$R = \frac{v_\infty^2}{g(n - 1)} \quad (2.97)$$

and

$$\omega = \frac{g(n - 1)}{v_\infty}. \quad (2.98)$$

If an airplane, which is initially in level flight, suddenly rolls into an inverted position, it will perform a *pull-down* manoeuvre. Analogously to (2.96) – (2.98), we obtain

$$F_R = L + W = W(n + 1), \quad (2.99)$$

$$R = \frac{v_\infty^2}{g(n + 1)} \quad (2.100)$$

and

$$\omega = \frac{g(n + 1)}{v_\infty}. \quad (2.101)$$

On the Manoeuvrability of an Aeroplane

For large n , we may argue that $n \approx n + 1$. The turn radii and turn rates for the different manoeuvres as given by (2.94), (2.95), (2.97), (2.98) and (2.100), (2.101) may then be approximated, respectively, by

$$R = \frac{v_\infty^2}{g n} \quad \text{and} \quad \omega = \frac{g n}{v_\infty}. \quad (2.102)$$

Using (2.5), this can be written as

$$R = \frac{2W}{\rho S C_L g} \quad \text{and} \quad \omega = g \sqrt{\frac{\rho S C_L n}{2W}}. \quad (2.103)$$

Hence, high manoeuvre performance (small minimum R , large maximum ω) is associated with large $C_{L\max}$ and n_{\max} . Depending on the velocity v_∞ , the maximum load factor n_{\max} is determined by the maximum lift coefficient $C_{L\max}$ or by the structural strength of the aircraft as described in the next Section.

According to (2.103), high manoeuvre performance is also associated with a low *wing loading* W/S . However, the wing loading is typically determined by factors other than manoeuvring, such as payload, range and maximum velocity. As a result wing loadings for light general aviation aircraft are relatively low, but those for high performance military aircraft are relatively large.

airplane	W/S [kg m ⁻²]
Wright Flyer (1903)	7
Spitfire (1936)	137
sailplane DG-1000	35
Cessna Skyhawk	69
Boeing 747	350 - 700
Airbus A-380	300 - 700
Eurofighter Typhoon	311
General Dynamics F-16	430

2.9 $V-n$ Diagram

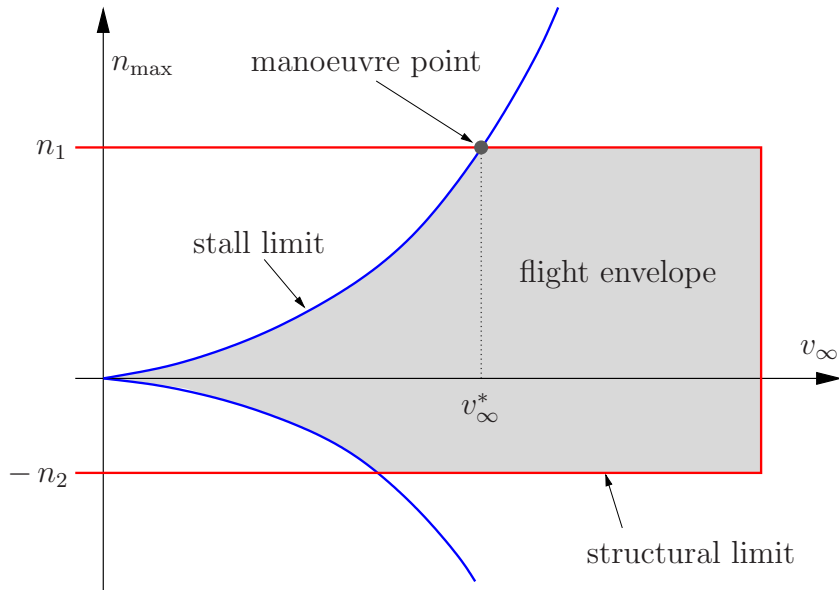
In the $V-n$ diagram, we display the maximum admissible value of the load factor n_{\max} against the freestream velocity v_{∞} .

From (2.5) it follows for the stall limit that

$$n_{\max} = \frac{\rho S v_{\infty}^2 C_{L\max}}{2W}. \quad (2.104)$$

The load factor n_{\max} is also subject to structural limitations of the aeroplane. A major limitation arises from the strength of the joints between light lift producing parts (wings) and the bulky heavy parts (fuselage) of the airplane.

The velocity v_{∞} is also subject to structural limitations. These may be due to *aeroelastic instabilities*, temperature effects, excessive dynamic pressure, *etc.*



Recalling (2.103), we identify the *manoeuvre point* where C_L and n are maximal and render the highest manoeuvre performance possible. The velocity v_{∞}^* is called the *corner velocity*.

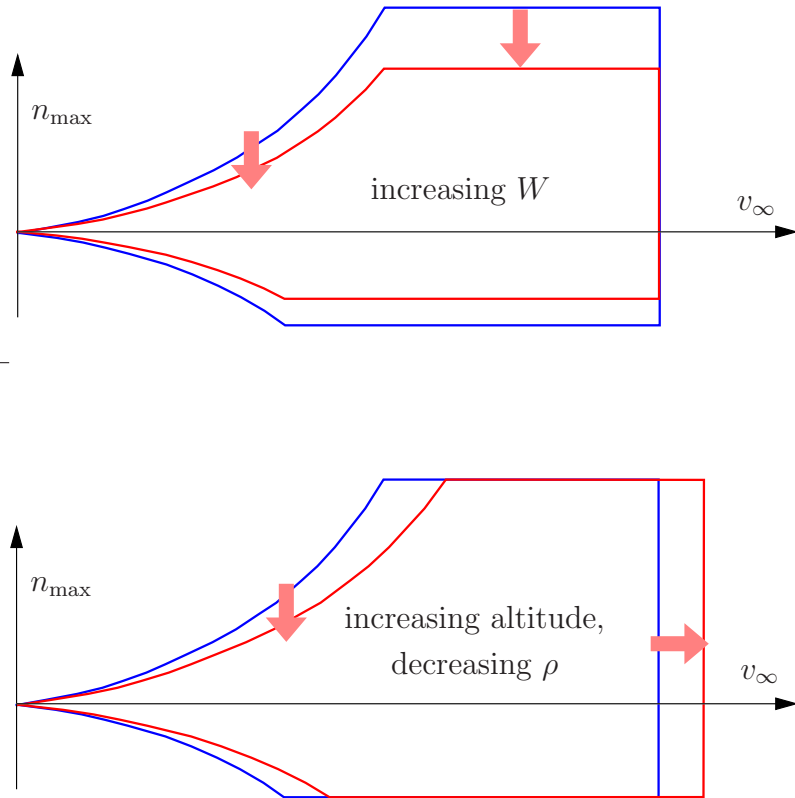
The area with all admissible pairs (n, v_{∞}) is denoted as the *flight envelope*.

Clearly, the $V - n$ diagram is an interface between the disciplines of *flight mechanics* and *airframe design*. It represents many of the load cases which the airframe has to withstand. The values for n_1 and n_2 as defined in the diagram are specified by the airworthiness authorities for particular aircraft. Typical load factors laid down in the *British Civil Airworthiness Requirements* (BCAR) are shown in the table.

	aeroplane type		
	normal	semi-aerobatic	aerobatic
n_1	$2.1 + \frac{24,000 \text{ lb}}{W + 10,000 \text{ lb}}$	4.5	6.0
n_2	1.0	1.8	3.0

For military aeroplanes, the value of n_1 is of the order of 10 and larger.

Effects of Weight and Altitude on the V - n Diagram



The effects of W and ρ on the stall limit are evident from (2.104).

Often, the structural limit arises from a maximum admissible lift force $L_{\max} = \text{const.}$ or maximum admissible difference force $(L - W)_{\max} = \text{const.}$, beyond which the airframe fails. It then follows from $L = nW$ that the structural limit n_{\max} decreases as W increases.

The maximum admissible velocity typically increases as ρ decreases. This may, for example, be due to the decrease of the dynamic pressure.

2.10 Energy Method for Accelerated Flight

Modern high performance aeroplanes are capable of highly accelerated climbs. Such manoeuvres can be analysed with the *energy method*.

First, we consider the *specific total aircraft energy* H_e , which is the sum of the potential and the kinetic energies of the aeroplane divided by the aeroplane weight, *i. e.*

$$H_e = \left(m g h + \frac{1}{2} m v_\infty^2 \right) \frac{1}{W} . \quad (2.105)$$

With $W = m g$, we may write

$$H_e = h + \frac{v_\infty^2}{2 g} . \quad (2.106)$$

We can then draw isolines of H_e in the altitude over velocity diagram, which are independent of the specific aeroplane under consideration, *i. e.* all aeroplanes flying at altitude h with velocity v_∞ have the same *energy level* H_e .

Next, we recall (2.1) whereby we assume that $\phi + \alpha$ is small, *i. e.*

$$m \frac{d v_\infty}{d t} = T - D - W \sin \gamma . \quad (2.107)$$

Rearranging with $W = m g$ gives

$$\frac{v_\infty T - v_\infty D}{W} = v_\infty \sin \gamma + \frac{v_\infty}{g} \frac{d v_\infty}{d t} . \quad (2.108)$$

We recognise the term on the left hand side as the ratio of the excess power over the aeroplane weight. This ratio is known as the *specific excess power* P_s . Furthermore, we recall from (2.37) that we have for the rate of climb *ROC*

$$ROC = \frac{d h}{d t} = v_\infty \sin \gamma . \quad (2.109)$$

We may then write (2.108) as

$$P_s = \frac{d h}{d t} + \frac{v_\infty}{g} \frac{d v_\infty}{d t} . \quad (2.110)$$

From the comparison of (2.106) and (2.110), we note that the specific excess power equals the time derivative of the energy level, *i. e.*

$$P_s = \frac{d H_e}{d t} . \quad (2.111)$$

P_s Diagram

The conclusion of (2.111) is that an aeroplane can change its energy state by the application of excess power. It is therefore essential to know how much excess power is available to the aeroplane, when it is flying with velocity v_∞ at altitude h . For this purpose, we draw contour lines of P_s in the h - v_∞ system. The contour line with $P_s = 0$ describes the *flight envelope* similar to the diagram on page 68. In the same diagram, we may plot contour lines of the energy level h_e . Typical P_s diagrams for a subsonic and a supersonic aeroplane are displayed below. Note that, due to Equation (2.4) for drag (thrust required), the contour lines for P_s depend on the aeroplane configuration and on the load factor. The irregular shape of the P_s contour lines for the supersonic aeroplane is due to the effect of the maximum drag associated with Mach numbers near $Ma_\infty = 1$ (compare Section 1.12).

zooms and dives: The pilot does not need to apply any excess power in order to change from one state (v_1, h_1) on a contour line of H_e to another state (v_2, h_2) on the same contour line. Such “zooms” ($h_2 > h_1$) and “dives” ($h_2 < h_1$) basically mean trading kinetic energy for potential energy or vice versa. Note, however, that these manoeuvres affect the specific excess power available to the pilot, since the thrust required and thrust available change with the velocity and altitude.

minimum time to climb: The P_s diagrams may be used to determine the minimum time required to climb to the maximum energy height. In fact, for fighter aircraft, it is advantageous to have a higher energy level than the adversary. Rearranging (2.111) gives

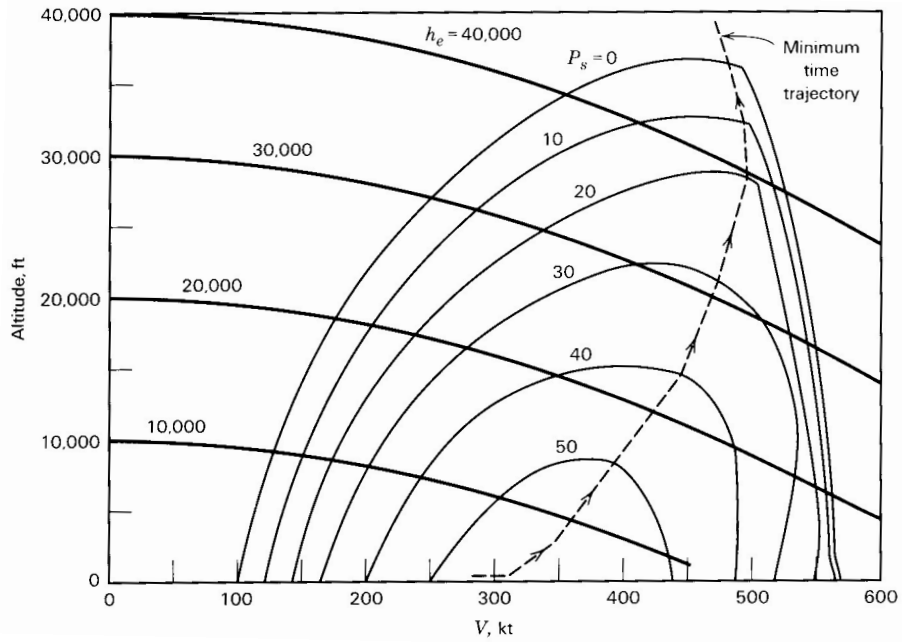
$$dt = \frac{dH_e}{P_s}, \quad (2.112)$$

which we integrate to obtain

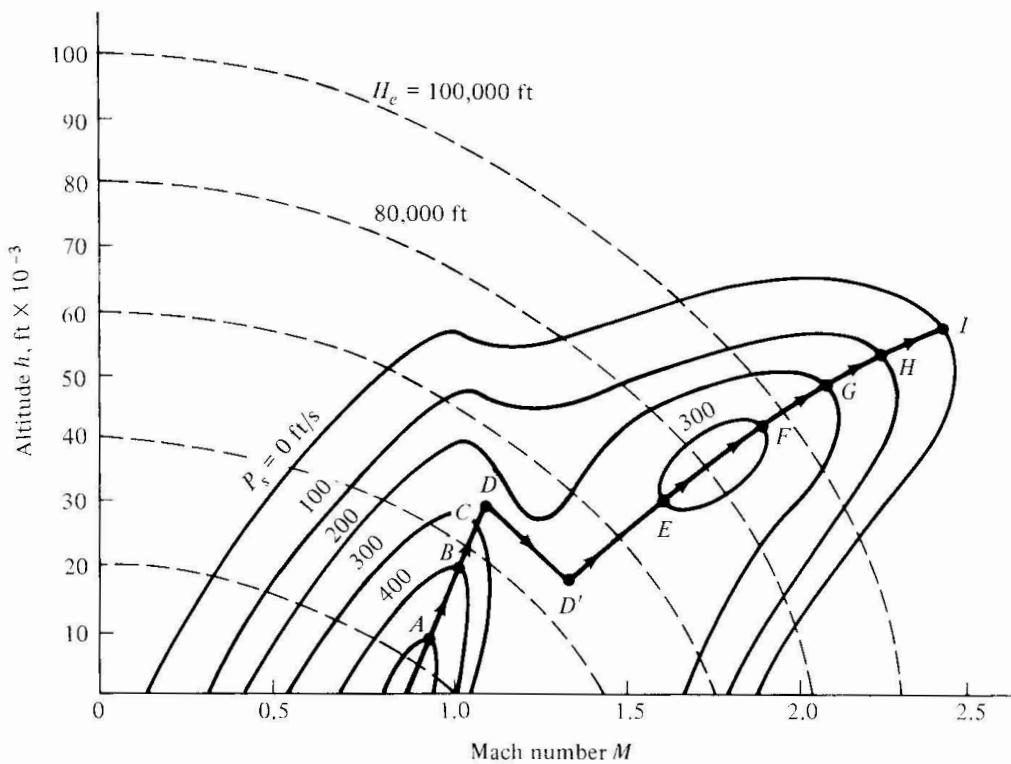
$$\Delta t = \int_0^{\Delta t} dt = \int_{H_{e,1}}^{H_{e,2}} \frac{1}{P_s} dH_e. \quad (2.113)$$

Thus, Δt is minimised by using $P_{s,\max}$ on each energy level. This is represented in the h - v_∞ system by the trajectory that connects the maxima of P_s on each energy level. In the diagram for the supersonic aeroplane, note the characteristic constant-energy dive to accelerate through the drag-divergence region near $Ma_\infty = 1$.

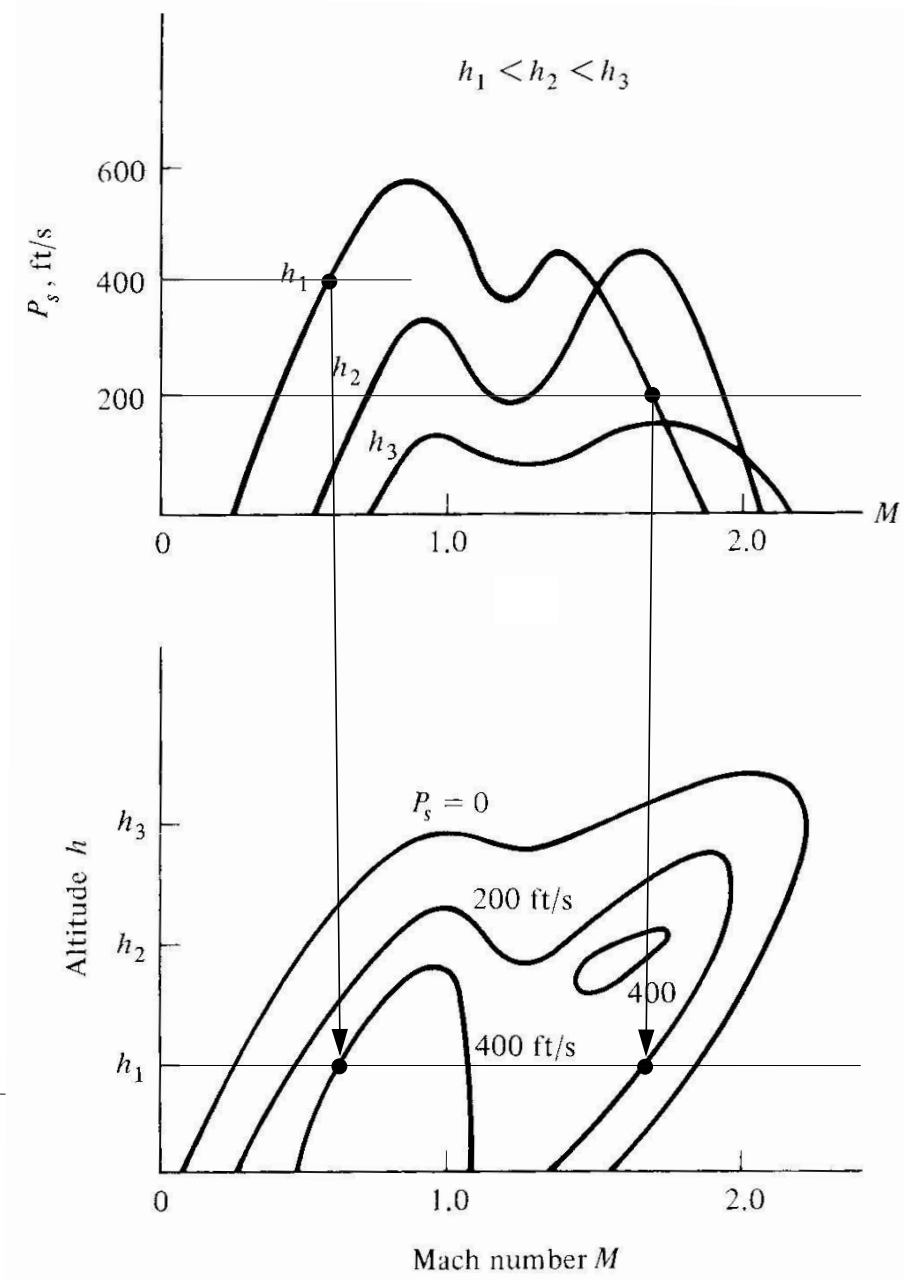
subsonic aeroplane



supersonic aeroplane



construction of P_s contour lines



Chapter 3

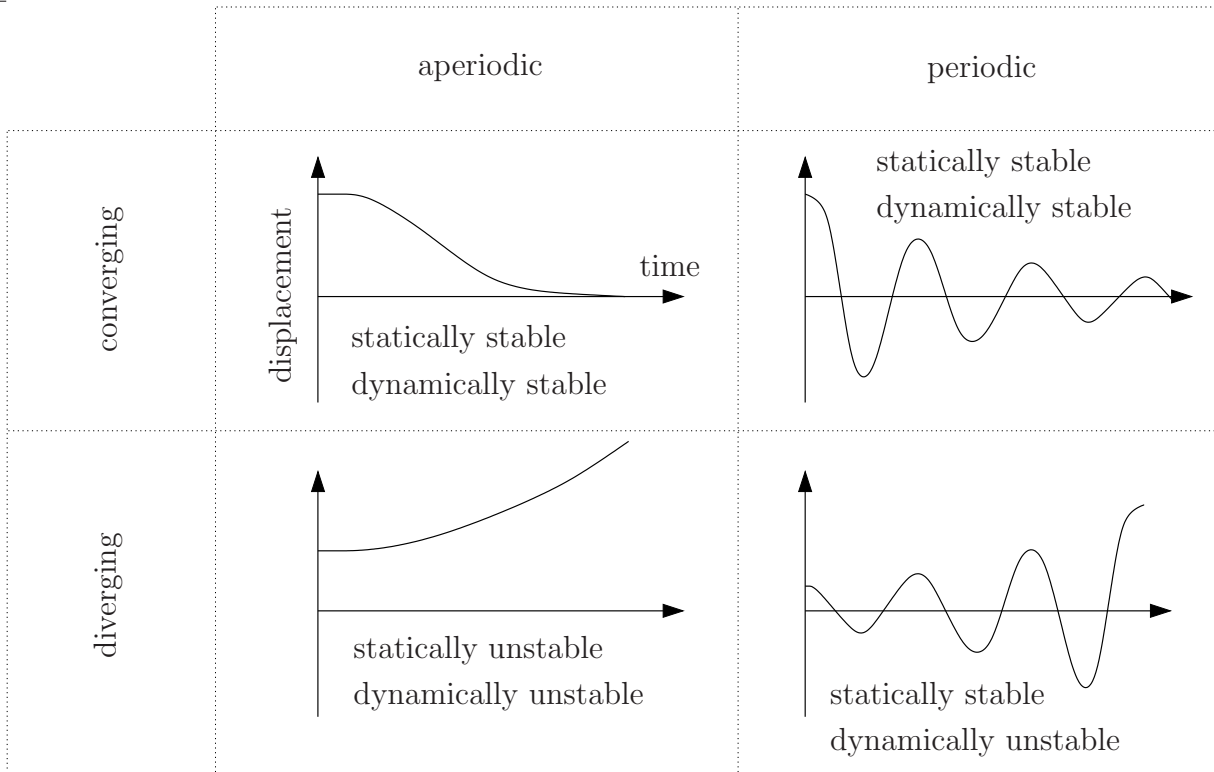
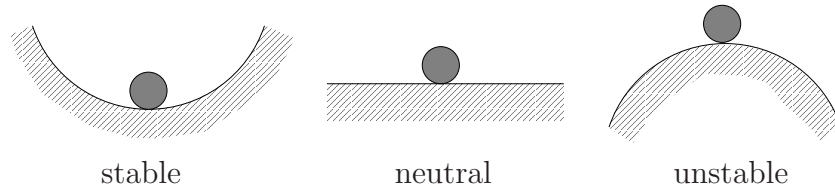
Static Stability and Control

3.1 Static and Dynamic Stability

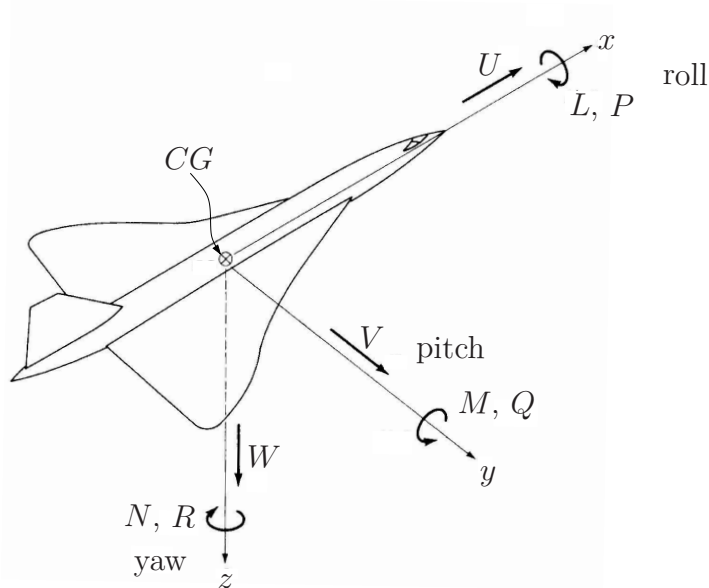
The analysis of the *static stability* of an aeroplane is concerned with the forces or moments acting on the aeroplane, which arise from disturbances such as wind gusts or temporary deflections of the control surfaces. The direction or orientation of these forces and moments should be such that the aeroplane is returned (at least initially) towards stable flight. The specific aeroplane configuration under consideration is then said to be “statically” stable. For unstable configurations, disturbances cause moments and forces which take the aeroplane further away from stable flight and, in the worst case, cause the loss of control.

It is important to understand that static stability is necessary, but not sufficient for stable flight. Only the additional consideration of *dynamic stability* ensures that a specific aeroplane configuration is really *stable*. Dynamic stability is concerned with the motion of the aeroplane following a disturbance. An aeroplane may be statically stable and dynamically unstable as illustrated in the diagrams below.

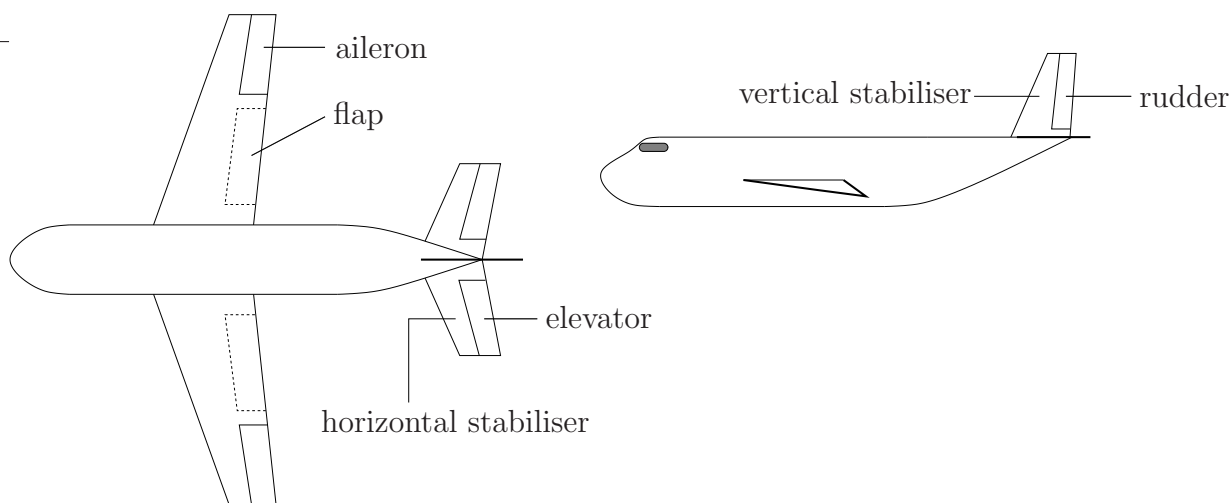
We distinguish three different states of static stability. A configuration may be *stable*, *i. e.* small disturbances cause forces which return the system into stable equilibrium. The state of the configuration may be *neutral*, *i. e.* disturbances do not cause any forces or moments, or it may be *unstable*, *i. e.* disturbances cause forces which remove the system further away from equilibrium.



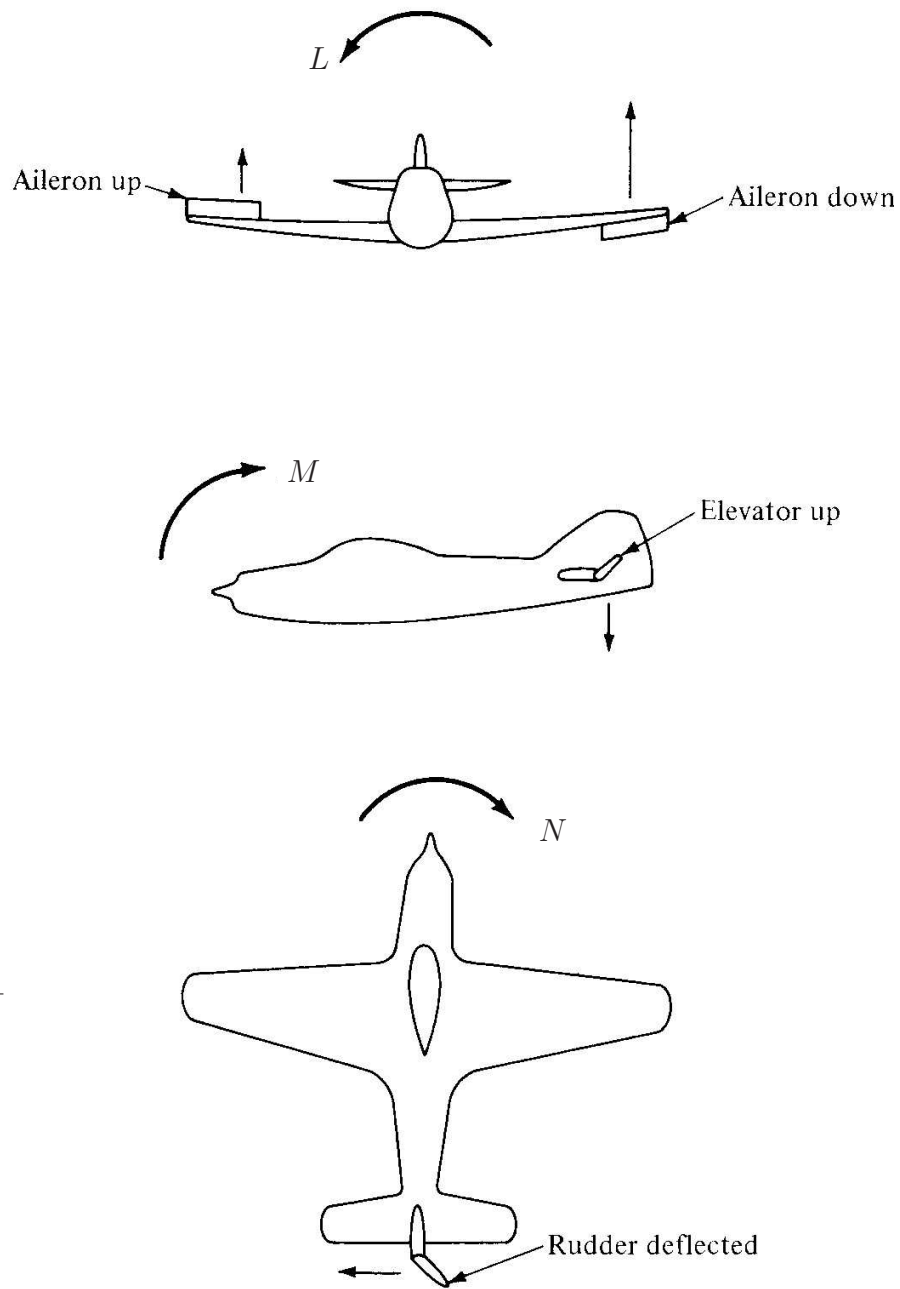
3.2 Aircraft Rotations and Control Surfaces



The rotations of the aeroplane with respect to the axis of a coordinate system that moves with the aeroplane as shown are known as *pitch*, *roll* and *yaw*. The associated angular velocities are denoted by Q , P and R , respectively. These rotational velocities are due to moments M , L and N as shown. The translational velocities along the axis are denoted by U , V and W .



Flaps are high-lift systems (compare Section 1.9), whereas *ailerons*, *elevators* and *rudder* are the conventional control surfaces.



By deflecting the control surfaces during flight the pilot can generate the moments L , M or N .

3.3 Longitudinal Static Stability

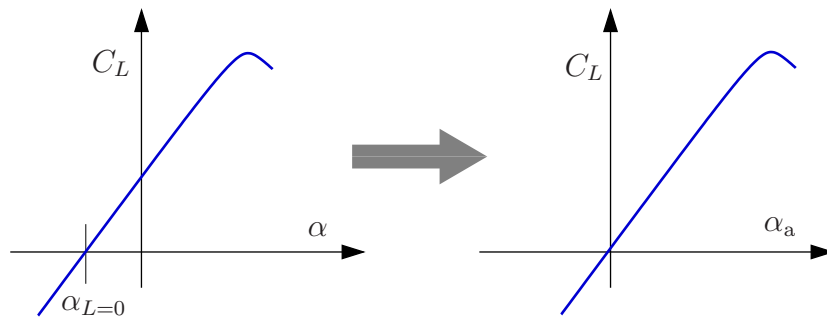
Longitudinal stability is concerned with the relation between the *pitching moment* M and the corresponding angular displacements. We define the pitching moment with respect to the centre of gravity CG of the aeroplane as

$$M = q_\infty S \bar{c} C_M, \quad (3.1)$$

where \bar{c} denotes the mean chord line.

Furthermore, for convenience, we introduce the *absolute angle of attack* α_a as

$$\alpha_a = \alpha - \alpha_{L=0}. \quad (3.2)$$

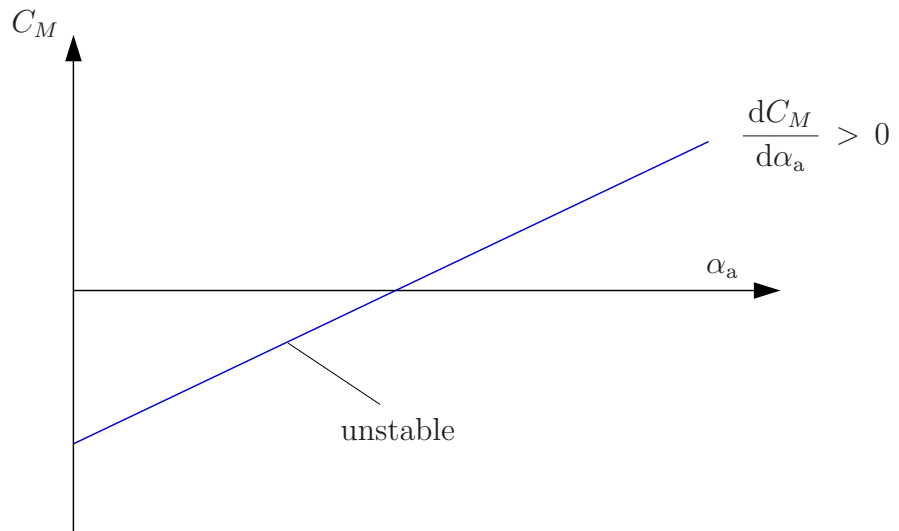
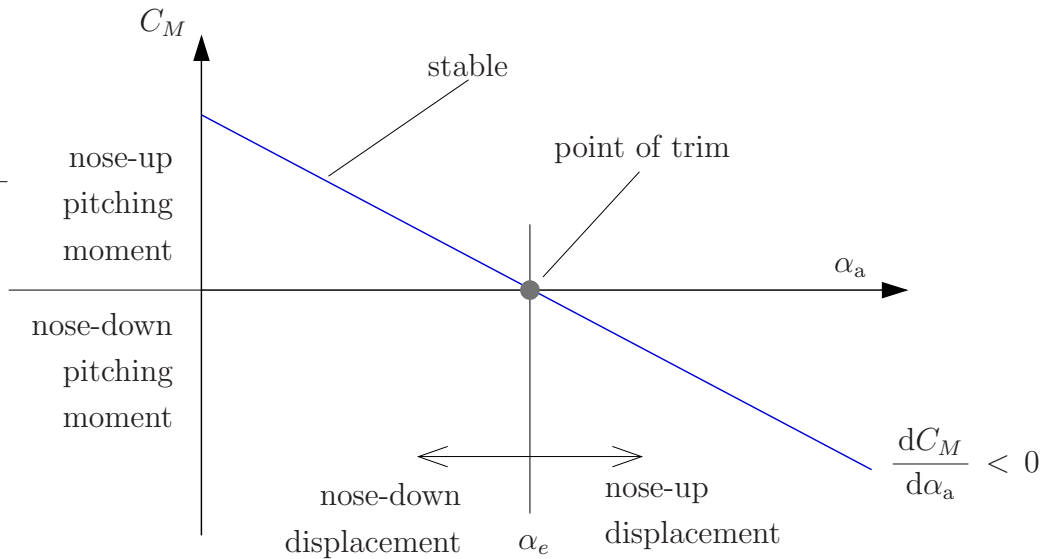


By means of wind tunnel tests, or by an analysis along the lines of the following pages, the pitching moment coefficient C_M can be represented as a function of the absolute angle of attack α_a . In the range of small α_a , this function is typically linear and shows one angle α_a for which C_M disappears. By definition, an increase of α_a corresponds to a nose-up rotation of the aeroplane with respect to the freestream velocity. For a stable configuration, that should generate a nose-down pitching moment, which returns the aeroplane to the undisturbed flight. Therefore, we conclude that a requirement for positive longitudinal stability is that the derivative $dC_M/d\alpha_a$ be negative, *i. e.*

$$\text{for longitudinal stability:} \quad \frac{dC_M}{d\alpha_a} < 0. \quad (3.3)$$

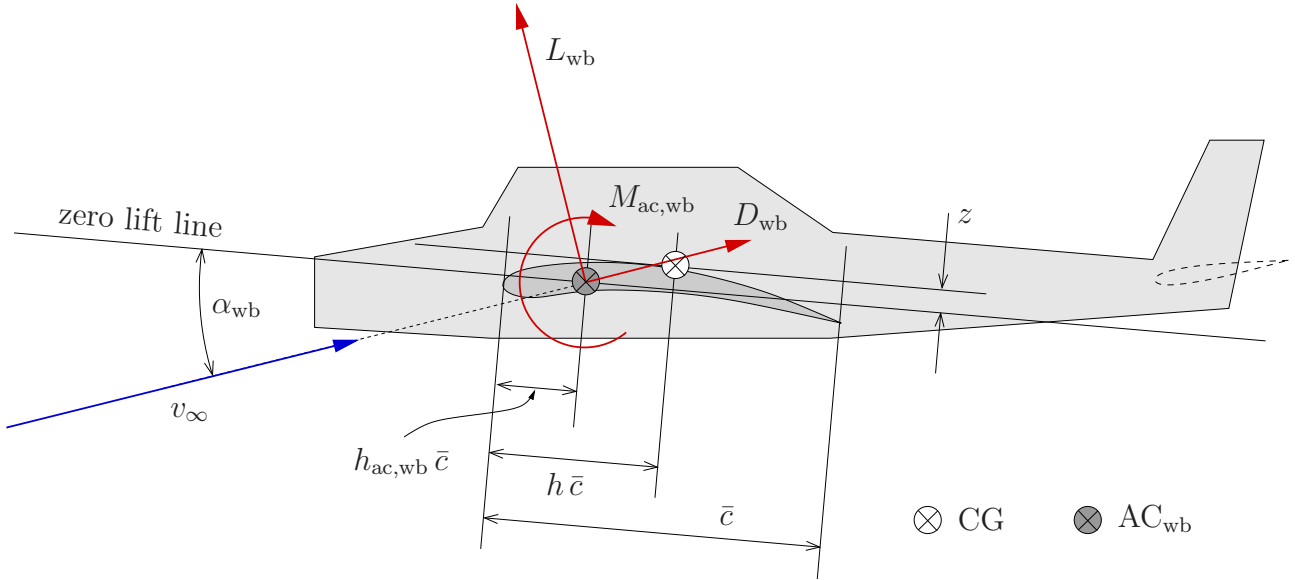
Steady and stable flight clearly requires $C_M = 0$. We say that for $C_M = 0$ the aeroplane is *trimmed*. The associated absolute angle of attack α_e is known as the *angle of trim*. With (3.3), it follows from $C_M = 0$ for some positive α_e that

$$\text{for longitudinal stability:} \quad C_M(\alpha_a = 0) > 0. \quad (3.4)$$



On the following pages, we derive an expression for C_M in terms of parameters which describe the configuration of the aeroplane. First, we will account for the contribution of the wings and the fuselage to the pitching moment, and second, we will study the contribution of the horizontal tail. The objective is to translate the conditions (3.3) and (3.4) for longitudinal stability into practical design requirements.

Contribution of Wings and Body to the Pitching Moment



The “body” of the aeroplane includes the fuselage and the engine nacelles. We then introduce the *aerodynamic centre of wing & body* AC_{wb} . Analogously to the aerodynamic centre of the airfoil as discussed in Section 1.8, this is the point with respect to which the aerodynamic moment $M_{ac,wb}$ is independent of the angle of attack. The angle α_{wb} denotes the absolute angle of attack for the wing & body combination. The quantities h and $h_{ac,wb}$ are dimensionless parameters and \bar{c} denotes the mean zero-lift chord also known as the *aerodynamic chord*. Note that h defines the location of the centre of gravity CG of the entire aeroplane.

The pitching moment of the wing & body combination with respect to the centre of gravity may then be written as

$$M_{cg,wb} = M_{ac,wb} + \bar{c} L_{wb} \cos \alpha_{wb} (h - h_{ac,wb}) + z L_{wb} \sin \alpha_{wb} - z D_{wb} \cos \alpha_{wb} + \bar{c} D_{wb} \sin \alpha_{wb} (h - h_{ac,wb}), \quad (3.5)$$

which we may divide by $S q_\infty \bar{c}$ to obtain

$$C_{M_{cg,wb}} = C_{M_{ac,wb}} + (h - h_{ac,wb}) C_{L_{wb}} \cos \alpha_{wb} + \frac{z}{\bar{c}} C_{L_{wb}} \sin \alpha_{wb} - \frac{z}{\bar{c}} C_{D_{wb}} \cos \alpha_{wb} + (h - h_{ac,wb}) C_{D_{wb}} \sin \alpha_{wb}. \quad (3.6)$$

Generally, the ratio z/\bar{c} is negligible and the angle of attack is small. With

$$\frac{z}{\bar{c}} \approx 0, \quad \sin \alpha_{wb} \approx 0, \quad \cos \alpha_{wb} \approx 1, \quad (3.7)$$

we may rewrite (3.6) as

$$C_{M_{cg,wb}} = C_{M_{ac,wb}} + (h - h_{ac,wb}) C_{L_{wb}}. \quad (3.8)$$

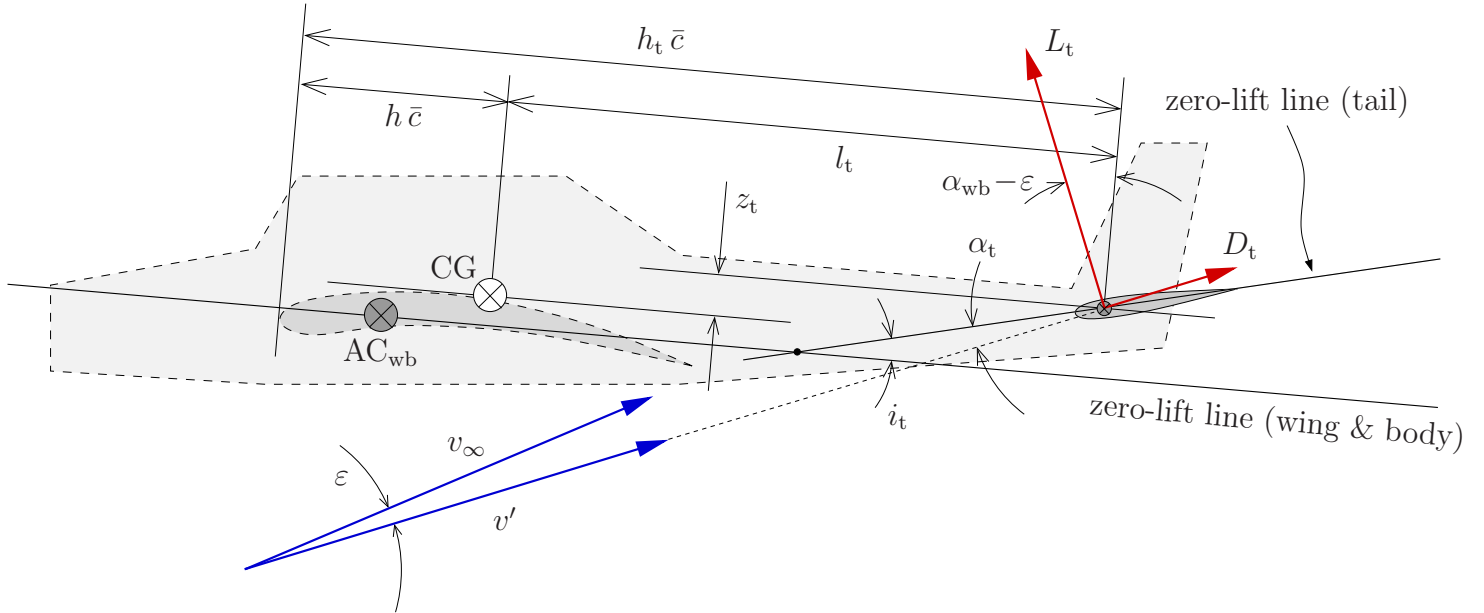
Using $C_{L_{wb}} = C_{L_{wb}\alpha} \alpha_{wb}$, with $C_{L_{wb}\alpha} = \frac{dC_{L_{wb}}}{d\alpha_{wb}}$, (3.9)

we obtain

$$C_{M_{cg,wb}} = C_{M_{ac,wb}} + (h - h_{ac,wb}) C_{L_{wb}\alpha} \alpha_{wb}. \quad (3.10)$$

The location of the aerodynamic centre as defined by $h_{ac,wb}$ and the parameters $C_{M_{ac,wb}}$ and $C_{L_{wb}}$ are usually determined by wind tunnel tests. Note that, for a wing with positive camber, the moment coefficient $C_{M_{ac,wb}}$ is generally negative.

Contribution of the Tail to the Pitching Moment



Generally, the aerodynamic moment $M_{ac,t}$ of the tail plane is negligible due to zero camber or due to the relatively small size of the tail. The angle i_t between the zero-lift lines of the wing & body combination and the horizontal tail is known as the *tail incidence angle*. The angle ε accounts for the downwash caused by the wing tip vortices. Due to the location of the tail plane behind the wings, this effect may be very pronounced and must not be neglected. The contribution of the tail to the moment $M_{cg,t}$ with respect to the centre of gravity is then obtained as

$$\begin{aligned} M_{cg,t} = & -l_t L_t \cos(\alpha_{wb} - \varepsilon) - z_t L_t \sin(\alpha_{wb} - \varepsilon) \\ & -l_t D_t \sin(\alpha_{wb} - \varepsilon) + z_t D_t \cos(\alpha_{wb} - \varepsilon). \end{aligned} \quad (3.11)$$

Division by $q_\infty S \bar{c}$ gives

$$\begin{aligned} C_{M_{cg,t}} = & -\frac{l_t S_t}{\bar{c} S} C_{L_t} \cos(\alpha_{wb} - \varepsilon) - \frac{z_t S_t}{\bar{c} S} C_{L_t} \sin(\alpha_{wb} - \varepsilon) \\ & -\frac{l_t S_t}{\bar{c} S} C_{D_t} \sin(\alpha_{wb} - \varepsilon) + \frac{z_t S_t}{\bar{c} S} C_{D_t} \cos(\alpha_{wb} - \varepsilon). \end{aligned} \quad (3.12)$$

With $\frac{z_t}{\bar{c}} \approx 0$, $\sin(\alpha_{wb} - \varepsilon) \approx 0$, $\cos(\alpha_{wb} - \varepsilon) \approx 1$, (3.13)

it follows that $C_{M_{cg,t}} = -\frac{l_t}{\bar{c}} \frac{S_t}{S} C_{L_t}$. (3.14)

The factor multiplying C_{L_t} in (3.14), which quantifies the effect of the tail, is known as the *horizontal tail volume* V_H , *i. e.*

$$C_{M_{cg,t}} = -V_H C_{L_t}, \quad \text{and} \quad V_H = \frac{l_t}{\bar{c}} \frac{S_t}{S}. \quad (3.15)$$

It is important to understand that V_H is not a purely geometrical parameter, but it depends on the location of the centre of gravity h . For the sake of clarity, we therefore rewrite (3.14) as

$$C_{M_{cg,t}} = -(h_t - h) \frac{S_t}{S} C_{L_t}. \quad (3.16)$$

The angle of attack α_t may be expressed as

$$\alpha_t = \alpha_{wb} - \varepsilon - i_t. \quad (3.17)$$

Due to the linear relations between angle of attack and lift coefficient (1.23) and between lift coefficient and induced angle of attack (1.29), we can assume a linear variation of ε with the absolute angle of attack α_{wb} , *i. e.*

$$\varepsilon = \varepsilon_\alpha \alpha_{wb}, \quad (3.18)$$

where $\varepsilon_\alpha = d\varepsilon/d\alpha$ can be determined by means of wind tunnel tests. The lift coefficient C_{L_t} can then be expressed as

$$C_{L_t} = C_{L_{t\alpha}} \alpha_{wb} = C_{L_{t\alpha}} \left((1 - \varepsilon_\alpha) \alpha_{wb} - i_t \right), \quad (3.19)$$

and (3.16) becomes

$$C_{M_{cg,t}} = -(h_t - h) \frac{S_t}{S} C_{L_{t\alpha}} \left((1 - \varepsilon_\alpha) \alpha_{wb} - i_t \right). \quad (3.20)$$

Note that due to the orientation of a positive tail incidence i_t the term $C_{L_{t\alpha}} i_t$ corresponds to a tail lift force which is directed downwards, whereas the term $C_{L_{t\alpha}} \alpha_{wb}$ with $\alpha_{wb} > 0$ is associated with a tail lift force that is directed upwards.

The Total Pitching Moment

The total pitching moment coefficient $C_{M_{cg}}$ is obtained from adding up the contributions of the wing & body and the tail.

$$C_{M_{cg}} = C_{M_{cg,wb}} + C_{M_{cg,t}} . \quad (3.21)$$

The expressions (3.10) and (3.20) for $C_{M_{cg,wb}}$ and $C_{M_{cg,t}}$, respectively, involve the absolute angle of attack of the wing & body combination α_{wb} . Based on the negligible influence of the tail on the orientation of the zero-lift line of the entire aeroplane, we may replace α_{wb} by the absolute angle of attack of the entire aeroplane α_a . Henceforth, for the sake of notational brevity, we also omit the subscript “cg”. Using (3.10), (3.20) and $\alpha_{wb} = \alpha_a$ we may rewrite (3.21) as

$$C_M = C_{M_{ac,wb}} + (h - h_{ac,wb}) C_{L_{wb}\alpha} \alpha_a - (h_t - h) \frac{S_t}{S} C_{L_t\alpha} \left((1 - \varepsilon_\alpha) \alpha_a - i_t \right) ,$$

or shorter,

$$C_M = C_{M_0} + C_{M_\alpha} \alpha_a , \quad (3.22)$$

with

$$C_{M_0} = C_{M_{ac,wb}} + (h_t - h) \frac{S_t}{S} C_{L_t\alpha} i_t \quad (3.23)$$

$$C_{M_\alpha} = (h - h_{ac,wb}) C_{L_{wb}\alpha} - (h_t - h) \frac{S_t}{S} C_{L_t\alpha} (1 - \varepsilon_\alpha) . \quad (3.24)$$

The Equations (3.22) – (3.24) express the pitching moment coefficient in terms of the location of the centre of gravity and in terms of some aerodynamic coefficients.

We now recall the requirement (3.4) for longitudinal stability and consider an aeroplane subjected to airflow at an absolute angle of attack equal to zero. The pitching moment coefficient then reduces to C_{M_0} . The condition (3.4) then requires that $C_{M_0} > 0$. For positively cambered wings we have $C_{M_{ac,wb}} < 0$. Thus, it follows from (3.23) that we can ensure that $C_{M_0} > 0$ by providing a sufficiently large positive tail incidence i_t (and tail volume). It is important to understand that this corresponds to a tail lift force which is directed downwards.

We conclude from (3.24) that the requirement (3.3), *i. e.* $C_{M_\alpha} < 0$, can be satisfied simply by providing sufficient tail volume.

Total Lift, Neutral Point and Static Margin

As a preliminary, we begin this subsection by considering the total lift of the aeroplane. Adding the contributions of wing & body and tail, we may write

$$\begin{aligned} L &= q S \left(C_{L_{wb}} + \frac{S_t}{S} C_{L_t} \right) = q S \left(C_{L_{wb}\alpha} \alpha_a + \frac{S_t}{S} C_{L_t\alpha} \alpha_t \right) \\ &= q S \left(\left(C_{L_{wb}\alpha} + \frac{S_t}{S} C_{L_t\alpha} (1 - \varepsilon_\alpha) \right) \alpha_a - \frac{S_t}{S} C_{L_t\alpha} i_t \right), \end{aligned} \quad (3.25)$$

where we have used (3.17) to eliminate α_t . The total lift coefficient may then be expressed as

$$C_L = C_{L0} + C_{L\alpha} \alpha_a \quad (3.26)$$

$$\text{with} \quad C_{L0} = -\frac{S_t}{S} C_{L_t\alpha} i_t, \quad C_{L\alpha} = C_{L_{wb}\alpha} + \frac{S_t}{S} C_{L_t\alpha} (1 - \varepsilon_\alpha). \quad (3.27)$$

Analogously to the airfoil or the wing & body combination, there exists a location with respect to which the total pitching moment of the aeroplane is independent of the angle of attack. This point corresponds to the aerodynamic centre of the entire aeroplane and it is known as the *neutral point* NP. Its location is denoted by the parameter h_n , such that $h_n \bar{c}$ is the distance between the leading edge of the wing and the neutral point. In (3.22) – (3.24), the parameter h denotes the location of the point of reference for the pitching moment. Therefore, h_n can be calculated by equating $C_{M\alpha}$ in (3.24) to zero and by replacing h with h_n . We obtain

$$0 = (h_n - h_{ac,wb}) C_{L_{wb}\alpha} - (h_t - h_n) \frac{S_t}{S} C_{L_t\alpha} (1 - \varepsilon_\alpha), \quad (3.28)$$

which renders

$$h_n = \frac{h_{ac,wb} C_{L_{wb}\alpha} + h_t \frac{S_t}{S} C_{L_t\alpha} (1 - \varepsilon_\alpha)}{C_{L_{wb}\alpha} + \frac{S_t}{S} C_{L_t\alpha} (1 - \varepsilon_\alpha)}. \quad (3.29)$$

With (3.27)₂ we can rewrite (3.29) as

$$h_n = \frac{1}{C_{L\alpha}} \left(h_{ac,wb} C_{L_{wb}\alpha} + h_t \frac{S_t}{S} C_{L_t\alpha} (1 - \varepsilon_\alpha) \right). \quad (3.30)$$

In some textbooks, the difference between the lift slopes $C_{L\alpha}$ and $C_{L_{wb}\alpha}$ is neglected (the effect of the tail is small). If we also ignore the dependency of the tail volume V_H on h , *i. e.* $h \ll h_t$ and $V_H \approx h_t S_t/S$ (see (3.15) and diagram on page 101), then we may rewrite (3.30) as

$$h_n = h_{ac,wb} + V_H \frac{C_{L_t\alpha}}{C_{L\alpha}} (1 - \varepsilon_\alpha) . \quad (3.31)$$

Based on the expression for $C_{L\alpha}$ in (3.27)₂ we can also rewrite (3.24) as

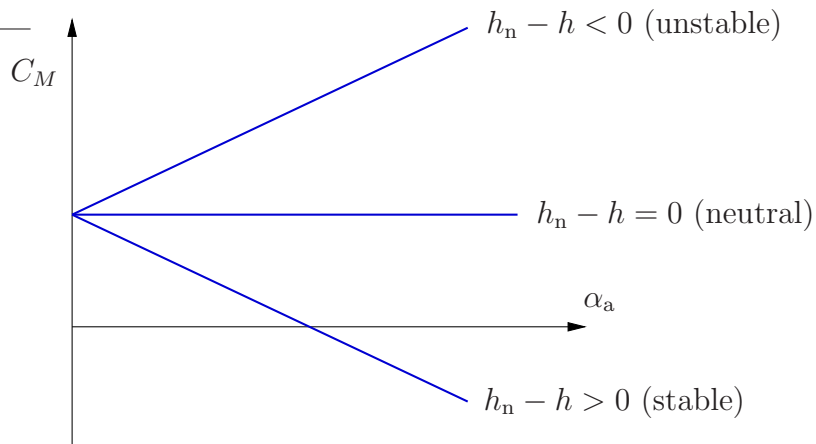
$$C_{M\alpha} = h C_{L\alpha} - \left(h_{ac,wb} C_{L_{wb}\alpha} + h_t \frac{S_t}{S} C_{L_t\alpha} (1 - \varepsilon_\alpha) \right) , \quad (3.32)$$

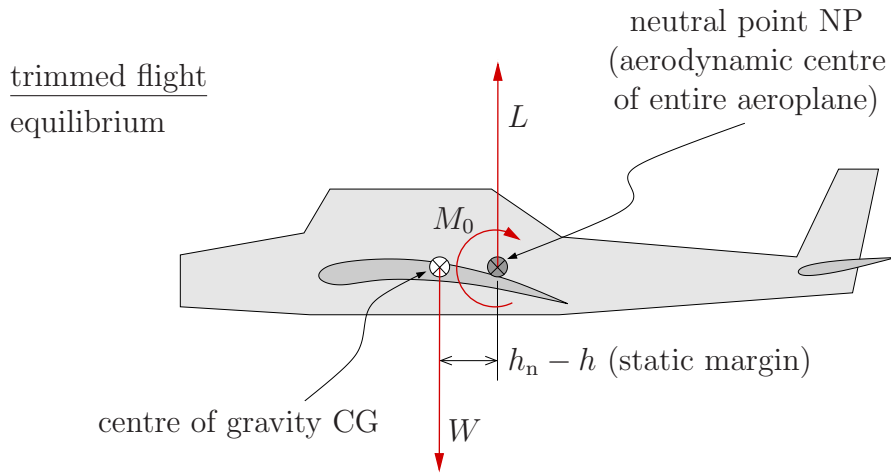
Using (3.30) to simplify (3.32) renders

$$C_{M\alpha} = (h - h_n) C_{L\alpha} . \quad (3.33)$$

This important result states that the slope $C_{M\alpha}$ of the moment curve is equal to the slope of the lift curve $C_{L\alpha}$ multiplied by the dimensionless distance of the centre of gravity behind the neutral point. According to (3.3), for static stability, $C_{M\alpha}$ must be negative. *Therefore, for a statically stable aeroplane the centre of gravity must be located ahead of the neutral point.*

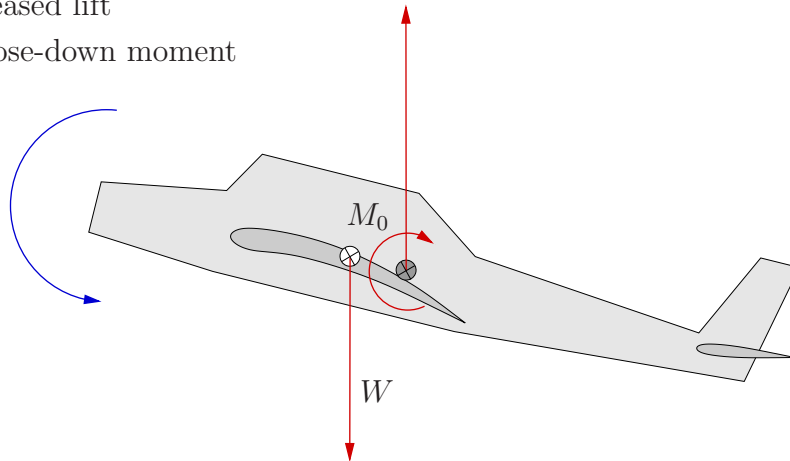
The quantity $h_n - h$ is known as the *static margin* SM, which must be positive to ensure static stability. Adequate static stability is achieved if the static margin is at least 5%.





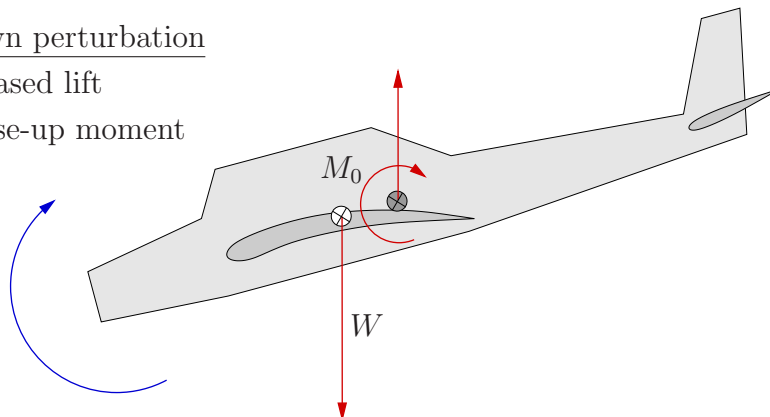
nose-up perturbation

- increased lift
- nose-down moment



nose-down perturbation

- decreased lift
- nose-up moment



Special Configurations

T-tail configuration: In a classically configured aeroplane, the horizontal tail is much smaller than the wings and therefore relatively close to the fuselage. Typically, a significant part of the tail is located inside the boundary layer of the fuselage. Due to skin friction, the airflow inside this boundary layer is slower than further away from the fuselage. This effect can be accounted for by introducing the *tail efficiency factor* η , *i. e.*

$$q_t = \eta q_\infty \quad \text{with} \quad \eta \leq 1, \quad (3.34)$$

where q_t is the dynamic pressure at the leading edge of the tail surface. For the *T-tail* configuration, we have $\eta = 1$. In these notes, we assume for simplicity that always $\eta = 1$.

Canard configuration: It follows from (3.23) that C_{M0} is positive only if the tail generates a lift force which is directed downwards. This may seem impractical with respect to the total lift, *i. e.* the lift of the wings has to counterbalance not only the weight but also the downward lift of the tail. Therefore, on some aeroplanes, the horizontal stabilisers are located ahead of the wings. Such horizontal stabilisers are known as *Canard surfaces*. The Canard surfaces generate upward lift which causes a positive pitching moment increment equivalent to the moment generated by the downward lift of a horizontal tail. Thus, the Canard surfaces stabilise the aeroplane and at the same time contribute to the total aeroplane lift.

A significant disadvantage of a Canard configuration is that the airflow over the wings is disturbed by the wake of the Canard surfaces. This adversely affects the generation of lift of the wings.

3.4 Longitudinal Control

Consider an aeroplane in trimmed configuration at straight level and unaccelerated flight. In order to fly faster, the pilot needs to increase the throttle setting and to reduce the angle of attack. In order to fly more slowly, he must reduce the throttle setting and increase the angle of attack. According to (3.22) the pitching moment depends exclusively on the aeroplane geometry and on the absolute angle of attack α_a . Therefore, the variation of α_a will lead to the loss of trim, unless the aeroplane geometry is changed to achieve trim for the new angle of attack. Two different strategies are available:

- *shifting the centre of gravity.*

Clearly this is impractical for complex aeroplanes. However, for simply configured sailplanes or gliders without control surfaces this is a viable strategy. It is discussed in more detail on the next page.

- *adjusting the tail plane configuration.*

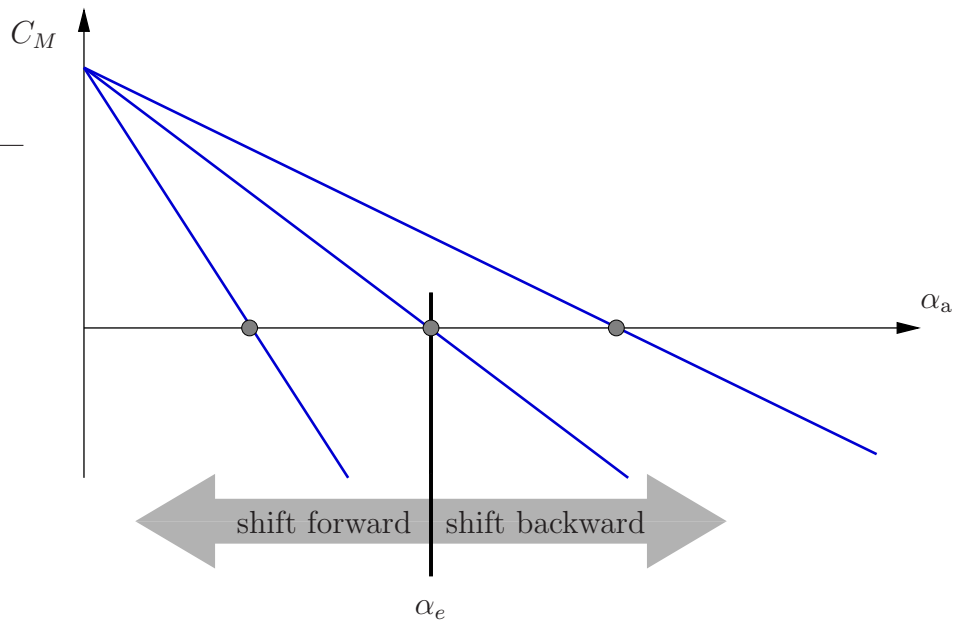
By adjusting the lift of the horizontal tail plane the total pitching moment may be reduced to zero such that the aeroplane is trimmed again. We distinguish different tail plane configurations, such as the *all moveable tail*, the *horizontal stabiliser-elevator* configuration or the *stabilator*, which are discussed on the following pages.

Shifting the Centre of Gravity

In order to study the effect of shifting the centre of gravity on the $C_M - \alpha_a$ diagram, we first assume

$$h \ll h_t \rightarrow \frac{h_t - h}{h_t} \approx 1 \rightarrow h_t - h \approx h_t. \quad (3.35)$$

It then follows from (3.22) – (3.24) that shifting the centre of gravity forward results in a smaller angle of trim α_e , whereas a backward shift increases α_e .



All-Movable Tail

In this configuration, the tail incidence i_t can be controlled by the pilot. In order to express the tail incidence associated with trim in terms of the total lift coefficient C_L (which easily relates to the freestream velocity by (2.5)) we note that (3.22) and (3.26) may be written, respectively, as

$$C_M = C_{M_{ac,wb}} + C_{M_i} i_t + C_{M_\alpha} \alpha_a \quad (3.36)$$

$$C_L = C_{L_i} i_t + C_{L_\alpha} \alpha_a, \quad (3.37)$$

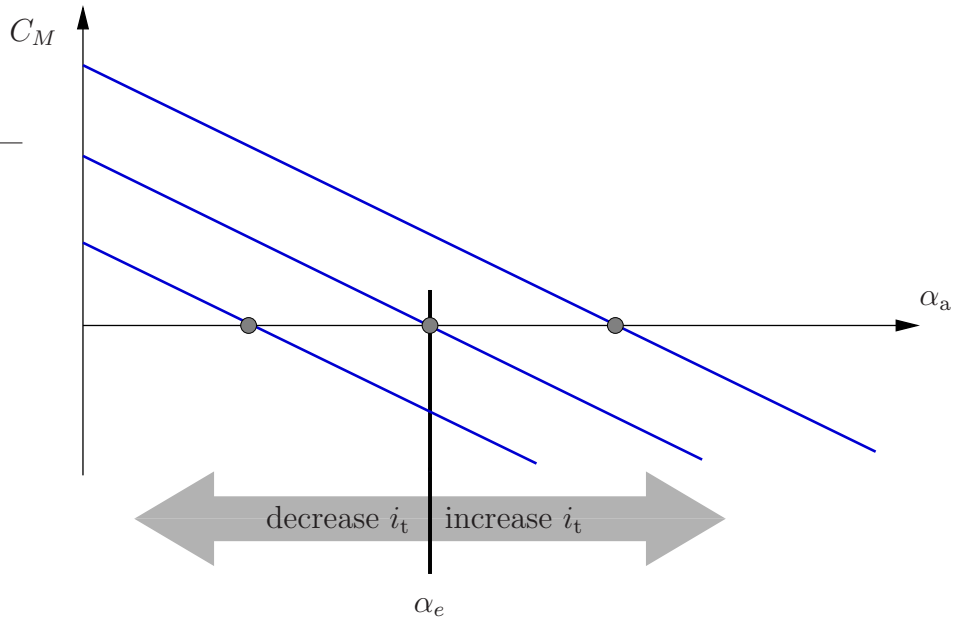
where

$$C_{M_i} = (h_t - h) \frac{S_t}{S} C_{L_t\alpha} \quad (3.38)$$

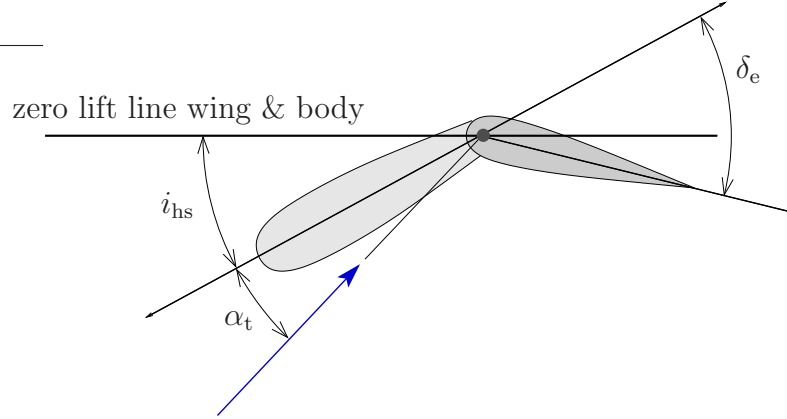
$$C_{L_i} = -\frac{S_t}{S} C_{L_t\alpha}. \quad (3.39)$$

Using (3.37) to eliminate α_a in (3.36), we obtain

$$i_t = -\frac{C_{M_{ac,wb}} C_{L_\alpha} + C_{M_\alpha} C_L}{C_{L_\alpha} C_{M_i} - C_{M_\alpha} C_{L_i}}. \quad (3.40)$$



Tail with Elevators



Recalling the discussion of flaps in Section 1.9, we conclude from (1.24)

$$C_{L_t} = C_{L_t\alpha} (\alpha_t + \tau \delta_e), \quad (3.41)$$

where τ is the effectiveness factor of the elevator flap. Setting the right hand side of (3.41) to zero, we find the angle $\alpha_{t,L=0} = -\tau \delta_e$, which renders zero lift and therefore defines the orientation of the zero lift line of the tail. The sum of $\alpha_{t,L=0}$ and the incidence i_{hs} of the fixed horizontal stabiliser corresponds to the tail incidence i_t in (3.36) and (3.37), which describes the zero lift line of the total tail, *i. e.*

$$i_t = i_{hs} - \tau \delta_e. \quad (3.42)$$

We may now use (3.42) in (3.36) and (3.37) to replace i_t . Next, we eliminate α_a , set C_M to zero and solve the resulting equation for δ_e . We obtain

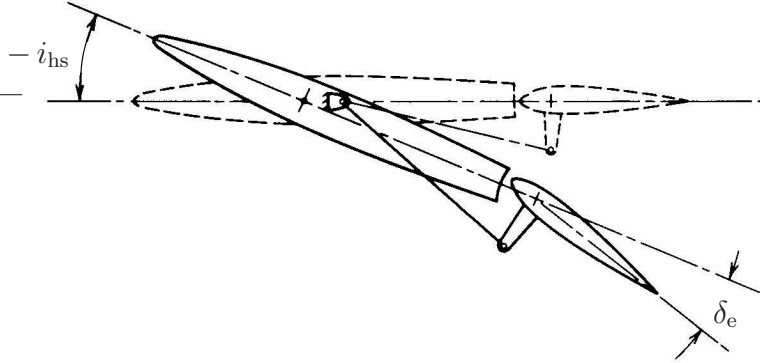
$$\delta_e = -\frac{C_{M_{ac,wb}} C_{L\alpha} + C_{M\alpha} C_L}{C_{L\alpha} C_{M\delta} - C_{M\alpha} C_{L\delta}} + \frac{i_{hs}}{\tau}, \quad (3.43)$$

which defines the elevator deflection, that renders trimmed flight for a given total lift coefficient C_L . The new expressions in (3.43) are defined as

$$C_{M\delta} = -\tau C_{M_i} = -\tau (h_t - h) \frac{S_t}{S} C_{L_t\alpha} \quad (3.44)$$

$$C_{L\delta} = -\tau C_{L_i} = \tau \frac{S_t}{S} C_{L_t\alpha}. \quad (3.45)$$

Stabilator



The stabilator configuration may be regarded as a horizontal stabiliser with an elevator, whereby the incidence i_{hs} of the stabiliser is variable. Furthermore, the elevator is linked to the fuselage as shown in the diagram. The elevator deflection is thus dependent on the incidence i_{hs} , *i. e.*

$$\delta_e = k_e i_{hs} + \delta_0 , \quad (3.46)$$

where k_e is the *linkage factor*. Using (3.46) in (3.42), we obtain

$$i_t = i_{hs} (1 - \tau k_e) - \tau \delta_0 . \quad (3.47)$$

Following the same procedure as for the fixed stabiliser-elevator configuration, we use (3.47) in (3.36) and (3.37) to replace i_t . We eliminate α_a , set C_M to zero and solve the resulting equation for i_{hs} . We thus obtain

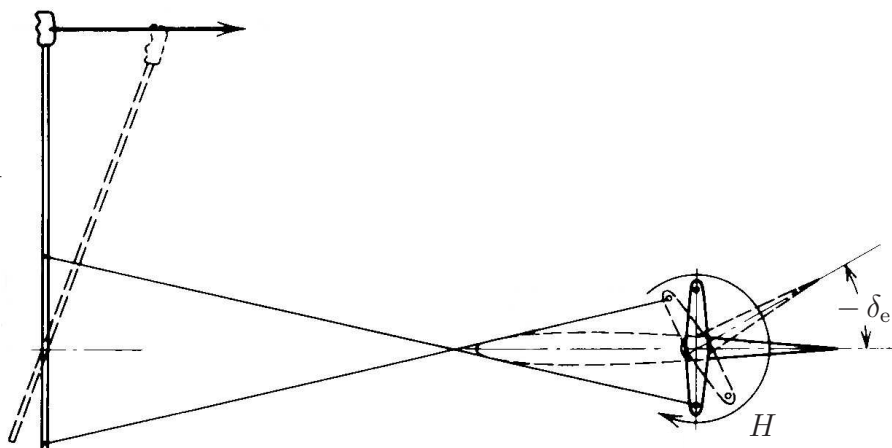
$$i_{hs} = - \frac{C_{M_{ac,wb}} C_{L\alpha} + C_{M\alpha} C_L}{C_{L\alpha} C_{Mi} - C_{M\alpha} C_{Li}} \frac{1}{1 - \tau k_e} + \frac{\tau \delta_0}{1 - \tau k_e} , \quad (3.48)$$

which defines the stabiliser incidence, that renders trimmed flight for a given total lift coefficient C_L .

The linkage factor k_e is independent of aerodynamics and depends only on the mechanical linkage of the elevator to the fuselage. It follows from (3.48) that a negative k_e increases the tail effectiveness in the sense of requiring smaller variations of i_{hs} to trim the aeroplane for a different velocity (angle of attack).

3.5 Stick-Free Longitudinal Static Stability

In large aeroplanes, hydraulic systems are commonly used to hold the moveable control surfaces in the desired position. However, small light aircraft, older ones as well as modern ones, are equipped with simple mechanical gear systems, which the pilot has to operate by means of sticks or wheels. These systems must be designed such that, for each point within the flight envelope ($V - n$ diagram), the forces and moments to be applied by the pilot lie within acceptable limits. It is the gear systems which can give proper “feel” to the pilot. “Elevator-down”, for example, should be associated with a push-forward of the stick (decrease angle of attack, accelerate), whereas “elevator-up” should be achieved by a pull-back of the stick (increase angle of attack, decelerate).



We have seen that the elevator angle of trim or the tail incidence of trim (moveable tails, stabilators) vary with the flight velocity. A mechanical gear system would therefore require that the pilot permanently holds on to the stick and exerts a force to keep it in the right position associated with trim for the desired velocity. This is clearly very impractical. Therefore, we will, in the following, consider what happens when the stick is left free, *i. e.* when the elevator is “floating”.

Tail with Elevators

For the horizontal stabiliser-elevator configuration, the *elevator hinge moment* H may be expressed as

$$H = \frac{1}{2} \rho v_\infty^2 S_e \bar{c}_e C_H, \quad (3.49)$$

where S_e and \bar{c}_e denote, respectively, the surface area of the elevator and the mean chord of the elevator. For symmetrical sections, the *hinge moment coefficient* C_H depends only on the angle of attack and on the elevator deflection and may be written as

$$C_H = C_{H\alpha} \alpha_t + C_{H\delta} \delta_e. \quad (3.50)$$

The coefficients $C_{H\alpha}$ and $C_{H\delta}$ correspond to the derivatives of C_H and are constant. If the elevator is floating, then the *hinge moment* is zero and (3.50) may be solved for δ_e to give

$$\delta_e = - \frac{C_{H\alpha}}{C_{H\delta}} \alpha_t. \quad (3.51)$$

Using (3.51) in (3.41) renders

$$C'_{L_t} = C_{L_t\alpha} \left(1 - \tau \frac{C_{H\alpha}}{C_{H\delta}} \right) \alpha_t, \quad (3.52)$$

where C'_{L_t} denotes the *stick-free tail lift coefficient*. The factor

$$F_e = 1 - \tau \frac{C_{H\alpha}}{C_{H\delta}} \quad (3.53)$$

is known as the *free elevator factor* and, for the configuration under consideration, $F_e < 1$. Thus, the floating elevator basically renders a new, smaller slope of the tail lift curve

$$C'_{L_t\alpha} = C_{L_t\alpha} F_e < C_{L_t\alpha}. \quad (3.54)$$

If we use $C'_{L_t\alpha}$ rather than $C_{L_t\alpha}$ and repeat the derivation of the location of the neutral point along the lines of Section 3.3, then we obtain the location of the *stick-free neutral point* h'_n as

$$h'_n = \frac{h_{ac,wb} C_{L_{wb}\alpha} + h_t \frac{S_t}{S} C_{L_t\alpha} F_e (1 - \varepsilon_\alpha)}{C_{L_{wb}\alpha} + \frac{S_t}{S} C_{L_t\alpha} F_e (1 - \varepsilon_\alpha)}. \quad (3.55)$$

Following the simplifying assumptions which lead to (3.31), we may write

$$h'_n = h_{ac,wb} + F_e V_H \frac{C_{L_t \alpha}}{C_{L \alpha}} (1 - \varepsilon_\alpha). \quad (3.56)$$

We may then formulate the criteria for *stick-free* longitudinal static stability

$$C_{M'_\alpha} = (h - h'_n) C_{L'_\alpha} < 0, \quad (3.57)$$

where $h'_n - h$ is the *stick-free* static margin. We conclude from (3.56) that, for $F_e < 1$, this is smaller than the *stick-fixed* static margin. Therefore, the longitudinal stability of an aeroplane with an elevator tail degrades as the stick is freed.

Stabilator and Stick-Free Trim

For the stabilator tail, we introduce a hinge moment coefficient C_H similar to the one for the elevator in (3.50),

$$C_H = C_{H\alpha} \alpha_t + C_{H\delta} \delta_e . \quad (3.58)$$

For the calculation of the free elevator factor F_e of the stabilator tail, we have to work with the absolute angle of attack α_a of the entire aeroplane since α_t is measured with respect to i_{hs} and i_{hs} is variable. With $\alpha_{wb} \approx \alpha_a$ and $i_t = i_{hs}$ the equation (3.17) for the tail angle of attack can be written as

$$\alpha_t = \alpha_a (1 - \varepsilon_\alpha) - i_{hs} . \quad (3.59)$$

Also, we recall (3.41) and (3.46), *i. e.*

$$C_{L_t} = C_{L_t\alpha} (\alpha_t + \tau \delta_e) \quad (3.60)$$

$$\delta_e = k_e i_{hs} + \delta_0 . \quad (3.61)$$

Setting C_H equal to zero and eliminating α_t , δ_e and i_{hs} renders, after some lengthy manipulation,

$$C'_{L_t} = C_{L_t\alpha} \left((1 - \varepsilon_\alpha) \left(1 - \frac{(1 - \tau k_e) C_{H\alpha}}{C_{H\alpha} - C_{H\delta} k_e} \right) \alpha_a + \frac{\tau C_{H\alpha} - C_{H\delta}}{C_{H\alpha} - C_{H\delta} k_e} \delta_0 \right) . \quad (3.62)$$

Thus, we obtain for the stick-free case

$$\frac{\partial C'_{L_t}}{\partial \alpha_a} = C_{L_t\alpha} (1 - \varepsilon_\alpha) \left(1 - \frac{(1 - \tau k_e) C_{H\alpha}}{C_{H\alpha} - C_{H\delta} k_e} \right) . \quad (3.63)$$

The comparison with

$$\frac{\partial C_{L_t}}{\partial \alpha_a} = C_{L_t\alpha} (1 - \varepsilon_\alpha) \quad (3.64)$$

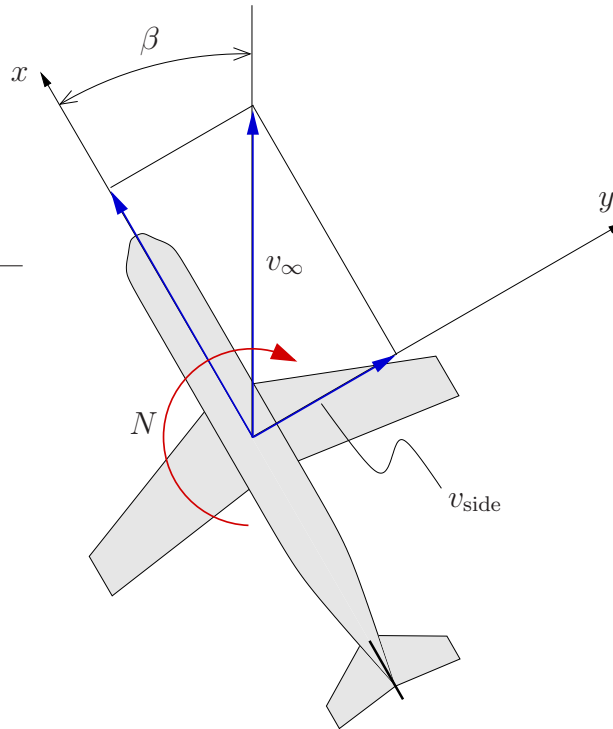
for the stick-fixed case renders the free elevator factor F_e for the stabilator tail as

$$F_e = 1 - \frac{(1 - \tau k_e) C_{H\alpha}}{C_{H\alpha} - C_{H\delta} k_e} . \quad (3.65)$$

It is a straightforward exercise to show that (3.55) – (3.57) also hold for the aeroplane with a stabilator tail. In most stabilator configurations, we find that k_e and $C_{H\delta}$ are negative whereas $C_{H\alpha}$ is always positive. Provided that $C_{H\alpha} < C_{H\delta} k_e$, we therefore get $F_e > 1$. Consequently, the longitudinal stability is improved by freeing the stick!

The linkage of the stabilator tail to the fuselage (k_e and δ_0) can be designed such that the aeroplane, flown with a free stick, always trims itself whenever the flight velocity is changed. For different locations of the centre of gravity, trim can be achieved by moving the attachment point of the link to the fuselage.

3.6 Directional Static Stability and Control

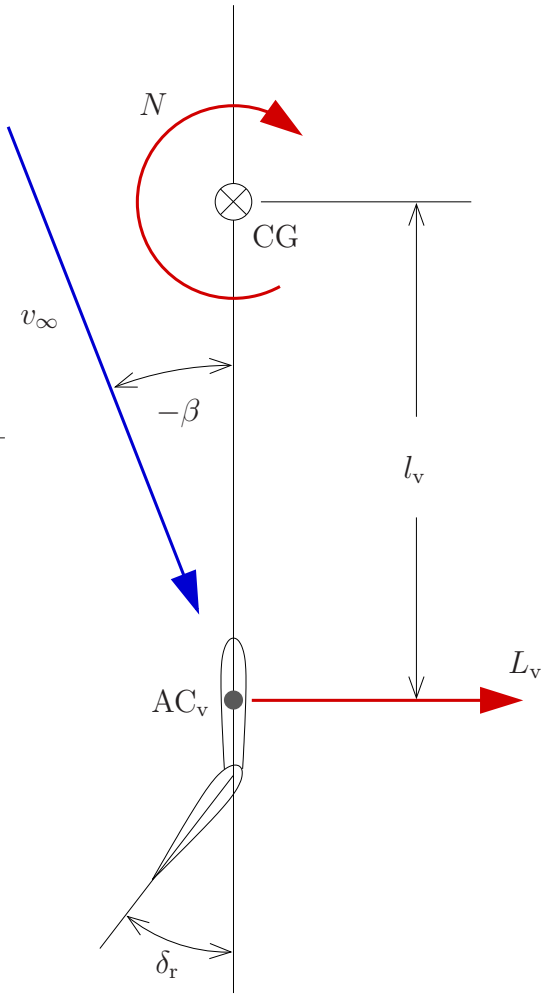


We define the *sideslip angle* β as illustrated. Furthermore, we introduce the yawing moment coefficient C_N by writing

$$N = q_\infty S b C_N . \quad (3.66)$$

For static stability, a perturbation β must generate a restoring positive yawing moment N . Therefore, directional static stability requires that

$$\frac{\partial C_N}{\partial \beta} = C_{N\beta} > 0 . \quad (3.67)$$



In the following we neglect the contribution of the wings & body to the yawing moment. The moment N is then generated by the lift force L_v of the vertical tail and we may write

$$N = -l_v L_v . \quad (3.68)$$

With

$$L_v = q_\infty S_v C_{L_v} \quad (3.69)$$

and

$$C_{L_v} = C_{L_{v\alpha}} (-\beta + \tau \delta_r) \quad (3.70)$$

we obtain

$$N = l_v q_\infty S_v C_{L_{v\alpha}} (\beta - \tau \delta_r) . \quad (3.71)$$

The comparison with (3.66) renders

$$C_N = \frac{l_v}{b} \frac{S_v}{S} C_{L_{v\alpha}} (\beta - \tau \delta_r) . \quad (3.72)$$

Note that the first two terms in (3.72) are known as the *vertical tail volume*

$$V_V = \frac{l_v}{b} \frac{S_v}{S} . \quad (3.73)$$

We may then define the constant coefficients

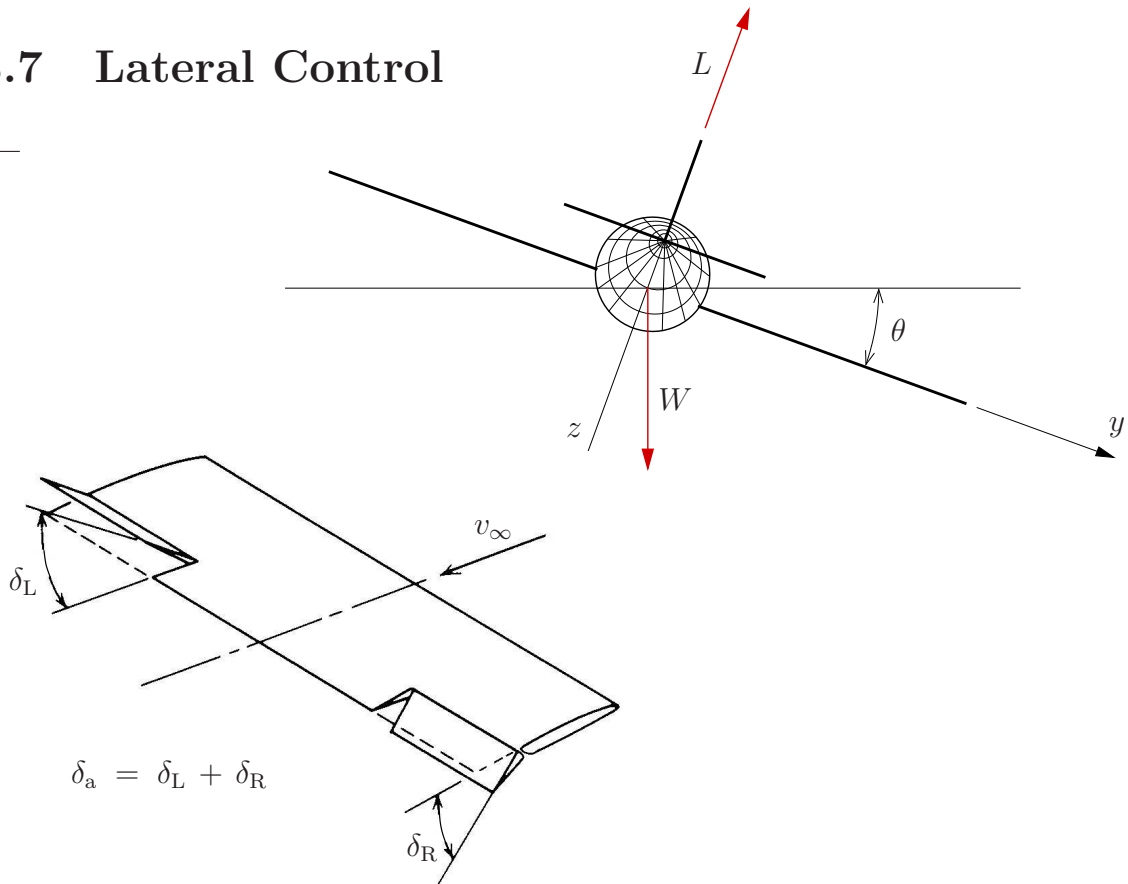
$$C_{N\beta} = \frac{l_v}{b} \frac{S_v}{S} C_{L_{v\alpha}} \quad (3.74)$$

and

$$C_{N\delta} = -\frac{l_v}{b} \frac{S_v}{S} C_{L_{v\alpha}} \tau . \quad (3.75)$$

It follows from (3.67) that the desired amount of directional stability can be achieved by choosing a sufficiently large tail volume V_V .

3.7 Lateral Control



The aeroplane can be rolled, *i. e.* the bank angle θ can be controlled, by deflecting the ailerons as illustrated. The aileron deflection δ_a is defined as the angle between the left and the right ailerons. The diagram shows positive aileron deflection (left aileron up, right aileron down).

The rolling moment L (not to be confused with the lift force!) may be expressed as

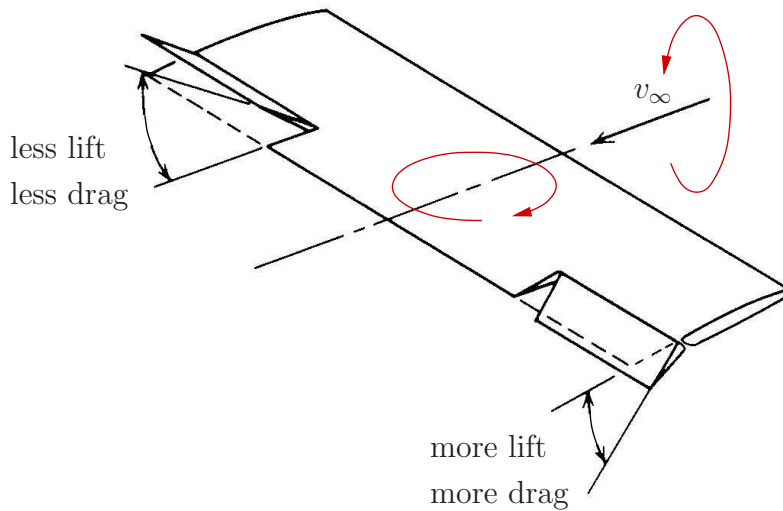
$$L = q_\infty S b C_l, \quad (3.76)$$

where C_l (lower case “l” to avoid confusion with lift coefficient) denotes the rolling moment coefficient. Since the ailerons represent the only direct mechanism to control roll, we have

$$C_l = C_{l\delta} \delta_a. \quad (3.77)$$

Note that for $\delta_a = 0$ the rolling moment disappears. Thus, a perturbation $\theta \neq 0$ generates neither a restoring nor a diverging rolling moment. The lateral static stability is neutral (be, however, aware of the *dihedral effect* discussed on page 127).

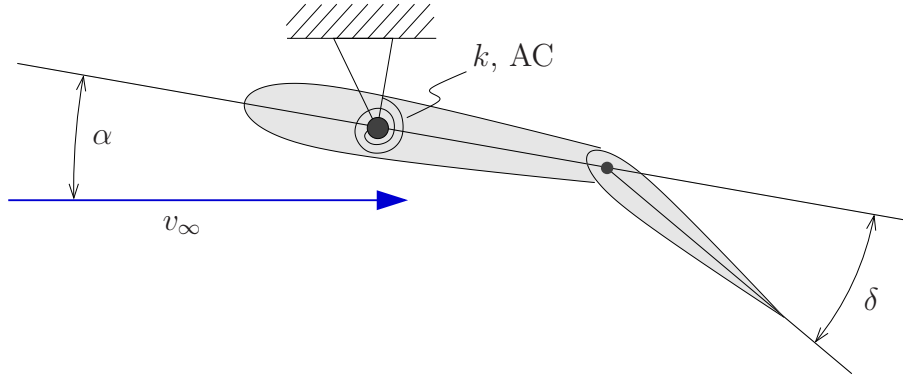
Adverse Yaw



Due to the effect of the aileron deflections on induced drag, a positive antisymmetric aileron deflection, which is intended to initiate a level left turn, generates an undesired positive yawing moment forcing the nose to the right. This phenomena is known as *adverse yaw*.

Adverse yaw can be reduced by applying asymmetric aileron deflection, such that the upward deflection on one side is larger than the downward deflection on the other (typically twice as big). This can be achieved by appropriately designed mechanical gearing systems and reduces the drag differential significantly. The parameter δ_a controlled by the pilot corresponds to the angle between the left and the right aileron and is not affected by the mechanical linkage.

Aileron Reversal



Consider a symmetric airfoil, supported in the aerodynamic centre by a rotational spring, with a flap. This experimental set-up is representative of the section of a wing near the wing tip. The stiffness of the spring corresponds to the torsional stiffness of the wing. If the spring (the wing) is rigid, then the positive deflection of the flap will generate lift. In the following we study the situation with $k < \infty$.

Due to the symmetry of the airfoil the pitching moment coefficient C_m is nonzero only for $\delta \neq 0$, *i. e.*

$$C_m = C_{m0} + C_{m\alpha} \alpha + C_{m\delta} \delta \quad (3.78)$$

with
$$C_{m0} = 0, \quad C_{m\alpha} = 0, \quad C_{m\delta} < 0. \quad (3.79)$$

The rotational displacement of the spring is equal to the angle of attack α . The internal moment of the structure must be in equilibrium with the aerodynamic loading. Rotational equilibrium formulated with respect to the support point may be written as

$$k \alpha = q_\infty c^2 C_{m\delta} \delta. \quad (3.80)$$

Solving (3.80) for α gives
$$\alpha = \frac{q_\infty c^2 C_{m\delta}}{k} \delta. \quad (3.81)$$

Using this in the expression for the lift coefficient (1.24) renders

$$C_l = C_{l\alpha} (\alpha + \tau \delta) = C_{l\alpha} \left(\frac{q_\infty c^2 C_{m\delta}}{k} + \tau \right) \delta. \quad (3.82)$$

From (3.82) we conclude that, due to $C_{m\delta} < 0$, there is a critical dynamic pressure q_∞ , for which the sign of the lift turns from positive to negative. This phenomena is known as *aileron reversal*. Due to warping of the wing, a positive deflection of the flap (or aileron) at high flight velocities causes a reduction of lift rather than an increase. In order to delay aileron reversal to higher velocities, we need to provide more structural stiffness to the wing (increase k), which typically leads to a larger aeroplane weight.

3.8 Coupling Effects

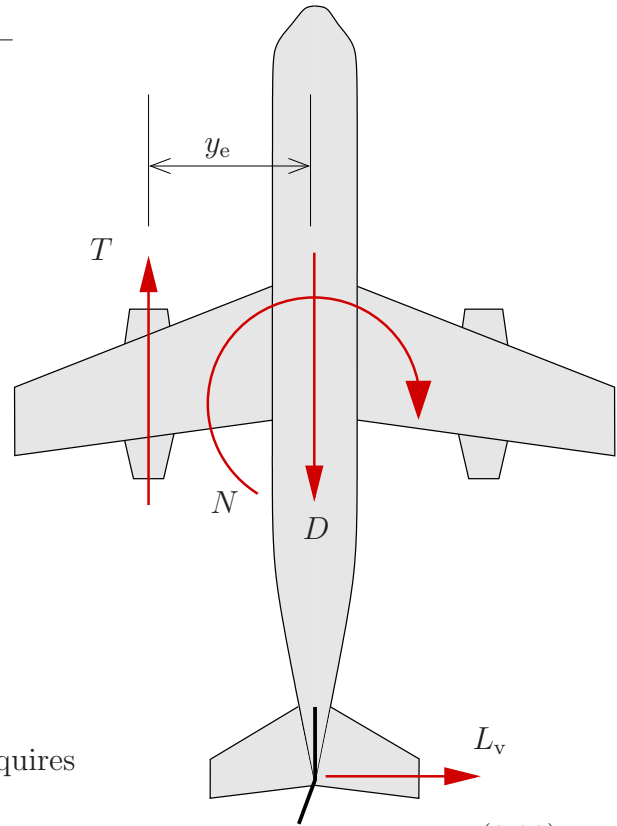
In this section, we briefly discuss some coupling effects between lateral and directional stability and control. Generally, longitudinal motion in the xz -plane is independent of lateral and directional motion. The latter are, however, very closely coupled such that we often speak of *lateral-directional stability and control*.

Coordinated Turn

A level turn is initiated by aileron deflection which rolls the aeroplane into the desired bank angle (compare Section 2.8). However, the roll primarily causes sideslip β and does not directly ensure that the aeroplane turns its nose into the desired direction. The yaw needed to coordinate the turn is, at least partly, provided by the vertical stabiliser, *i. e.* by $C_{N\beta} > 0$ (see (3.67)). However, specifically in the presence of adverse yaw, the vertical stabiliser may not generate sufficient yaw. A certain rudder deflection is then required to achieve a *coordinated turn*, such that the x -axis is always tangential to the flight path. In a coordinated turn the yaw rate and the bank angle are consistent, such that the gravity experienced by the pilot and the passengers is always perpendicular to the wings, *i. e.* they do not feel subjected to any forces to the right or to the left.

Asymmetric Engine Failure

Consider a twin engine aeroplane with one engine suddenly failing. The pilot has to trim the aeroplane with only one engine and then try to reach the nearest airport.



Rotational equilibrium in the xy -plane requires

$$T_R y_e + N = 0 . \tag{3.83}$$

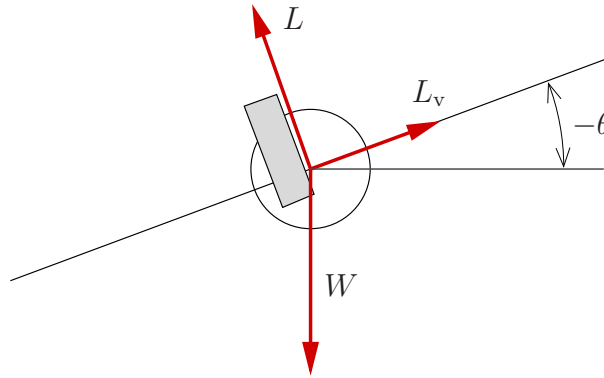
For trimmed controllable flight the sideslip has to vanish (or at least be very small), such that $\beta = 0$. Recalling $T_R = q_\infty S C_D$ and using (3.71) in (3.83) then gives

$$C_D y_e - l_v \frac{S_v}{S} C_{L_v \alpha} \tau \delta_r = 0 . \tag{3.84}$$

Solving for δ_r and using $V_V = \frac{l_v}{b} \frac{S_v}{S}$ renders

$$\delta_r = \frac{C_D y_e}{V_V C_{L_v \alpha} \tau b} , \tag{3.85}$$

which is the rudder deflection needed to balance the asymmetric thrust. Note that (3.85) is important for the design of vertical tail and rudder, since the vertical tail volume V_V must be large enough to keep δ_r in the linear range, *i. e.* to avoid stall at the vertical tail.



It remains to balance the sideways lift force generated by the rudder deflection. This can be done by rolling the aeroplane such that a component of weight is used to counterbalance the sideways lift L_v . Assuming that θ is small we may write

$$-W \theta = L_v . \quad (3.86)$$

Using (3.85) and $L = W$ for small θ we obtain

$$\theta = -\frac{L_v}{L} = -\frac{q_\infty S_v C_{L_v \alpha} \tau \delta_r}{q_\infty S C_L} = -\frac{C_D}{C_L} \frac{y_e}{l_v} . \quad (3.87)$$

minimum control speed: A sudden asymmetric engine failure will result in a sudden yawing moment. This is accompanied by a rolling moment due to the lift differential on the two wings, which results from the different airspeeds of the wings. The pilot needs to react quickly with the appropriate rudder and aileron deflections. This requires the control surfaces to be sufficiently effective at the current flight velocity. Recalling that rudder and aileron lift forces are proportional to q_∞ , it follows that there exists a minimum velocity below which control of the aeroplane can not be recovered.

Similarly, the equations (3.85) and (3.87) suggest that there is a maximum drag coefficient C_D beyond which the rudder deflection δ_r and the bank angle θ become impractical. Recalling that the (induced) drag increases as the velocity decreases, we conclude that this renders a minimum flight velocity for which asymmetric thrust can be counterbalanced by rudder deflection and roll.

The minimum velocity for which controlled trimmed flight can be recovered and maintained is known as the *minimum control speed* v_{MC} . It represents a critical design factor. Engine failures at smaller flight velocities usually result in fatal accidents.

Rolling Moment with Sideslip – Dihedral

Generally, it follows from positive sideslip (sideslip to the right) that the lift force generated by the right wing is larger than the one generated by the left wing and vice versa. The lift force differential then causes a rolling moment, which rolls the aeroplane towards the direction opposite to the sideslip. This phenomena is known as the *dihedral effect* and may be expressed as

$$C_{l\beta} < 0. \quad (3.88)$$

Generally, a value of $C_{l\beta}$ slightly smaller than zero is desirable for the handling of the aeroplane. If $C_{l\beta}$ is positive or $|C_{l\beta}|$ is too large, then the aeroplane becomes difficult to fly.

Now consider a positive rolling perturbation, *i. e.* the aeroplane is suddenly banked by the angle θ . Consequently, the lift force is tilted to the right and causes positive sideslip. Due to (3.88) a negative restoring rolling moment is generated. Thus, the dihedral effect may be seen as providing static stability with respect to perturbations of the bank angle.

The parameter $C_{l\beta}$ is determined mainly by the *dihedral angle* Γ . For each wing, the sideslip velocity may be decomposed into components parallel and perpendicular to the wing surface as illustrated. Depending on its orientation, the perpendicular component displaces the freestream velocity v_∞ such that the angle of attack decreases or increases. Therefore, we conclude that the larger Γ is chosen, the more lift is generated on the wing facing the sideslip wind, and consequently the larger is the resulting rolling moment.

In the presence of wing sweep, the component of the sideslip parallel to the wing surface has a similar effect as is illustrated below. However, we recall that the primary design criteria for wing sweep is the drag divergence at high flight velocities.

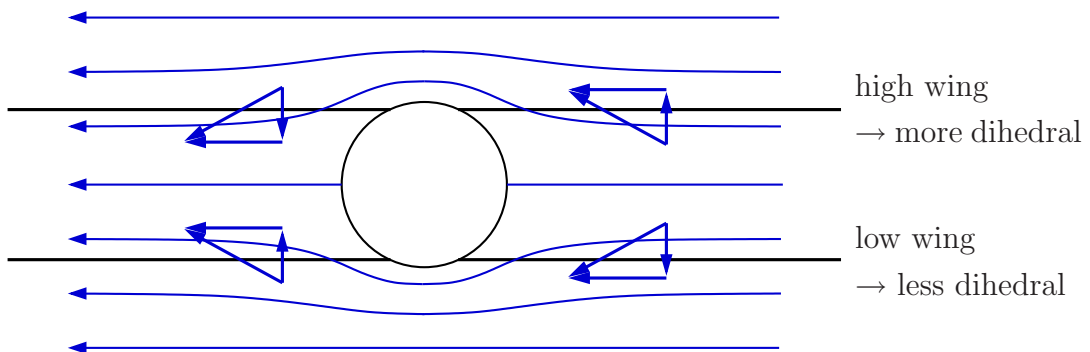
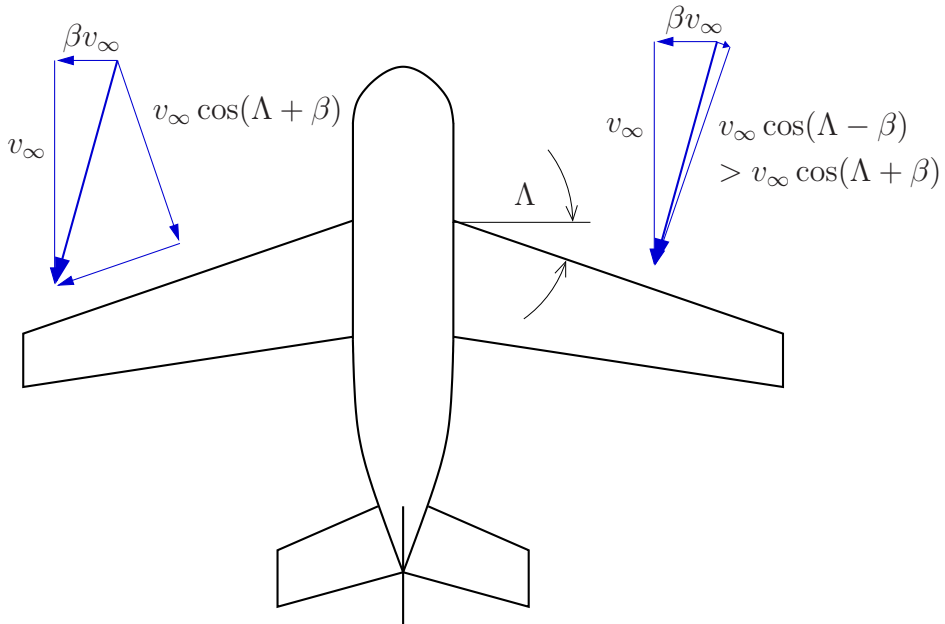
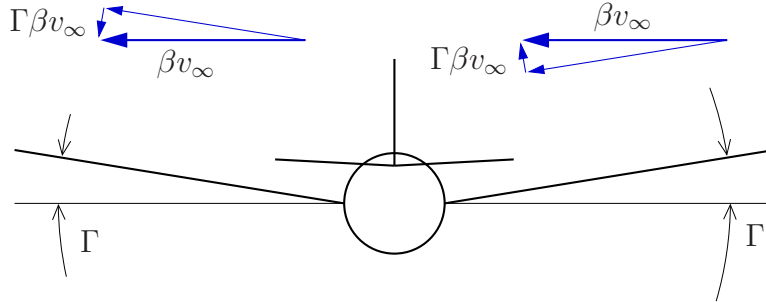
Finally, the dihedral effect depends significantly on the placement of the wings on the fuselage. In fact, some aeroplanes with high wings (and/or large wing sweep) have a negative dihedral angle Γ in order to avoid an excessive dihedral effect.

decrease angle of attack

$$\Delta\alpha = -\beta\Gamma$$

increase angle of attack

$$\Delta\alpha = +\beta\Gamma$$



Other Coupling Effects

rolling moment with rudder deflection: In a classically configured aeroplane, the vertical tail with the rudder is situated at some distance above the centre of gravity of the aeroplane. Consequently, any horizontal lift force of the vertical tail and rudder generates a rolling moment with respect to the centre of gravity.

rolling moment with yaw rate: While the aeroplane is yawing in the positive direction, the left wing experiences a larger freestream velocity than the right wing. This lift force difference results in a positive rolling moment. Vice versa, a negative yaw rate produces a negative rolling moment.

yawing moment with roll rate: While the aeroplane is rolling, the freestream velocities on the two wings are displaced by a component vertical to the wing. Consequently, the lift force is tilted forward on one wing and backwards on the other. This results in a yawing moment.

There exist other, more complicated coupling effects, which are beyond the scope of these notes.